SDC-91-00087

SDC
SOLENOIDAL DETECTOR NOTES

ISOLATED ELECTRON PATTERN LOGIC DESIGN AND PERFORMANCE AT THE SSC

November 11, 1991

W.H. Smith, J. Lackey, T. Gorski, and W. Temple
University of Wisconsin

SDC Note SDC-91-00087
November 11, 1991

Isolated Electron Pattern Logic Design and Performance at the SSC

W.H. Smith, J. Lackey, T. Gorski, W. Temple
University of Wisconsin

1 Introduction

A major requirement of the SDC First Level Trigger is the detection of electrons from inclusive W and Z production with 50% efficiency for triggering on the events that enter the detector fiducial volume. The anticipated rate of electrons from these sources is 3 KHz at the nominal SSC design luminosity of 10^{33}. However, these must be detected against a background rate of an average of 1.6 events occuring at the beam crossing frequency of 16 nsec. This input rate of 10^8 interactions every second must be reduced by a factor of at least 10^3 to 10^4 by the first level trigger. This report is a conceptual design for digital pattern logic to trigger on isolated electrons and photons in the SDC calorimeter. This logic is fully pipelined with 16 nsec clocking. This document outlines the design of this logic and presents simulation results on its performance.

The isolated electron pattern logic is part of a calorimeter trigger based on several quantities. Among these are: the total energy deposited in the calorimeter, the sum of transverse energy, missing p_T, along with the number and energies of jets and electrons[2]. The trigger design presented here requires fast signal detection. The philosophy of this trigger is to collect information at the rate of the crossing frequency in order to minimize the probability of event overlap confusing the trigger. This does not imply that the full calorimeter data acquisition systems collect information at this rate. This does mean that the subset of information used by the trigger is acquired at the crossing frequency.

The calorimeter design assumes scintillator readout by some type of photomultiplier device. The calculations required for the calorimeter trigger include summing all of the energies from pulseheights recorded in the photomultipliers every 16 nsec. In addition, calculation of the transverse energy and missing p_T requires energies from pulseheights, multiplied by geometric factors. The calorimeter trigger starts with the assignment of EMC and HAC sections to trigger towers. An analog sum is made of all of a trigger tower's EMC sections and a second sum is made of all its HAC sections. These are then flash-digitized. The trigger must form the transverse energy and missing p_T sums. Given an EMC or HAC trigger tower sum of energy E_i located at polar angle θ_i and azimuthal angle ϕ_i, the sums may be formed from the quantities E_i (total energy), $E_i \sin\theta_i$ (transverse energy) and the components $E_i \sin\theta_i \cos\phi_i$ (missing E_x) and $E_i \sin\theta_i \sin\phi_i$ (missing E_y). The digitized HAC and EMC pulseheight from each of the trigger towers is stored. multiplied by lookup tables containing these geometric factors and injected into summing networks.

The formation of jet, isolated muon and isolated electron triggers in a pipelined fashion is considerably more complicated than making sums. The detection of jets requires preservation of tower information that would be lost in a global sum. The detection of an electron requires evidence of electromagnetic energy. This is done by comparing energy deposited in the first interaction length of the calorimeter with that deposited later on a tower by tower basis. The determination of the isolation of an electron requires checking the towers bordering on the electron "candidate" tower for energy below some minimum threshold ("quiet").

The proposed design uses tables to make local tests on the amount of energy in an individual trigger tower. The ratio of HAC to EMC energy is also tested. The results of these tests are encoded and passed forward with the energy sums to a search table that looks for matches with desired patterns. Local energy sums and tests are also made.

Although the design described in this document is applied to the task of identifying isolated electrons, it is essentially a general purpose isolated particle detector. Any particle which can be characterized in terms of its energy depositions into the electromagnetic and hadronic compartments of the calorimeter is eligible for isolation detection. The design is reconfigured to detect isolated alternate particle types simply by reprogramming the memory lookup tables which correlate the electromagnetic and hadronic energy depositions.

The identification of an electron involves correlating information from the tracking and calorimeter systems. Identification of an electron in the calorimeter requires detecting isolated electromagnetic energy. The first step is to find a calorimeter trigger tower with energy in the electromagnetic compartment and little or no energy in its hadronic compartment (i.e. typically $E_{HAC} < 0.1 * E_{EMC}$). Next the towers adjacent to this tower are checked for having little or no energy in both electromagnetic and hadronic compartments. This establishes electromagnetic energy that is transversely and longitudinally isolated. Since electrons may share energy among towers, and the criteria for electron isolation needs to be relaxed for more energetic electrons, the design allows for the ratio of HAC to EMC energy to identify an electron tower to change with energy, allows for different definition of the quiet towers used in transverse isolation with different energy electron towers, and has provision for up to six energy thresholds. The latter is necessary in order to allow for different energy thresholds for single, dilepton, and multilepton events.

2 General Overview

Figure 1 shows a hardware block diagram for the Isolated Electron Trigger. Photomultiplier Tube (PMT) currents for the EMC and HAC sections of each trigger tower are digitized in a FADC to produce a value for the current. These digitized values are supplied as address to a Memory Lookup Tables (MLUs) which both convert the energy to a 12-bit linear scale for the production of jet and total/missing energy sums, and also determine a state for the trigger tower, known as an Encode Tower Type (ETT) code. This code classifies a tower as electromagnetic, quiet or hadronic. The FADC and MLUs are organized in a pipeline architecture, so as to be able to sample new PMT currents and produce a new ETT code for each 16ns bunch crossing. The pipeline length will be approximately 3 crossing clocks.

The ETT codes are used to reflect the state of the trigger tower as it pertains to isolated electron triggering. The code is 3-bits wide, and thus can reflect 8 different states for the trigger tower. All of the states are programmable through the VME downloadable memory lookup tables. Two of the code values, 0 and 7, are reserved to specific states. Code 0 is reserved to indicate towers which are below all pertinent energy thresholds (i.e., "quiet"). Code 7 is reserved to indicate towers which are hadronic in energy content. The other 6 codes can be programmed to indicate that the tower are either electromagnetic or quiet in nature, at different energy levels. This capability allows for different definition of the quiet towers used in transverse isolation with different energy thresholds for electron towers. The example ETT codes below and the following discussion show a full 6-Electron threshold configuration for the ETT code. At the end of this *General Overview* section, an alternate example configuration is shown, with a second quiet threshold inserted at code 4.

ETT code definitions for 6-Electron threshold configuration:

- **Quiet.** (Code 0.) This state indicates that the energy deposition in the tower is below all electron energy thresholds.
- **E_1 Electron.** (Code 1.) This state indicates an energy deposition was detected corresponding to the passage of an electron at or above energy threshold 1.
- **E_2 Electron.** (Code 2.) This state indicates an energy deposition was detected corresponding to the passage of an electron at or above energy threshold 2.
- **E_3 Electron.** (Code 3.) This state indicates an energy deposition was detected corresponding to the passage of an electron at or above energy threshold 3.
- **E_4 Electron.** (Code 4.) This state indicates an energy deposition was detected corresponding to the passage of an electron at or above energy threshold 4.
- **E_5 Electron.** (Code 5.) This state indicates an energy deposition was detected corresponding to the passage of an electron at or above energy threshold 5.
- **E_6 Electron.** (Code 6.) This state indicates an energy deposition was detected corresponding to the passage of an electron at or above energy threshold 6.
- **Non-Electron.** (Code 7.) This state indicates an energy distribution corresponding to something other than an electron or quiet tower (hadron).

An ETT code exists for each trigger tower. The size of the trigger tower and the resulting granularity of the search grid of the isolated electron detection, in terms of η-ϕ coordinates, depends upon the summing of the PMT currents supplied to the FADC. A trigger tower size of .05 x .05 is achieved if the EMC and HAC PMT currents of each tower are digitized separately. If the currents from groups of 4 towers (in a 2x2 layout) are summed together before digitization, then the trigger tower size becomes 0.1 x 0.1. In either case, there is no effect on the structure of the ETT code, or the logic which operates upon it.

The next step in isolated electron detection is to organize the towers into 8x8 regions, for the application of their ETT data to a pattern recognition ASIC. Each 8x8 region, hereafter referred to as a "grid", has a 3-bit ETT code for each of its 64 trigger towers, for a total of

192 bits of ETT data. This data is applied via a common bus to 6 instances of a Pattern Recognition ASIC (PRA). All PRAs operate on the same ETT data simultaneously; each at a different electron threshold level. For each PRA, the electron threshold is determined by a select mask, which is under computer control. The select mask identifies the threshold level at which the PRA will identify a tower as containing an electron. Towers with ETT codes below that threshold level will appear as quiet to the PRA **for pattern recognition purposes.**

Each PRA searches for isolated electron electrons at its respective threshold level in 49 possible locations within the grid. The rules for this search are described in a subsequent section. The output of the PRA is a flag word which indicates the presence of any isolated electrons within regions of the grid. These regions consist of 2x2 trigger tower geometries which are fully confined within the grid, and 1x2 or 1x1 trigger tower geometries which occupy the edges or corners of the grid. There are a total of 25 regions in an 8x8 grid: 9 confined 2x2 regions, 12 1x2 edge regions, and 4 1x1 corner regions.

Note that the logic within the PRA for decoding the ETT codes is designed in such a way that **two PRAs operating at different thresholds cannot each find an isolated electron in the same location**; the higher thresholds have priority. Each PRA can accept a new grid of ETT data every 16ns bunch crossing. The latency through the PRA to the production of the flag word is approximately 3 crossing clocks.

In addition to the PRAs, the ETT data bus is monitored by the quiet detect logic. This logic checks the raw ETT codes for the grid to detect regions which are completely quiet (all towers at ETT code 0), and produces a resulting flag word indicating which of the 25 regions is quiet. The region geometries exactly correspond to those used by the PRAs as described above.

The flag words from all of the 6 PRAs and the quiet detect logic are fed to the electron threshold decoder logic. This logic examines the flag words, and produces a 3-bit isolated electron code for each region. This code reflects the threshold at which an isolated electron was found, if the region was completely quiet, or if no isolated electron was found in the region.

For the 6-Electron threshold case, these codes are defined as follows:

- **Region Completely Quiet.** (Code 0.) This code indicates that all towers in the region were completely quiet (all had an ETT code of 0).
- E_1 **Isolated Electron.** (Code 1.) This code indicates that an isolated electron at threshold 1 was located in the region.
- E_2 **Isolated Electron.** (Code 2.) This code indicates that an isolated electron at threshold 2 was located in the region.
- E_3 **Isolated Electron.** (Code 3.) This code indicates that an isolated electron at threshold 3 was located in the region.
- E_4 **Isolated Electron.** (Code 4.) This code indicates that an isolated electron at threshold 4 was located in the region.

- E_5 **Isolated Electron.** (Code 5.) This code indicates that an isolated electron at threshold 5 was located in the region.

- E_6 **Isolated Electron.** (Code 6.) This code indicates that an isolated electron at threshold 6 was located in the region.

- **Not Isolated, Not Quiet.** (Code 7.) This code indicates that the region did not contain an isolated electron, and was also not completely quiet.

Despite the apparant similiarity, these isolated electron codes should not be confused with the ETT codes. Whereas the ETT codes refer to the raw state of individual trigger towers, the isolated electron codes refer to regions of trigger towers after an isolation cut has been performed. Code value 7 provides a good example of the difference between the two definitions. Whereas ETT code 7 refers to a trigger tower which is hadronic, isolated electron code 7 refers to a region which is not completely quiet, and did not contain an isolated electron. [As it turns out, however, a region with a tower at ETT code 7 (hadronic tower) does indeed map to isolated electron code 7 (non-quiet, non-isolated region).]

The threshold encoder logic also contains a self-test feature, in which all PRAs are set to the same threshold, and their flag words subjected to a bitwise comparison. As the PRAs are identical, their output flags should also be identical. This feature will identify a lack of total agreement between the six PRAs.

Once the isolated electron codes are generated, the final step before matching with the track and showermax data in the level 1 trigger is the combination of edge/corner partial regions of adjacent grids into 2x2 trigger tower composite regions which fall across grid boundaries. This is performed by the edge/corner region checking logic described in a later section. The result produced by this logic is a map of uniform 2x2 tower regions for the entire calorimeter, each with a 3-bit isolated electron code.

As stated previously, the ETT codes 1-6 may be configured to be additional quiet states instead of electromagnetic thresholds. This is accomplished merely be reprogramming the selected ETT codes in the downloadable MLU via the VME interface to reflect the definition change for the additional quiet states. These additional quiet states will be visible as to all electron thresholds having higher ETT code values, and will not be visible to the thresholds with lower ETT code values. In addition, those PRAs which previously monitored those thresholds are disabled by the controlling processor. The result is that towers with significant energy content can be considered as quiet under certain circumstances for the purpose of detecting isolated electrons at the higher energy thresholds.

In the example below, electron threshold 4 is replaced with a second quiet threshold, resulting in the following altered ETT code definition. The gap created by the loss of a threshold is filled by the reprogramming of one or more of the remaining electron thresholds. The result is a configuration with a single quiet threshold for the bottom 3 electron thresholds, and two quiet thresholds for the top 2 electron thresholds.

- **First Quiet.** (Code 0.) This state indicates that the energy deposition in the tower is below all electron energy thresholds. This threshold is unchanged from the original definition.

- **E_1 Electron.** (Code 1.) This state indicates an energy deposition was detected corresponding to the passage of an electron at or above energy threshold 1.
- **E_2 Electron.** (Code 2.) This state indicates an energy deposition was detected corresponding to the passage of an electron at or above energy threshold 2.
- **E_3 Electron.** (Code 3.) This state indicates an energy deposition was detected corresponding to the passage of an electron at or above energy threshold 3.
- **Second Quiet Threshold** (Code 4.) This state provides an additional quiet threshold which is visible to to electron thresholds 5 and 6, but not to electron thresholds 1 through 3. This threshold is for towers which have significant energy deposition but may nonetheless be considered quiet for detecting electrons at higher energy thresholds.
- **E_5 Electron.** (Code 5.) This state indicates an energy deposition was detected corresponding to the passage of an electron at or above energy threshold 3.
- **E_6 Electron.** (Code 6.) This state indicates an energy deposition was detected corresponding to the passage of an electron at or above energy threshold 5.
- **Non-Electron.** (Code 7.) This state indicates an energy distribution corresponding to something other than an electron or quiet tower (hadron).

Continuing the example, the following isolated electron codes result. Note that code 0, *Region Completely Quiet*, is formulated exclusively from the first quiet threshold, ETT code 0. Code 5, previously occupied by isolated electrons at ETT code 4, now becomes an empty/undefined state.

- **Region Completely Quiet.** (Code 0.) This code indicates that all towers in the region were completely quiet (all had an ETT code of 0).
- **E_1 Isolated Electron.** (Code 1.) This code indicates that an isolated electron at threshold 1 was located in the region.
- **E_2 Isolated Electron.** (Code 2.) This code indicates that an isolated electron at threshold 2 was located in the region.
- **E_3 Isolated Electron.** (Code 3.) This code indicates that an isolated electron at threshold 3 was located in the region.
- **Empty/Undefined.** (Code 4.) This code is empty/undefined. ETT code 4 has been reassigned to a second quiet, and the PRA operating at threshold 4 has been disabled. The encoder logic will not generate this code for any region.
- **E_5 Isolated Electron.** (Code 5.) This code indicates that an isolated electron at threshold 5 was located in the region.
- **E_6 Isolated Electron.** (Code 6.) This code indicates that an isolated electron at threshold 6 was located in the region.
- **Not Isolated, Not Quiet.** (Code 7.) This code indicates that the region did not contain an isolated electron, and was also not completely quiet.

3 Memory Lookup Tables

Figure 2 shows a block diagram of the memory lookup table architecture for a single logical tower. It shows a pipeline consisting of the Flash ADCs (FADCs) that digitize the raw PMT or summed PMT signals, a fiber-optic interface to transfer the raw data off the detector, and a group of memory lookup tables, operating at the 16ns crossing clock rate. The pipeline begins with photo-multiplier tube currents of the tower EMC and HAC sections connected to a pair of FADCs. (Note that if the trigger tower size in η-ϕ coordinates is to be .05x.05, then this corresponds to a single physical tower. If the trigger tower size corresponds to .1x.1, then this corresponds to 4 physical towers in a 2x2 arrangement, with their currents summed in the analog domain.)

The output of the FADCs is a raw digital value which reflects the energy content in that section of the tower. These values are represented in the figure as being 8 bits compressed on a nonlinear scale, although it could be represented using other formats, including 8-bits mantissa with 4-bits exponent or 8-bits mantissa with 1-bit range and 1-bit overflow. The EMC and HAC digital values are transmitted together on a single optical fiber off the detector, where they are received and separated again for application to the MLUs.

There are three MLU blocks in the design. The first MLU compares the raw EMC and HAC energies to produce the ETT code. This code is used for the isolated electron detection which is subsequently described in this document. The other two MLU convert the raw EMC and HAC energies to a 12-bit linear scale, so that they can be applied to a summation tree for use in the jet threshold and total/missing transverse energy triggers.

4 Pattern Recognition ASIC (PRA)

The PRA performs the task of examining the ETT codes for 8x8 trigger tower regions ("grids") to detect those trigger towers containing isolated electrons. A PRA is configured with a static threshold select under computer control to select the desired electron energy threshold. This select controls how the ETT data is decoded within the PRA. During normal operation, six PRAs, one for each electron threshold, simultaneously operate on the same ETT data for each grid in the calorimeter. During self-test mode, all PRAs operate on the same threshold, and should produce identical results.

Figure 3 shows a block diagram of the PRA. Processing within the PRA occurs in three major stages: ETT decoding to Q/E bits, finding isolated electrons in the isolated electron detection blocks, and mapping the results of the isolation detection into fixed physical regions.

The first stage of processing is the ETT decoding. The top three edges of Figure 3 show the 3-bit ETT codes of 64 trigger towers (192 bits total) entering the chip. The ETT code for each trigger tower is compared to the threshold selected for the PRA. The result of this comparison is the Q and E bits. The Q bit is active if the ETT code is less than the threshold–the tower is considered quiet. The E bit is active if the

tower exactly matches the threshold–the tower is considered electromagnetic. The Q and E bits are merely a repackaging of the tower state into a format which is more convenient to the pattern recognition logic. The comparisons are performed on an individual tower basis.

In the next layer into the PRA, the Q/E bits are buffered for distribution into 49 isolated electron detection blocks. Each of these blocks examines a single 4x4 tower zone on the grid known as a "template," to determine if an isolated electron is present. The templates are placed on the grid in a 7x7 array, such that they are offset one tower horizontally and/or vertically from their neighbors. This positioning covers all of the areas on the grid where an isolated electron may occur. As stated previously, one isolated electron detection block is assigned to each template, for a total of 49. Each block produces binary flags indicating which of the trigger towers within its template contained an isolated electron.

The last step of processing in the PRA is to map the isolated electron flags for individual trigger towers from the detection blocks into 25 fixed regions. These regions correspond to 9 fully confined 2x2 trigger tower regions, 12 edge 1x2 or 2x1 trigger tower regions, and 4 corner 1x1 trigger tower regions. The result of the mapping is called the "region flag word", a 25-bit word that contains a binary flag for each region, indicating if that region contained an isolated electron or not.

The three major stages of processing are described in greater detail in subsequent subsections. To summarize, the ETT codes for an 8x8 group of 64 trigger towers are tested against the selected threshold. The results of the comparison are passed into the array of 49 isolated electron detection blocks, each located at one of the possible sites of an isolated electron, and each of which examines the state of the towers in one 4x4 template area to detect isolated electrons within that area. Each block produces binary flags for those trigger towers within its template which may contain an isolated electron. All of the individual trigger tower flags from the 49 isolated electron detection blocks are then mapped into 25 fixed regions on the grid and delivered to the output pins of the PRA.

In terms of technology, this preliminary design assumes a BiCMOS Gate Array technology, utilizing 1.0/1.5-micron CMOS features, with a 1.5-micron bipolar commercial process. The design would require approximately 220 TTL I/O pins. The chip would run at a 16ns clock rate. We have evaluated implementing this design with one vendor and have a resulting gate count of approximately 18,000 gates.

4.1 ETT Decoding to Q/E Bits

Figure 4 shows the decoding of tower ETT codes to Q/E bits at all six electron thresholds. In order to be usable by the isolated electron blocks, the ETT code must first be converted into a Q and E bit for each tower. This is performed by comparing the value of each ETT code to the threshold selected for the PRA. If the ETT code is < the threshold, then the Q bit is active. and the tower is considered quiet. If the ETT code exactly matches the threshold, then the E bit is active, and the tower is electromagnetic at the correct threshold for detection by the PRA. If the ETT code is > the threshold, then neither bit is active, and the tower appears as a non-electron,

non-quiet tower to the PRA. This situation covers the cases where the tower contains a hadron or an electron at a higher threshold, in which case the isolation cut will be performed by a different PRA operating at a higher threshold. One PRA operates at each of the six thresholds.

Figure 5 contains a block diagram of the ETT decoding section in the PRA. The 64 ETT codes are received as TTL data by the input buffers. They are then converted to Q/E bits by the method described above in 64 identical decoding blocks. The Q/E bits are then passed to the first stage 16ns pipeline register at time "T1" in the design. From the pipeline registers, they are sent to fanout buffers.

4.2 Isolated Electron Detection Blocks

As stated above, there are a total of 49 isolated electron detection blocks in each PRA. Each block operates on a 4x4 section of towers known as a template. The purpose of the block is to examine the Q/E bits of the 16 towers to determine if an isolated electron is present within the bounds of the template, centered on the inner 2x2 towers.

The templates are placed on the grid in in a 7x7 array, such that they are offset one tower horizontally and/or vertically from their neighbors. The templates on the edges of the grid are placed so that one row or column of the template is actually off the grid. Towers which occupy an off-grid location are assumed to be quiet by the logic. This may result in the detection of electrons in edge towers, which are isolated on the current grid, but have not as yet passed isolation checking with adjacent towers on other grids. These electrons are mapped into edge/corner regions which will undergo final isolation checking with similiar regions in subsequent logic. With this placement, the templates examine all 49 possible locations for an isolated electron.

An isolated electron is present in the template if both of the following conditions are met:

1. One or more E bits is active in the inner 2x2 region. Any remaining towers in the inner 2x2 have their Q bit active.
2. All of the towers in the outer region (outside the inner 2x2) which are adjacent to active E bits in the inner 2x2 (including diagonal connections) have their Q bit active. Those towers in the outer region which are not in contact with an active E bit are considered to be "don't cares."

Note that the definition of an isolated electron allows for cases where up to 4 E-bits are set in the inner 2x2.

To determine if an isolated electron is present in a template, the detection blocks utilize a combinatorial function referred to as an Evaluation Function. This function provides a bit, called the F-value, which is active if an isolated electron is present in the template. The general case of the Evaluation Function is shown in Figure 7. The C_1 through C_4 subfunctions check that any E bits set in the inner towers are adjacent to Q bits in the outer towers in the 4 corners of the template. The D subfunction is used to defer evaluation of an isolated electron candidate to the next template to the right or below. This is to avoid the condition where the same isolated electron

is detected in more than one template. (The D subfunction has special cases which apply for right-edge, bottom-edge, and bottom-right-corner templates, as indicated by the active-high signals *BOTTOM* and *RIGHT* in the definition.) The N subfunction is used to detect Non-Electron type towers or towers above the selected threshold in the inner 2x2 region.

Figure 9 contains a block diagram of the isolated electron detection section in the PRA. The Q/E bits arrive from the T1 pipeline register at the fanout buffers. These buffers distribute the Q/E bits to the 49 detection blocks. As the 49 templates overlap each other, a given tower may reside in up to 16 individual templates. As a result, a given Q/E bit may have 30 to 40 individual loads. The purpose of the buffers is to distribute this loading in the most efficient method possible. In spite of the presence of a given tower in many templates, an electron can only satisfy the isolation conditions in a single template.

Each detection block has boolean outputs, known as tower E-flags, for 2 or 4 of its inner 2x2 towers. These flags correspond to trigger tower locations in the template where an isolated electron may be assigned. When the detection block has an active F-value, it examines the E bits on the candidate towers to determine which tower contained the electron. The tower for which the E bit is active has its E-flag set active, while all other E-flags in the template are set inactive. For cases where multiple E bits are active in the template, the assignment is still only made to one tower. The E bits are examined according to a set priority, depending on the location of the template in the grid.

There are four template types, based on their location on the grid. Examples of these types are shown in Figure 8. In the examples, the tower to which the electron will be assigned is indicated with a bold outline. The template types are described below:

Non-Right, Non-Bottom Edge Templates. This group is comprised of the 36 upper-left templates on the grid. For these templates, isolated electrons will only be assigned to the left two towers of the inner 2x2 (indicies B1 and C1 in figure 7). This follows from the fact that any isolated electron within the template which does not have an E bit set in at least one of these two towers will be deferred to the template to the right. The rule for mapping in these templates is that if the E bit is set at location B1 in the template, then the electron is assigned to the tower at B1. Otherwise, if the E bit is set at location C1, then the electron is assigned to the tower at C1.

Bottom, Non-Right Edge Templates. This group is comprised of the leftmost 6 templates on the bottom edge of the grid. For the same reason as above, the assignment can again only be made to B1 and C1. However, in this case, the priority is reversed, such that C1 has higher priority over B1. This guarantees that an isolated electron on the edge of the grid that is detected in these templates will be mapped to an edge region in the region flag word.

Right, Non-Bottom Edge Templates. This group is comprised of the upper 6 templates on the right edge. For these templates, isolated electrons can be assigned to any of the inner 2x2 regions, according to the following priority. If the E bit at location B2 (upper right in the inner 2x2) is active, then the electron is assigned to the tower at B2. Otherwise, if the E bit at C2 is active, then the

electron is assigned to C2. B1 is the next tower in priority, and finally C1. The intent is to make sure that the electron is first assigned to a right edge region if possible, and then to a top edge region if the template is on the top edge, and then finally to the fully confined electron C1.

Bottom, Right Edge Template. This template is the special case at the lower right corner of the grid. The priority is the same as for the group immediately above, with the exception that the priority for B1 and C1 have been reversed. Thus, this template first attempts to assign the electron to the right edge, and then to the bottom edge, before assigning it to the confined electron B1.

The examples demonstrate how isolated electron assignment to individual towers varies with the template type. The priority is always to assign isolated electrons to towers on the edge of the grid, if possible, so that they will undergo further checking with regions from adjacent grids.

A total of 112 tower E-flags are produced by the 49 detection blocks. This includes 2 flags each from the 42 non-right edge templates (84), and 4 each from the 7 right-edge templates (28). These 112 bits are sent to the next stage 16ns pipeline register, at time "T2" in the design. From there, they will be used for region flag word generation.

4.3 Region Flag Word Generation

As stated previously, the PRA generates a region flag word for each grid of ETT data. Figure 10 shows the bit definition of the word and the mapping of the 25 regions onto the 8x8 grid of trigger towers. Note that for each region, an E-flag is defined. An E-flag is active if any of the towers in its region contains an *isolated* electron. Note that due to the nature of isolation, a maximum of one isolated electron would be found in any region. Note also the placement of the region boundaries. Those towers which are completely confined within the grid are placed in 2x2 regions. Electrons found within these regions have already been determined to be properly isolated. Those towers which are on the edge of the grid are placed in 1x2 edge or 1x1 corner partial regions. Electrons found in these regions have been determined to be isolated with respect to other towers on this grid, but require further isolation checking with towers in adjacent grids. This checking is described in a subsequent section.

The 25 region E-flags are produced from the 112 tower E-flags produced by the detection blocks using OR logic. Figure 11 contains a block diagram of the region flag word generation section in the PRA. There are 25 independent OR gates, one for each of the 25 regions. Each OR gate has 1 to 8 inputs on it, depending on the region. The number of inputs to a gate corresponds to the total number of tower E-flags from overlapping templates which map into that region. Each of the 112 tower E-flags acts as an input to the OR gate for the 2x2 region which contains that tower. The output of each OR gate is an E-flag for the region, which indicates if any tower within that region contained an isolated electron.

From the OR logic, the E-flags are passed to a 16nsec pipeline register at chip time "T3". From there, the signals go through the output buffers of the chip, and driven as TTL data to the 25 output pins.

4.4 PRA Summary

The PRA constitues a 3-stage, 16ns pipeline, which accepts a new grid of ETT data and produces a new region flag word on each clock cycle, with a latency of 2 clocks between input and output. It is optimized for six thresholds, using a 3-bit ETT code. It requires approximately 220 TTL I/O pins, plus power and ground. It will operate on a single +5V source. It will be fabricated using BiCMOS Gate-Array technology. Power consumption will be dependent in part on the density of non-quiet towers, as the more often each ETT code changes state, the more resulting switching and thus power consumption there will be inside the ASIC. Monte Carlo studies are in progress to determine the switching rates which will be seen by the ASIC. It is anticipated, however, that the switching rates will be low enough (below 10%) such that power consumption in the ASIC will be manageable.

5 Quiet Detect Logic

As shown in Figure 1, the quiet detect logic monitors the ETT data bus in parallel with the six PRAs. Its purpose is to detect 2x2 regions (using the same region geometry as is used by the PRAs as defined in Figure 10) which are completely quiet. Like the PRAs, it delivers its 25 flags ("Q-flags") to the threshold encoder logic 3 crossing clocks after sampling the ETT data. These flags will be used to help determine the isolated electron code for the region, and indirectly, through the code, can be used by the muon trigger subsystem because they identify quiet $.2\eta$ x $.2\phi$ regions in the calorimeter.

The quiet detect logic occupies 3 pipeline stages. The first pipeline stage of the logic makes a Q-flag for each tower by NORing the 3 ETT code bits together. The result will be active Q-flags for those towers which had an ETT code of 0. The next stage ANDs together the 1, 2, or 4 tower Q-flags (depending on the region) to form region Q-flags. These Q-flags will be active only if *all towers in the region are completely quiet.* The final stage of the pipeline is merely for timing compatibility with the PRAs, so that the region Q-flags are delivered to the threshold encoder logic on the same clock cycle as the region E-flags from the PRAs.

6 Threshold Encoding

As shown in Figure 1, the electron threshold encoder logic operates on the region flag words produced by the six PRAs and the quiet detect logic. Its function is to encode the E-flags and Q-flags on a region-by-region basis to produce a 3-bit isolated electron code for each region. The isolated electron codes are described in the *General Overview* section.

The isolated electron code is defined so that each state corresponds to one of the seven flags being active. State 0 corresponds to the Q-flag from the quiet detect logic being active, states 1-6 correspond to an E-flag from the PRAs at threshold levels 1-6 respectively being active, and state code 7 is the exception, corresponding to none

of the flags being active. (Note that in programmed configurations where additional quiet states are defined, there will be empty isolated electron codes. This is due to the fact that a given PRA is disabled when its corresponding ETT code is defined as quiet, and therefore will not generate any active E-flags.) The code is produced from the Q/E-flags using a variation of a common 8-to-3 priority encoder. This encoder will be implemented using commercial Programmable Logic Device (PLD) architecture, such as a 16R4, 22V10, or similiar device, which are commonly available in 20 or 24-pin packages. A total of 25 identical encoder blocks are needed for the 25 regions. These will occupy either 13 or 25 PLDs, depending on whether one or two blocks are programmed per PLD. The encode operation from the Q/E-flags to the isolated electron codes should take 1 crossing clock.

Residing alongside the encoder blocks in the PLDs is the self-test logic. This self-test logic provides a quick test of the proper operation of the PRAs. The self-test must be performed while the logic off-line. During self-test mode, the six PRAs are set to the same threshold, and test ETT data is applied. If all PRAs are functioning correctly, then their E-flags should all be identical, from region to region (although the "correct" value for any given region is a function of the ETT test data.) The self-test logic within the PLDs checks the E-flags for the condition where there is a disagreement between the E-flags for the six PLDs. Each PLD will produce a single "Mismatch Error" signal for the one or two region encoder blocks it contains. The "Mismatch Error" signals are logged into memory and subsequently reported to the processor controlling the test via the VME interface.

Once a mismatch error has been found, the identity of the failing PRA can be determined by operating the PRAs at their normal thresholds, and examining the isolation codes produced using additional ETT test data.

7 Partial Region Resolution

Partial region resolution is term given to the task of recombining the partial 1x2 edge and 1x1 corner regions at the edges of 8x8 grids into 2x2 tower regions. It is the means by which isolation checking is performed across grid boundaries, and provides a final check of the assumption made in the PRA isolation cut that all towers just beyond the edges of the grid are quiet. The result of the recombination is a 2x2 tower region geometry of isolated electron codes across the entire calorimeter.

Figure 12 shows the mating of four adjacent grids in the calorimeter. Composite 2x2 regions are produced by pairing up adjacent 1x2 edge regions, and by grouping up quads of 1x1 corner regions. In this manner the isolated electron codes of the individual partial regions are compared against each other. The largest isolated electron code of the partial regions becomes the code for the composite 2x2 region. The reasoning for this lies in the definition of the code. A tower that contains an isolated electron at a lower threshold will appear as quiet to a higher threshold. This is demonstrated in the decoding of the ETT codes into Q/E bits for the PRAs, as shown in Figure 4. The same principle applies when combining regions. A region with a lower threshold code which is adjacent to a region with an isolated electron at a higher threshold code will appear as quiet to that region, and the higher threshold code dominates over the

composite region. Note that by assigning the non-quiet, non-electron code a value of 7, this code dominates over all isolated electron codes. This is consistent with the fact that a hadronic tower could not by definition be adjacent to a tower with an isolated electron.

Figure 13 provides some examples of partial region resolution. The resolution of partial regions is performed as a final step before matching the isolated electron codes with the the hit data from the showermax and tracking subsystems. The basic logic block for this process will be a 2-to-1, 3-bit magnitude selector. This block will act as a 2-input MAX function, to deliver the larger of two input magnitudes to the output.

7.1 Partial Grids

One noteworthy feature of the PRA design is the ability to operate on reduced size grids of ETT data, and to still produce usable output results. This feature offers significant flexibility in the mapping of towers into regions in the end-cap sections of the calorimeter. Valid partial grids are formed by biasing 2x2 groups of input tower ETT codes to the PRA to the quiet state. This has the effect of relocating the edge/corner regions (and possibly deleting old regions). With some of their towers biased to quiet, 2x2 regions which used to be completely confined become 1x2 edge or even 1x1 corner regions. These partial regions can then be treated in exactly the same matter as is described above.

Towers must be biased to quiet in 2x2 groups which fall across normal region boundaries shown in Figure 10. This rule ensures that no fully confined 2x2 regions will be adjacent to the edge of the grid. Under normal circumstances, 2x2 regions would be biased to quiet starting at one or two edges of the grid, and continuing until the desired partial grid geometry was obtained. The resulting new edge/corner regions of the reduced geometry would then be matched with similiar regions from adjacent full or partial grids.

8 Design Summary

The Isolated Electron Trigger design consists of three principal sections: the MLU section, the PRA and threshold encoder section, and the edge/corner resolution section. The scope of the design in these sections is at the one tower, grid (8x8 towers) and calorimeter (all towers) levels, respectively.

The MLU section has two types of memory lookups. The first type compares the energy content of the EMC and HAC sections of the trigger tower to produce an ETT code. The second type provides linearization and normalization and produces a 12-bit linear energy for both the EMC and HAC sections of the trigger tower. The architecture of the MLU section is flexible with respect to changes in format of both the input and output energies.

The PRA and threshold encoder section uses an ASIC to detect isolated electrons in 8x8 regions of towers referred to as grids. PRAs operate on the ETT codes generated by the MLU sections in a pipeline fashion to produce the region flag words. A

PRA is dedicated to each of the six mutually exclusive thresholds in the ETT code. Within a PRA, 49 overlapping 4x4 regions known as templates are examined using combinatorial logic to determine the presence of isolated electrons. For output, the grid is mapped into 25 regions as shown in Figure 10. Those regions fully confined on the grid are 2x2 towers in dimension, while those regions on the edges are 1x2, and the four corner regions are 1x1. Alongside the PRAs on the ETT data bus is the quiet detect logic, which examines the same 25 regions to determine which of those regions are completely quiet. The isolation results of the PRAs and the quiet detect logic output flags are encoded into a 3-bit isolated electron code for each of the 25 regions. This code indicates whether the region was completely quiet, contained an isolated electron at one of the six thresholds, or neither.

The edge/corner resolution section performs the final level of isolation checking across grid boundaries. It does this by forming composite 2x2 tower regions out of the 1x2 edge and 1x1 corner regions of the grids. The isolated electron code for these composite regions is simply the largest value from the component partial regions. The result of edge/corner resolution is a uniform group of 3-bit isolated electron codes for all 2x2 regions in the calorimeter. During the resolution the isolated electron codes for fully combined regions are propagated alongside the partial regions, so as to maintain the proper timing relationship for matching with the tracker/showermax hits.

8.1 Physical Partitioning

The SDC level 1 trigger baseline design is described in [2]. A preliminary version of the physical implementation may be found in [1].

The principal sections described above in the design summary fall neatly along possible PCB card boundaries. The first card, the "MLU card", receives the fiber-optic data for 16 trigger towers, and contains the MLUs for linearization of the energy values and generation of the ETT codes for these towers. Assuming the 16 towers represent a 4x4 region on the calorimeter, this card also contains the 12-bit adder trees for producing the bottom level of energy sums for the jet threshold and total/missing energy triggers.

The next card, the "PRA card", resides in the same crate with 4 MLU cards, which deliver their ETT codes to it over the backplane. The PRA card contains the hardware necessary to process the ETT codes into isolated electron codes for one grid. This includes the six PRA ASICs, the quiet detect logic and the electron threshold decoder logic. Through its frontpanel, the PRA card delivers the 3-bit isolated electron codes for the 25 regions (75 bits total) to the edge/corner resolution logic.

A single "Calorimeter" crate contains 8 MLU cards and 2 PRA cards. It also contains the additional standard cards, such as a processor, voltage monitor, and cards to interface to the clock, level 1, and level 2 subsystems. Finally, though not part of the isolated electron design, this crate could contain one or more instances of an "Energy Card", which continued the summation of energies for jet threshold and total/missing energy triggers.

The edge/corner recombination is performed as one of the functions of a "Match card". This card receives the tracker/showermax hit data in 2x2 trigger tower resolution

format for an 8x8 tower area. It would also receive the isolated electron codes for the corresponding area. This area, however, would be offset from the PRA grid such that it recieved from 4 separate Calorimeter crates the codes necessary to resolve all partial regions within that 8x8 area. Once the partial regions are resolved, the card proceeds with the task of matching isolated electrons with tracker/showermax hits.

In conclusion, the above partitioning scheme envisions some three card types which are wholly or partially dedicated to the isolated electron pattern logic. The scheme anticipates the tight integration of this subsystem at the circuit level with the other calorimeter triggers at one end, and with the matching logic on the other. The design utilizes a feed-forward approach starting with the fiber-optic link from the detector, through the MLU cards to the PRA cards on Calorimeter crates, and finally to the matching logic.

9 Simulation Results

9.1 Introduction

In order to simulate the performance of the electron trigger logic, 20000 Drell-Yan W, 20000 Drell-Yan Z, 120000 QCD twojet events from 20-200 GeV, and minbias events corresponding to a poisson distribution with mean 1.6 events per crossing were generated using the Monte Carlo program ISAJET. The events were integrated over three beam crossings, using a scintillator calorimeter shaping function from ZEUS. The energy deposit in the calorimeter which resulted was simulated by the program SIM3, from Greg Sullivan at the University of Chicago. The electronics as described in this document was then simulated in detail to determine how many events the proposed trigger would find. A trigger tower size of .1x.1 in η and ϕ was used for η <2, and twice that for η >2. The simulation was run on Symmetric MultiProcessor Silicon Graphics Inc. 4D/380s at the Physics Detector Simulation Facility of the SSC Laboratory.

The primary goal was to find electrons produced by W's and Z's. Figure 14 shows the HAC/EMC ratio in towers where electrons from W's and Z's deposited significant portions of their energy, plotted versus their η location. Only the events with HAC energy greater than 0.5 GeV are shown: the energy shown is "as seen by the trigger", i.e., after summing physical towers into trigger towers and converting the energies to a nonlinear scale. On the scale used, any energy of less than 0.5 GeV E_t appears as 0, and so is not shown on this plot. Thus the vast majority of electrons do not appear on this plot, since their HAC/EMC ratio is 0. This shows that the HAC/EMC ratio we can expect increases with η. Therefore, in the barrel calorimeter, or for $\eta < 1.6$, we decided that a tower meets the HAC/EMC requirement to contain an electron if its HAC/EMC ratio is less than 0.04. In the endcap calorimeter, or for $1.6 < \eta < 3$, we defined that the HAC/EMC ratio must not exceed 0.1. Figure 15 shows this ratio plotted against the E_t deposited in the EMC section of the tower. Because few background particles have very high E_t, it would be possible to loosen the ratio requirements for high E_t electrons. As the figure shows, the current simulation does not give obvious reason for doing so. Figure 16 shows the energy deposited in trigger

towers immediately adjacent to the trigger tower where a W or Z electron hit, plotted versus the η location. Again, only towers where the E_t deposited was greater than 0.5 GeV are shown, so the vast majority of towers adjacent to electrons are not shown. It seems clear that no possible cut will include all the electrons, and that the cut here must also be looser at higher η values. In the simulation, a trigger tower in the barrel region ($\eta < 1.6$) was determined to be non-quiet, non-electron if its HAC E_t was less than 1 GeV. A trigger tower in the endcap region ($1.6\eta < 3$) was determined to be non-quiet, non-electron if its HAC E_t was less than 2 GeV. Utilizing the feature described in Section 2 to insert a second quiet threshold, electrons with $E_t > 45$ GeV were allowed to be adjacent to towers with more energy in them. For this purpose, endcap towers with less than 4 GeV E_t were considered to meet the second quiet threshold requirement; in the barrel region a 2 GeV threshold was used.

In QCD twojet events which were identified by the trigger as isolated electrons under these cuts, the simulation looked for high E_t photons and electrons going into the appropriate trigger tower. Figure 17 shows the HAC/EMC ratio in towers from QCD twojet events where no high E_t electron or photon deposited its energy, but which the trigger logic identified as containing an isolated electron. This shows that further tightening of the HAC/EMC cuts would indeed result in lower background rates. The cuts chosen in this document were therefore chosen to be as tight as possible without losing many W and Z events.

Only the η <3 region of the calorimeter was simulated. Following the trigger logic design, the energies deposited in the calorimeter were first converted to an eight bit logarithmic scale. For each tower, a lookup table returned the ETT code for the tower. Then the pattern logic was done for each 8x8 region of trigger towers. The isolated electron codes were put in an array so that the region matching was automatically done. Subsequently, the threshold number for the highest transverse energy isolated electron found in the barrel and endcap were returned. It is worth noting that no communication between different regions was assumed except as noted in this document.

In order for the trigger to find an isolated electron, there must be at least one trigger tower between the electron and the edge of the calorimeter. Thus, for the trigger tower sizes used, it is only possible to find isolated electrons in the region η <2.8. ISAJET generated a cross section of $.62\times10^{-5}$ mb Drell-Yan W events which produced an electron from a W with η <2.8. Thus a trigger looking in the η <3 region of the calorimeter for electrons from W's should find no more than this cross section. In the figures following, the success at finding W events is expressed as a percentage of the W cross section which decays to electrons which have η <2.8. Thus 50% W efficiency corresponds to a cross section of $.31\times10^{-5}$ mb. For the Drell-Yan Z events, a cross section of 1.7×10^{-6} mb were Z events producing at least one electron having η <2.8. We will say that Z efficiency is our rate of success at finding these events. Events with virtual photons instead of Z's were ignored. A 50% Z efficiency corresponds to a cross section of $.86\times10^{-6}$ mb. A cross section of 1.0×10^{-6}mb corresponded to Z events generating two electrons with η <2.8. We will say that Z two-electron efficiency is our rate of success at finding these events. A 50% Z two-electron efficiency corresponds to a cross section of $.51\times10^{-6}$ mb. For the QCD background, the rates are expressed in kHz, where 1 mb corresponds to 1000 kHz at the SSC design luminosity of 10^{33} cm^{-2}

sec^{-1}.

9.2 W Efficiency

Figure 18 shows the trigger logic's success in finding W events, plotted versus the E_t of the electron from the W in the event. Only events which actually produced a W decaying into an electron with η <2.8 were taken into consideration. An event was considered successful if the trigger logic identified an electron above threshold in the calorimeter. A threshold of 20 GeV E_t was used. In this and subsequent efficiency plots in this document, variable histogram channel sizes, all multiples of 1 GeV, were chosen to assure the presence of at least 100 counts per channel. It is apparent from this plot that even at 80 GeV one electron has escaped our trigger. In fact, upon examination it was found that in a tower immediately adjacent was over 2 GeV E_t, and that there was nothing in any other surrounding towers. This event would have passed an offline trigger cut, but to pass a real trigger would have required a different algorithm. Most electrons that the trigger missed, however, were found upon examination to have deposited their energy into multiple trigger towers, and thus did not make the energy cut. A perfect trigger with a threshold of 20 GeV transverse energy would have 83.5% W efficiency. Our trigger, with threshold of 20 GeV, has 75.4% W efficiency, or, in other words, finds 90.3% of the W events it theoretically might. Of the electrons with more than 25 GeV E_t, we find 96.3%. Of those with more than 30 GeV E_t, we find 97.7%. Figure 19 shows the trigger logic's success in finding W events, plotted versus the E_t of the electron from the W in the event, for a threshold of 30 GeV E_t. A perfect trigger with a threshold of 30 GeV transverse energy would have 61.1% W efficiency. Our trigger, with threshold of 30 GeV, has 48.5% W efficiency, or, in other words, finds 79.3% of the W events it theoretically might. The efficiency rises with E_t, so that by a value of 35 GeV, the trigger finds 91.6%. Of the electrons with more than 40 GeV E_t, this trigger finds 95.4%.

The efficiency with which we find electrons varies with location in the calorimeter, as would be expected. Thus we now divide the calorimeter into two parts- the "barrel" and "endcap" regions. There is a real physical division of the calorimeter, over which information is not shared until late in the trigger process. In this simulation, we placed this division at $\eta = 1.6$, so that we had 16 trigger towers in η before the separation. We found isolated electrons bordering on this division by using the edge-checking algorithm described above, so that until a late stage of the simulation there was no information shared between the two parts. However, the logic is set up so that there is no loss in efficiency finding electrons at the boundary- instead there is an increase in the rate of false triggers there.

Below we look at how the efficiency in the two regions. Electrons found are assigned to .2x.2 $\eta - \phi$ squares in a grid covering the calorimeter. The η boundaries are at .1, .3, .5, etc. Thus the region between $\eta = 1.5$ and $\eta = 1.7$ spans the physical boundary between the endcap and barrel. If an electron deposits some of its energy in towers in this overlapping region, then it might be thought by the trigger logic to be either in the barrel or the endcap. Because of this inherent ambiguity, we defined the division as follows. When ISAJET generated a W electron with $\eta < 1.55$, we called that electron a barrel electron, and a W electron with $\eta > 1.55$ was called an endcap

electron. If a barrel electron had $\eta < 1.45$, so that it should not deposit energy into the .2 η region spanning the barrel and endcap, then we required that the trigger find an electron in a .2x.2 region where $\eta < 1.5$. If an electron had $1.45 < \eta < 1.55$, we allowed the trigger logic to find it anywhere in the calorimeter. An electron was said to be in the endcap region if it has $\eta > 1.55$. For such electrons, we required that the trigger find an isolated electron in a .2x.2 region with $\eta > 1.5$.

We now restrict our attention to the barrel section of the calorimeter. Thus we consider only W events which decay to an electron with $\eta < 1.55$. Figure 20 shows the trigger logic's success in finding W events in the barrel region, plotted versus the E_t of the electron from the W in the event. An event was considered successful if the trigger logic identified an electron above threshold in the barrel calorimeter. A threshold of 20 GeV E_t was used. A perfect trigger which looked for electrons only in the barrel region with a threshold of 20 GeV E_t would have 47.2% W efficiency. In the barrel region our trigger, with threshold of 20 GeV, has 43.4% W efficiency, or, in other words, finds 92.0% of the W events it theoretically might. Of the electrons with more than 25 GeV E_t, this trigger finds 97.4%. Of the electrons with more than 30 GeV E_t, the trigger finds 98.3%. Figure 21 shows the trigger logic's success in finding W events, plotted versus the E_t of the electron from the W in the event, for a 30 GeV E_t threshold. A perfect trigger which looked for electrons only in the barrel region with a threshold of 30 GeV transverse energy would have 34.6% W efficiency. In the barrel region our trigger, with threshold of 30 GeV, has 28.5% W efficiency, or, in other words, finds 82.3% of the W events it theoretically might. Of the electrons with more than 35 GeV E_t, the trigger finds 93.6%. At the 30 GeV threshold, the trigger finds 96.3% of W electrons exceeding 40 GeV E_t.

We now restrict our attention to the endcap section of the calorimeter. Thus we consider only W events which deacy to an electron with $1.55 < \eta < 2.8$. Figure 22 shows the trigger logic's success in finding W events in the endcap region, plotted versus the E_t of the electron from the W in the event. An event was considered successful if the trigger logic identified an electron above threshold in the endcap calorimeter. A threshold of 20 GeV E_t was used. A perfect trigger which looked for electrons only in the endcap region with a threshold of 20 GeV E_t would have 36.3% W efficiency. In the endcap region our trigger, with threshold of 20 GeV, has 31.9% W efficiency, or, in other words, finds 88.0% of the W events it theoretically might. Of the electrons with more than 25 GeV E_t in the endcap, we find 94.8%. Of the electrons with more than 30 GeV E_t, the trigger finds 96.8%. Figure 23 shows the trigger logic's success in finding W events, plotted versus the E_t of the electron from the W in the event, for a 30 GeV E_t threshold. A perfect trigger which looked for electrons only in the endcap region with a threshold of 30 GeV transverse energy would have 26.6% W efficiency. In the endcap region our trigger, with threshold of 30 GeV, has 20.0% W efficiency, or, in other words, finds 75.4% of the W events it theoretically might. Of the electrons with more than 35 GeV E_t which it might find, this trigger finds 89.0%. Of the electrons with more than 40 GeV E_t which it might find, this trigger finds 94.1%.

The primary reason for the slow turn-on in efficiency of the trigger is that the energy cut used by the trigger is the energy in one trigger tower. Thus the trigger underestimates the energy of an electron which splits its energy between towers. Also, in

the endcap the curve never reaches 100% efficiency because some of the events do not meet the isolation criteria.

9.3 Z Efficiency

We now examine our success in finding Z events in the calorimeter. Figure 24 shows the trigger logic's success in finding Z events, plotted versus the E_t of the electron from the Z in the event. Only events which actually produced a Z decaying into an electron with η <2.8 were taken into consideration. An event was considered successful if the trigger logic identified an electron above threshold in the calorimeter. A threshold of 20 GeV E_t was used. The plot shows that, for instance, one very high E_t electron was missed. In fact, further investigation showed it to be a 235 GeV E_t electron at $\eta = 2.6$, and that it deposited 25 GeV E_t in the HAC and less than 200 GeV E_t in the EMC, thus missing the cut. Thus, it would not have passed an offline trigger which required an EMC/HAC ratio of 10, though physically it was indeed an isolated electron. A perfect trigger with a threshold of 20 GeV transverse energy would have 88.4% Z efficiency. Our trigger, with threshold of 20 GeV, has 83.8% Z efficiency, or, in other words, finds 94.8% of the Z events it theoretically might. Of the events with electrons of more than 25 GeV E_t which it might find, this trigger finds 98.5%. Of the events with electrons of more than 30 GeV E_t which it might find, this trigger finds 99.3%. Figure 25 shows the trigger logic's success in finding Z events, plotted versus the E_t of the electron from the Z in the event, for a 30 GeV E_t threshold. A perfect trigger with a threshold of 30 GeV transverse energy would have 73.8% Z efficiency. Our trigger, with threshold of 30 GeV, has 66.0% Z efficiency, or, in other words, finds 89.5% of the Z events it theoretically might. Of the events with electrons of more than 35 GeV E_t which it might find, this trigger finds 96.8%. Of the events with electrons of more than 35 GeV E_t which it might find, this trigger finds 98.2%.

Figure 26 shows our success rate in finding both electrons from a Z which sends two electrons into the $\eta < 2.8$ region of the calorimeter, versus the E_t of the lower energy electron of the pair. With an E_t threshold of 14 GeV, a perfect trigger would have 94.9% Z two-electron efficiency. Our trigger, with a threshold of 14 GeV, finds both electrons from Z's in 94.6% of the events in which it is possible to do so, giving us a Z two-electron efficiency of 90.1%. Of the events with two electrons over 17 GeV E_t, we find both electrons in 97.3%. Of the events producing two electrons over 20 GeV E_t, we find both in 98.1%.

9.4 Comparison with Offline Trigger

The above-described figures show how well the trigger finds isolated electrons which are actually physically existent. We now consider how well it finds isolated electromagnetic particles which an offline trigger actually would find; i.e., we describe the performance of our trigger in finding events which a theoretical trigger with perfect calorimeter information would find.

We now define the offline trigger we used. A group of 1-4 trigger towers all with a common vertex shall be called a cluster. When we look for an isolated electron, a

trigger tower shall be in the cluster if it contains at least 2 GeV E_t EMC energy. A trigger tower cluster passes the offline trigger if it passes a HAC/EMC ratio cut and an isolation ratio cut. The HAC/EMC ratio is simply the HAC energy deposited in the trigger tower cluster divided by the EMC energy deposited in the trigger tower cluster. The isolation ratio is the total energy deposited in the towers adjacent to the cluster, divided by the EMC energy deposited in the cluster. Two cases will be considered- a "loose" cut, where both ratios are required to be above .1, and a "tight" cut, with both ratios required to be above .04. The tight cut was chosen to approximately match the cuts used in the simulation of the proposed trigger.

In the following figures, the procedure was as follows:

1. If an electron or a photon produced by a Drell-Yan event (or an accompanying minbias event) deposited 5 GeV or greater E_t in the calorimeter, then we considered the trigger tower in which it deposited the most energy. This tower was the "primary" tower.
2. If a tower adjacent to the primary tower had 2 GeV or greater E_t in its EMC, then it was added to the cluster.
3. All towers in a cluster were required to touch at some vertex- if not, the cluster was not allowed.
4. If the trigger tower cluster passed the offline trigger, then it was assigned an E_t value equal to its EMC E_t.
5. If the isolated electron logic, using a given threshold, found an electron in the .2x.2 area in which the primary trigger tower lay, then it was considered successful.
6. The ratio of the number of particles found by both the isolated electron logic and the offline trigger was divided by the total number of particles passing the offline trigger. The result was plotted as a function of the E_t value assigned in step 4.

This procedure was done using the trigger tower sizes of .05x.05, .1x.1, and .15x.15. We restricted our attention to events which could be isolated inside the $\eta < 2$ region of the calorimeter. This restriction was made to simplify the offline trigger algorithm, which otherwise would have had to operate over the change in tower size at $\eta = 2$. Figure 27 shows our trigger logic's success, using a 20 GeV threshold, in finding electrons from Drell-Yan events which passed the offline trigger with a tower size of .05 and loose cuts. We see that the W electron with E_t of 80 GeV mentioned before as being missed, does pass the loose offline trigger. Also, we note that though the trigger very quickly achieves about 93% efficiency on these events, it does not quite ever achieve 100% efficiency. The actual efficiency for events with $E_t > 30$ GeV was 98%, and for events with $E_t > 40$ GeV was 99.2%. In Figure 28, which shows our trigger logic's success with events passing the offline trigger on a trigger tower size of .10, is not very different. If we add towers together to form trigger towers of .15x.15, we get a similar curve, as shown in Figure 29. This seems to indicate that the Drell-Yan electrons which are isolated with a given tower size are very well isolated. Figure 30 shows our trigger logic's success, using a 20 GeV threshold, in finding particles from Drell-Yan events which passed the offline trigger with a tower size of .05 and tight

cuts. Here we see little difference from Figure 28, suggesting that the ratios chosen for the cuts do not make a large difference for Drell-Yan electrons. Figure 31 shows our trigger logic's success in finding particles from Drell-Yan events which passed the offline trigger with a tower size of .10 and tight cuts. This cut is the closest to our actual trigger cuts, but again the performance is roughly the same. Finally, Figure 32 shows our trigger logic's success in finding particles from Drell-Yan events which passed the offline trigger with a tower size of .15 and tight cuts.

The conclusion drawn from the above seems to be that, for Drell-Yan events, and thus presumably for W's and Z's in general, the trigger performance is roughly the same for almost any offline trigger. On the other hand, in addition to finding electrons from W's and Z's, we may be interested in finding isolated photons and electrons from other particles. Also, we considered how the performance versus an offline cut might be with particles not so naturally isolated as those produced by Drell-Yan events. Thus we considered the efficiency with which our trigger found electromagnetic particles from QCD twojet events which passed the offline trigger. Figure 33 shows our trigger logic's success, using a 20 GeV threshold, in finding particles from QCD events which passed the offline trigger with a tower size of .05 and loose cuts. Despit the bad statistics, it is apparent that the trigger does not nearly so well here as with Drell-Yan events; never indeed does it become three-quarters efficient. This signifies not only that for such electrons the trigger could not be well-duplicated by such an offline trigger, but that many background events would pass this offline trigger that this proposed version rejects. Figure 34 shows the trigger logic's success in finding particles from QCD events which passed the offline trigger with a tower size of .10 and loose cuts. Here, though it never becomes fully efficient, the turn-on is much faster, indicating that much of the energy resolution difficulty apparent in Figure 33 is due to our summing of four physical towers to create larger trigger towers. Figure 35 shows our trigger logic's success in finding particles from QCD events which passed the offline trigger with a tower size of .15 and loose cuts. Here, while the turn-on suffers compared to the .10 case, the eventual efficiency reached is higher, indicating that a greater degree of isolation makes it easier for our trigger to find particles. Figure 36 shows our trigger logic's success, using a 20 GeV threshold, in finding particles from QCD events which passed the offline trigger with a tower size of .05 and tight cuts. Here, though the turn-on is very slow, the efficiency does eventually reach 95%. Figure 37 shows our trigger logic's success in finding particles from QCD events which passed the offline trigger with a tower size of .10 and tight cuts. The turn-on here is improved over the .05 case (Figure 36), and this case is the offline trigger which ought to be closest to the cuts used in our simulation. Figure 38 shows our trigger logic's success in finding particles from QCD events which passed the offline trigger with a tower size of .15 and tight cuts. We conclude that while many different cuts will result in roughly the same efficiency for nicely isolated electrons, such as those from W's and Z's, it is more difficult to say exactly how different trigger algorithms will deal with arbitrary electrons and photons. However, the proposed trigger does seem to bear a certain resemblance to the offline trigger described, with appropriate cuts.

9.5 Background Rates

We now consider the background rates from QCD twojet events for various combinations of thresholds in the barrel and endcap calorimeters. For this purpose we consider triggers in the .2 η regions beyond 1.5 to be in the endcap. Figure 39 shows the QCD background rate plotted against W efficiency (as defined above) over the whole $\eta < 3$ calorimeter, for various combinations of thresholds. The points plotted are the results from combinations of thresholds for which no other single combination gave both a lower rate and higher efficiency. We see that 50% W efficiency is achieved with a background rate of 1.9 kHz. This is achieved with a threshold of 30 GeV in the barrel and 28 GeV in the endcap. Note that this is without any track matching. Figure 40 shows the QCD background rate plotted versus W efficiency, requiring that a 10 GeV or greater p_t track point to an η value consistent with the .2x.2 region in which the trigger finds a particle. This makes no attempt to realistically simulate the tracking system, but rather simply assumes the tracker finds all particles with some error in momentum measurement. So long as an ideal tracker is used, there is no improvement in using the shower max detector, so no results with it are presented here. This figure shows that we achieve 50% W efficiency with a QCD background of 0.9 kHz, using 26 GeV and 32 GeV E_t thresholds in the barrel and endcap regions respectively. Figure 41 shows the QCD background rate plotted against Z efficiency (as defined above) over the whole $\eta < 3$ calorimeter, for various combinations of thresholds. We see that 50% Z efficiency is achieved with a background rate of 0.7 kHz. This is achieved with a threshold of 40 GeV in the barrel and 34 GeV in the endcap. Figure 42 shows the QCD background rate ploted versus Z efficiency, requiring that a 10 GeV or greater p_t track point to an η value consistent with the .2x.2 region in which the trigger finds a particle. This figure shows that we achieve 50% Z efficiency with a QCD background of 0.4 kHz, using 38 GeV and 36 GeV E_t thresholds in the barrel and endcap regions respectively.

In Figure 43, we show the background rate if we require that an event have two electrons above a given threshold, versus our efficiency at getting both electrons from a Z event (Z two-electron efficiency). Here we achieve 91% Z two-electron efficiency with a background rate of 6 Hz by using a uniform thresholds of 14 GeV E_t over the entire calorimeter. In Figure 44, we in addition require tracks of 10 GeV p_t, and find that we achieve 96% efficiency with a background rate of about 10 Hz, using a threshold of just 8 GeV E_t everywhere. Of course, the statistics here are quite bad.

We now restrict our attention to the barrel region, or to $\eta < 1.5$. When considering a portion of the calorimeter, W efficiency is expressed as a fraction of the total W's that might be found in the whole calorimeter. Thus, W efficiency for a pair of thresholds can be approximately found by adding together their W efficiencies in the two parts of the calorimeter. Figure 45 shows the QCD background rate plotted against the threshold in the barrel region. This plot is roughly comparable to Figure 3 in [3], which describes the performance of an ideal trigger in the central region. Shown are points for:

- A trigger which just required that there be a tower with EMC E_t over threshold.
- A trigger which required that a tower with HAC/EMC ratio $< .04$ be over threshold. This was done by just requiring there be a tower with an appropriate

ETT code.

- The isolated electron logic described in this document.
- The isolated electron logic, together with a 10 GeV track.

Figure 46 shows the QCD rate versus W efficiency in the barrel region for the isolated electron logic with and without tracking. Naturally, for very low threshold values, some electrons from W's do not meet the tracking requirements. Figure 47 shows the QCD rate versus E_t threshold in the endcap region ($\eta > 1.5$) for the isolated electron logic. Figure 48 shows the QCD rate versus W efficiency in the endcap region for the isolated electron logic.

We now summarize the effect of using the perfect tracker on rates. First, we consider the effect on the rates in the entire calorimeter. However, the tracker is used only in the barrel region. Without the tracker, in order to achieve 68% W efficiency, a background rate of 5.2 kHz is needed. With the tracker, the rate is down to 2.4 kHz to get 68% efficiency. Considered another way, what W efficiency can we achieve with a background rate of below 2 kHz? Without the tracker, we can get 51% W efficiency with a background rate of 1.9 kHz. With the tracker, we achieve 63% W efficiency with a background rate of 1.75 kHz. With respect to Z efficiency, Without the tracker, in order to achieve 80% Z efficiency, a background rate of 4.8 kHz is needed. With the tracker, the rate is down to 2.7 kHz to get 80% Z efficiency. What Z efficiency can we achieve with a background rate of below 2 kHz? Without the tracker, we can get 68% Z efficiency with a background rate of 1.9 kHz. With the tracker, we achieve 75% W efficiency with a background rate of 2.0 kHz.

If we consider only the barrel region, where the tracker actually operates, we get the following. In order to achieve 36% W efficiency looking only in the barrel region, we take a rate of 2.6 kHz without the tracker. However, with the tracker we achieve 36% W efficiency from just the barrel with a rate of 0.6 kHz. This is 64% efficiency for the electrons from W's that enter the barrel. In order to achieve a background rate in the barrel of below 1.5 kHz, without the tracker, we can get 30% W efficiency in the barrel. This is 53% efficiency for the electrons from W's that enter the barrel. With the tracker, we achieve 45% W efficiency with a background rate of 1.5 kHz. This is 80% efficiency for the electrons from W's that enter the barrel.

9.6 Second-Level Trigger Implications

In many Z events we find two electrons. For such events we can reconstruct the invariant mass of the Z. If we do so, using only the .2x.2 locations of the electrons found, and the EMC energy deposit in the highest trigger tower in the .2x.2 region (values easily available to the second-level trigger), the reconstructed invariant mass of Z particles is shown in Figure 49. Currently, the statistics are insufficient to determine whether the Z cross-section can be separated from background with this information.

9.7 Source Code Availability

Inquiries about the code used in this simulation should be E-mailed to:
temple@pdsf.ssc.gov or temple@wishep.physics.wisc.edu.

References

[1] T. Gorski, J. Lackey, W.H. Smith, *Level 1 Trigger Decision Design for the SDC*, SDC Note SDC-91-00088, 1991.

[2] W. H. Smith, T. Gorski, J. Lackey, *SDC Trigger Preliminary Conceptual Design*, SDC Note SDC-91-00090, 1991.

[3] A. Lankford, et al., *Conceptual Design of the SDC Trigger from the SDC Trigger Group*, SDC note SDC-91-00098, 1991.

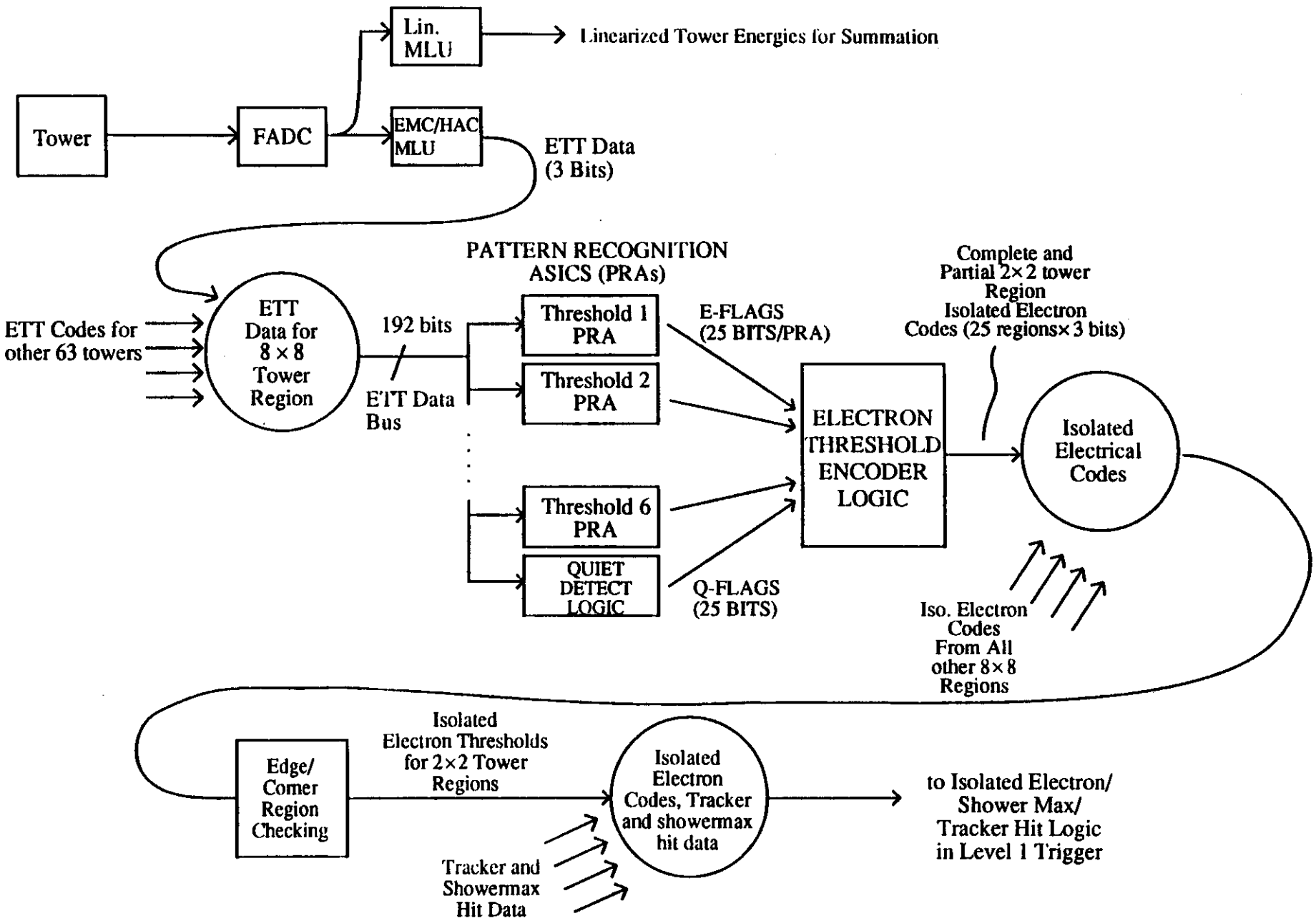

Figure 1. Hardware Block Diagram

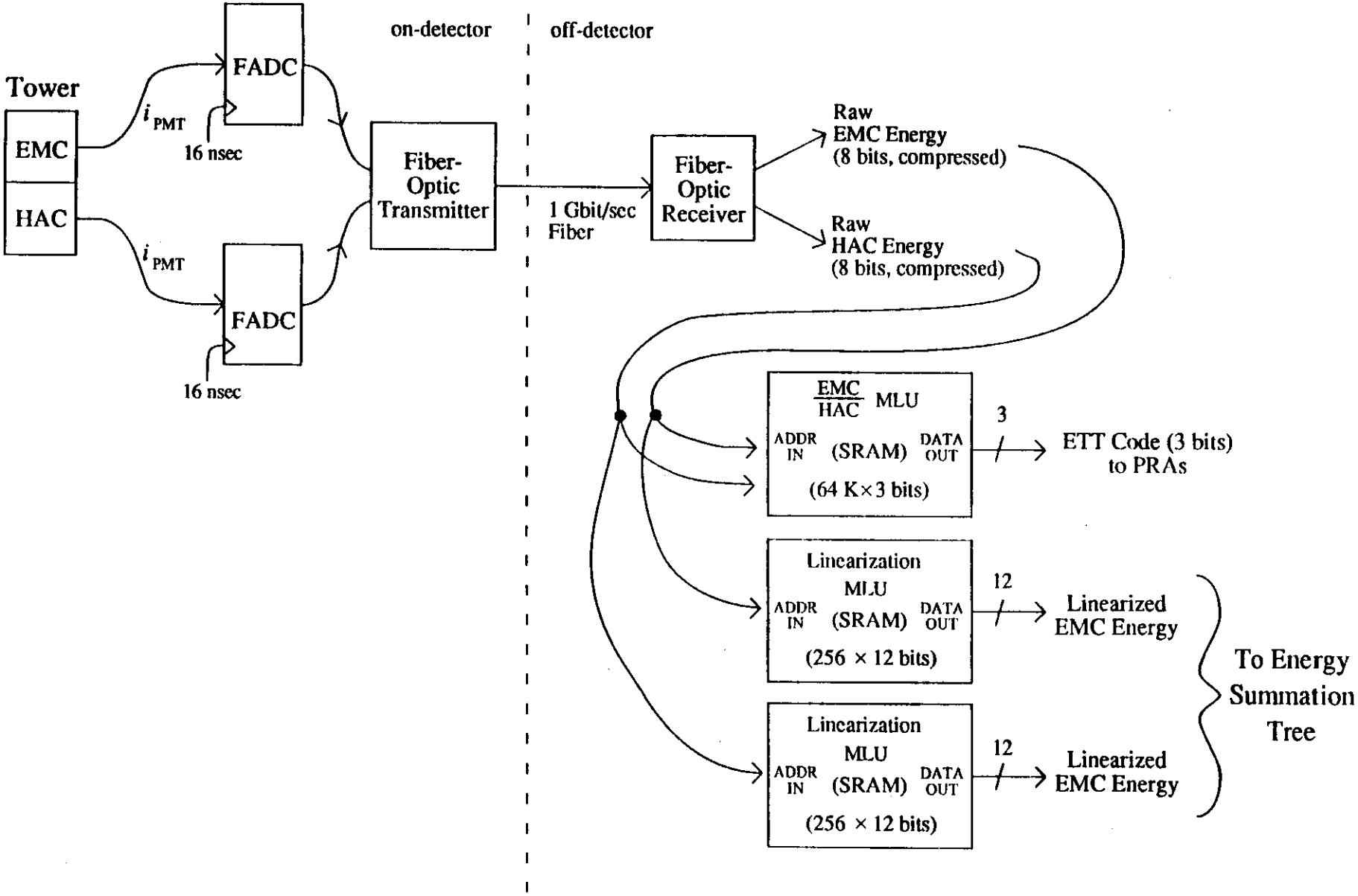

Figure 2. Memory Lookup Table Architecture

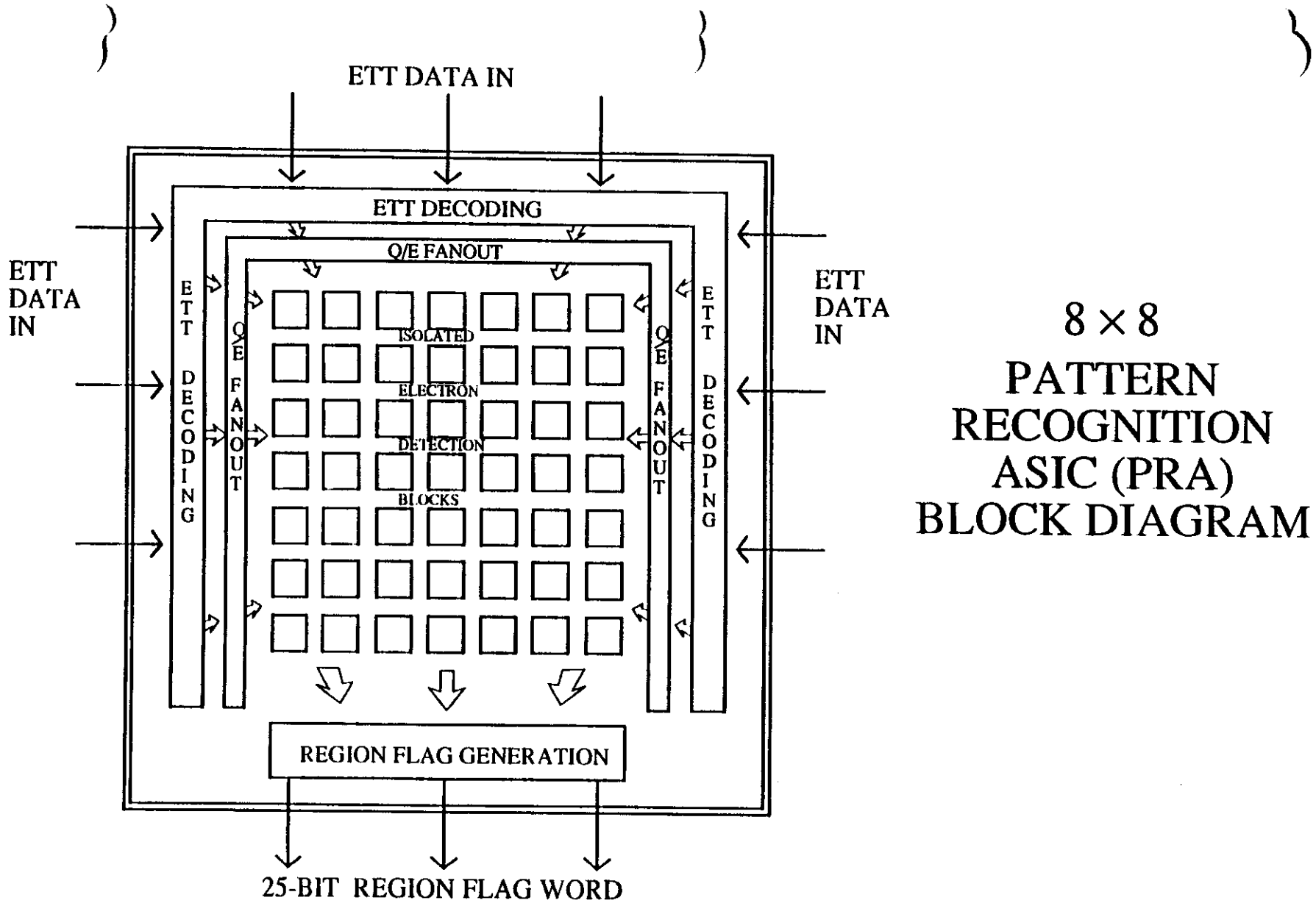

Figure 3. PRA Block Diagram

Tower ETT Code

Selected Threshold \ Q/E	0	1	2	3	4	5	6	7
1	Q	E	—	—	—	—	—	—
2	Q	Q	E	—	—	—	—	—
3	Q	Q	Q	E	—	—	—	—
4	Q	Q	Q	Q	E	—	—	—
5	Q	Q	Q	Q	Q	E	—	—
6	Q	Q	Q	Q	Q	Q	E	—

Figure 4. Decoding of ETT Codes to Q/E bits at all thresholds

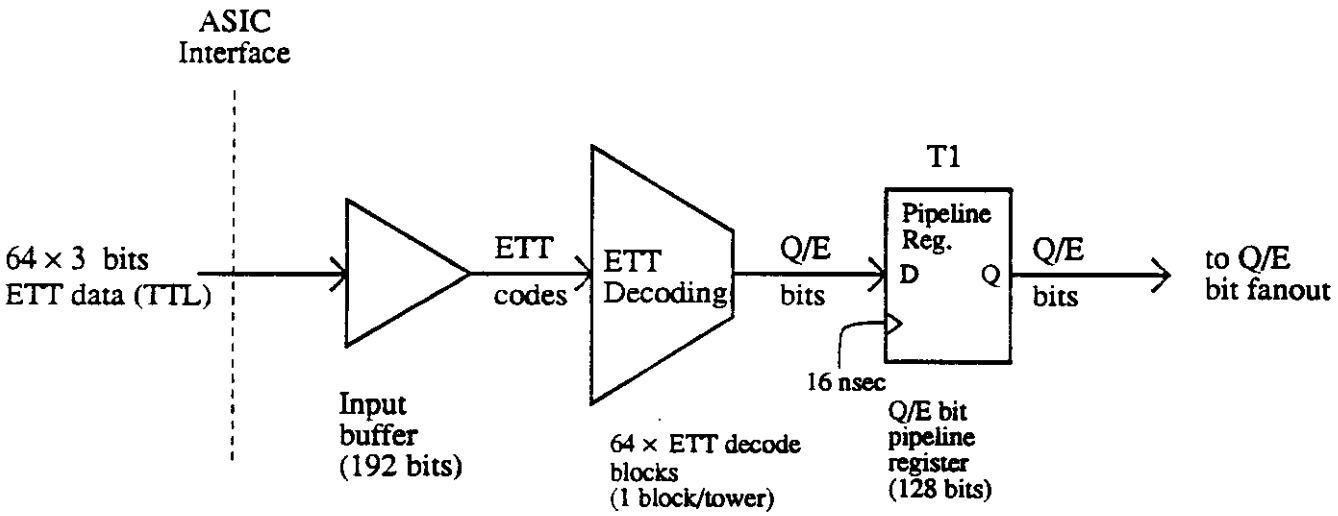

Figure 5. Block Diagram of
ETT Decoding Section of PRA

Q	Q	Q	Q
Q	E	E	Q
Q	E	Q	Q
Q	Q	Q	X

Q	Q	Q	Q
Q	E	E	Q
Q	Q	Q	Q
X	X	X	X

X	Q	Q	Q
Q	Q	E	Q
Q	E	Q	Q
Q	Q	Q	X

Q	Q	Q	X
Q	E	Q	X
Q	E	Q	X
Q	Q	Q	X

Q	Q	Q	X
Q	E	Q	X
Q	Q	Q	X
X	X	X	X

Q	Q	Q	Q
Q	E	E	Q
Q	E	E	Q
Q	Q	Q	Q

Figure 6: Examples of Isolated Electrons.
"X" denotes towers for which state is a "don't care."

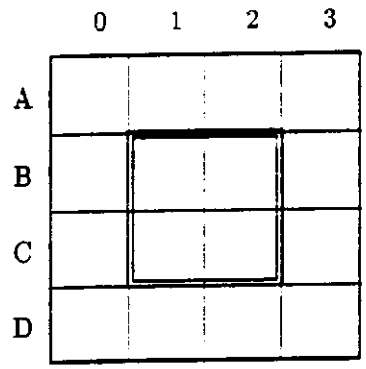

Blank Template Showing Inner 2x2 Region.
Active E bits must be found in the inner 2x2 region, completely surrounded by Q bits.

Evaluation Function:

Definition: F is TRUE if the template contains an isolated electron centered within the inner 2x2 region.

$F = C_1 \cdot C_2 \cdot C_3 \cdot C_4 \cdot \overline{D} \cdot \overline{N}$, where:

$$\begin{aligned}
C_1 &= (Q_{A0} \cdot Q_{A1} \cdot Q_{B0}) + (\overline{E_{B1}} \cdot Q_{A1} \cdot Q_{B0}) + (\overline{E_{B1}} \cdot Q_{A1} \cdot \overline{E_{C1}}) + \\
&\quad (\overline{E_{B1}} \cdot Q_{B0} \cdot \overline{E_{B2}}) + (\overline{E_{B1}} \cdot \overline{E_{B2}} \cdot \overline{E_{C1}}) \\
C_2 &= (Q_{D0} \cdot Q_{D1} \cdot Q_{C0}) + (\overline{E_{C1}} \cdot Q_{D1} \cdot Q_{C0}) + (\overline{E_{C1}} \cdot Q_{D1} \cdot \overline{E_{B1}}) + \\
&\quad (\overline{E_{C1}} \cdot Q_{C0} \cdot \overline{E_{C2}}) + (\overline{E_{C1}} \cdot \overline{E_{C2}} \cdot \overline{E_{B1}}) \\
C_3 &= (Q_{D3} \cdot Q_{D2} \cdot Q_{C3}) + (\overline{E_{C2}} \cdot Q_{D2} \cdot Q_{C3}) + (\overline{E_{C2}} \cdot Q_{D2} \cdot \overline{E_{B2}}) + \\
&\quad (\overline{E_{C2}} \cdot Q_{C3} \cdot \overline{E_{C1}}) + (\overline{E_{C2}} \cdot \overline{E_{C1}} \cdot \overline{E_{B2}}) \\
C_4 &= (Q_{A3} \cdot Q_{A2} \cdot Q_{B3}) + (\overline{E_{B2}} \cdot Q_{A2} \cdot Q_{B3}) + (\overline{E_{B2}} \cdot Q_{A2} \cdot \overline{E_{C2}}) + \\
&\quad (\overline{E_{B2}} \cdot Q_{B3} \cdot \overline{E_{B1}}) + (\overline{E_{B2}} \cdot \overline{E_{B1}} \cdot \overline{E_{C2}}) \\
D &= (Q_{B1} \cdot Q_{C1} \cdot \overline{BOTTOM}) + (Q_{B1} \cdot Q_{B2} \cdot \overline{RIGHT}) + (Q_{B1} \cdot Q_{B2} \cdot Q_{C1} \cdot Q_{C2}) \\
N &= (\overline{E_{B1}} \cdot \overline{Q_{B1}}) + (\overline{E_{B2}} \cdot \overline{Q_{B2}}) + (\overline{E_{C1}} \cdot \overline{Q_{C1}}) + (\overline{E_{C2}} \cdot \overline{Q_{C2}})
\end{aligned}$$

Figure 7: Evaluation Function Definition.
Note special conditions on the D subfunction for templates on the bottom and right edges of the grid.

	0	1	2	3
A	X	Q	Q	Q
B	Q	Q	**E**	Q
C	Q	E	Q	Q
D	Q	Q	Q	Q

Column 3 and Row D off-grid, assumed quiet

	0	1	2	3
A	Q	Q	Q	Q
B	Q	E	Q	Q
C	Q	**E**	Q	Q
D	Q	Q	Q	Q

Bottom, Right Edge Template Examples

	0	1	2	3
A	Q	Q	Q	X
B	Q	**E**	Q	X
C	Q	E	Q	X
D	Q	Q	Q	X

	0	1	2	3
A	X	Q	Q	Q
B	Q	Q	E	Q
C	Q	**E**	Q	Q
D	Q	Q	Q	X

Non-Right, Non-Bottom Edge Template Examples

	0	1	2	3
A	Q	Q	Q	X
B	Q	E	Q	X
C	Q	**E**	Q	X
D	Q	Q	Q	Q

— Row D off-grid, assumed quiet

Bottom, Non-Right Edge Example

	0	1	2	3
A	Q	Q	Q	Q
B	Q	E	**E**	Q
C	Q	Q	Q	Q
D	X	X	X	Q

Column 3 off-grid, assumed quiet

Right, Non-Bottom Edge Example

Figure 8. Examples of Isolated Electron Assignments to Towers. Isolated Electrons are assigned to Towers with bold outline.

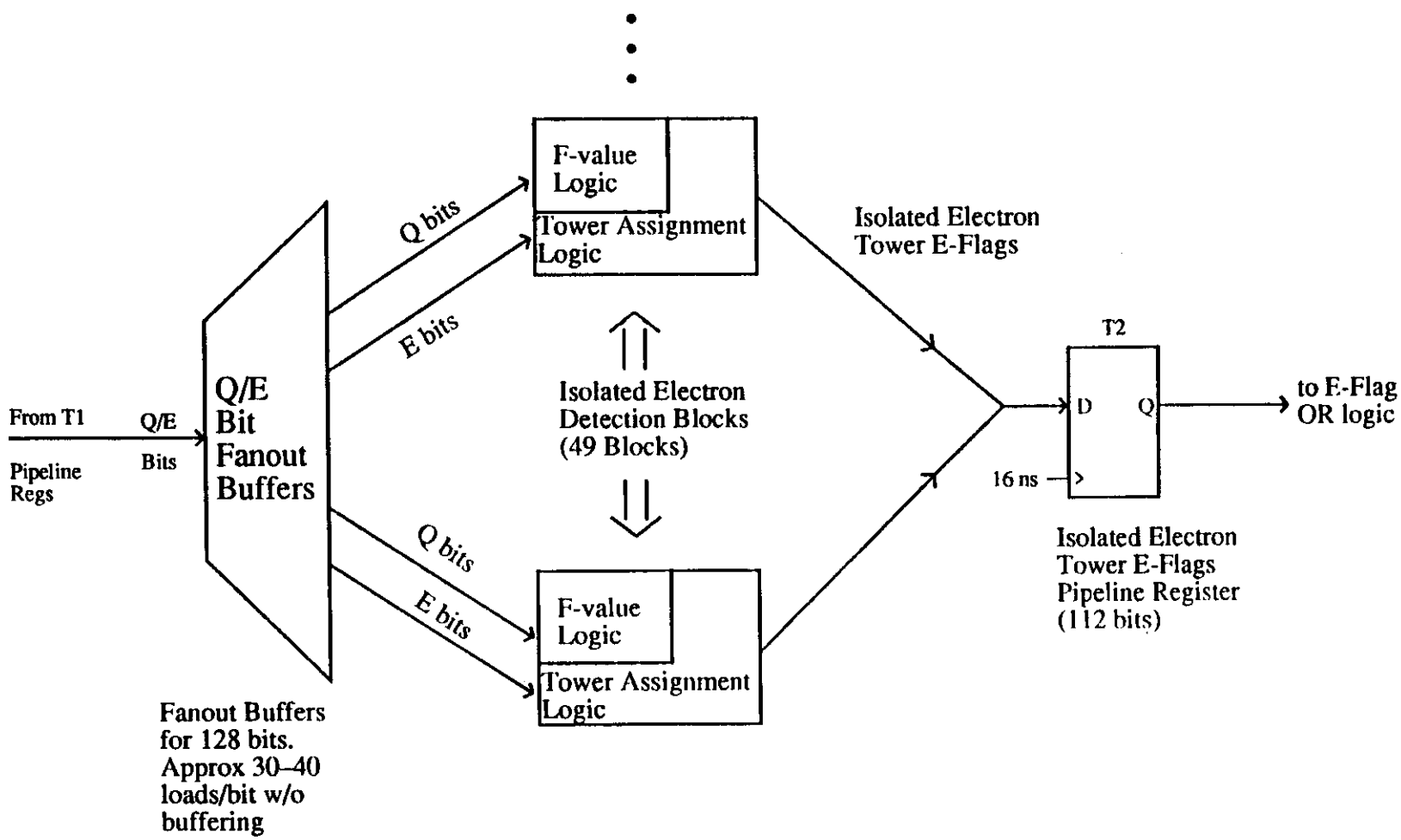

Figure 9. Block Diagram of Isolated Electron Block Section of PRA.

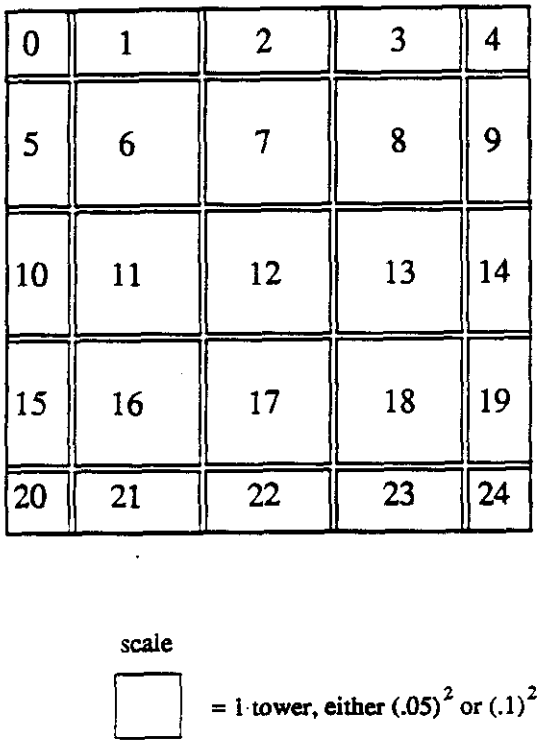

Bit#	Description	
0	Region 0	E-Flag
1	Region 1	E-Flag
2	Region 2	E-Flag
3	Region 3	E-Flag
4	Region 4	E-Flag
5	Region 5	E-Flag
6	Region 6	E-Flag
7	Region 7	E-Flag
8	Region 8	E-Flag
9	Region 9	E-Flag
10	Region 10	E-Flag
11	Region 11	E-Flag
12	Region 12	E-Flag
13	Region 13	E-Flag
14	Region 14	E-Flag
15	Region 15	E-Flag
16	Region 16	E-Flag
17	Region 17	E-Flag
18	Region 18	E-Flag
19	Region 19	E-Flag
20	Region 20	E-Flag
21	Region 21	E-Flag
22	Region 22	E-Flag
23	Region 23	E-Flag
24	Region 24	E-Flag

Figure 10. Region Flag Word Definition

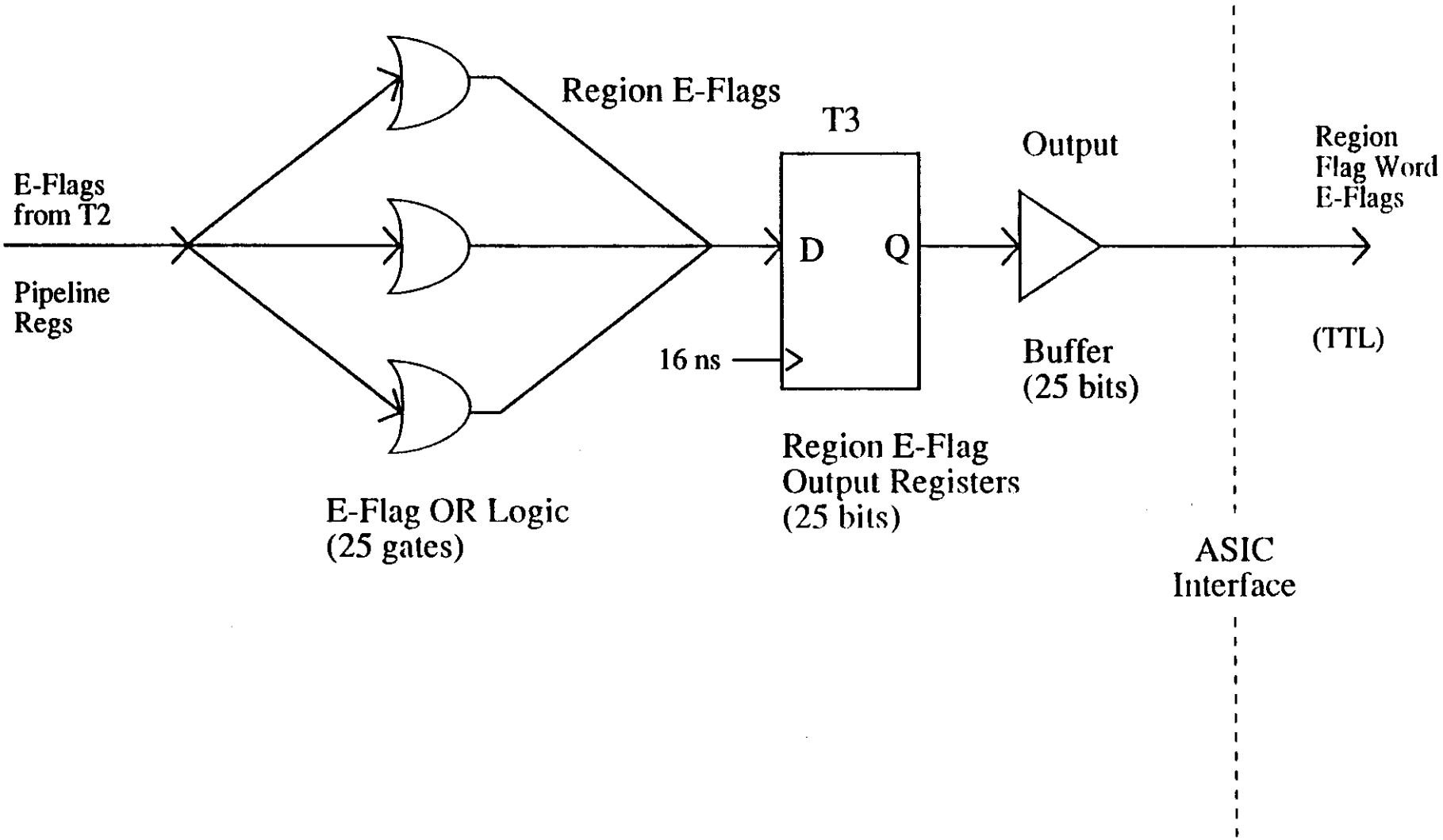

Figure 11. Block Diagram of Region Flag Word Section of PRA

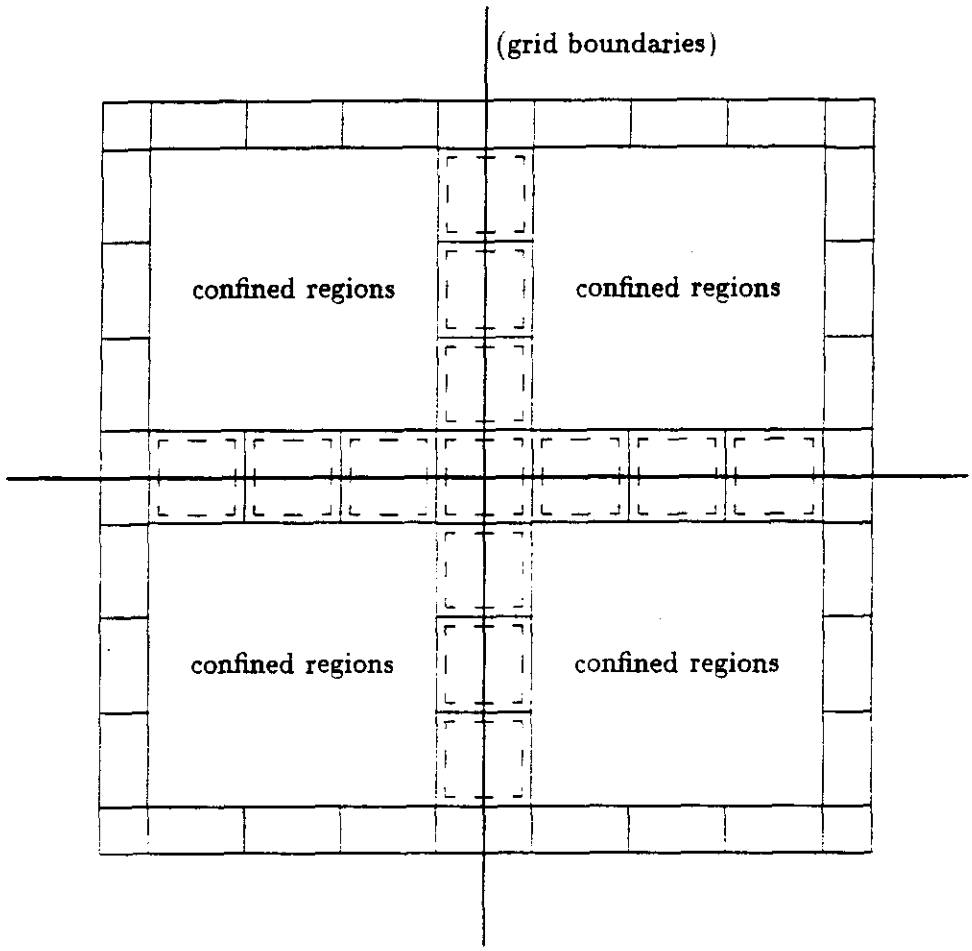

Figure 12: Four Adjacent Grids showing formation of 2x2 composite regions from edge and corner partial regions.

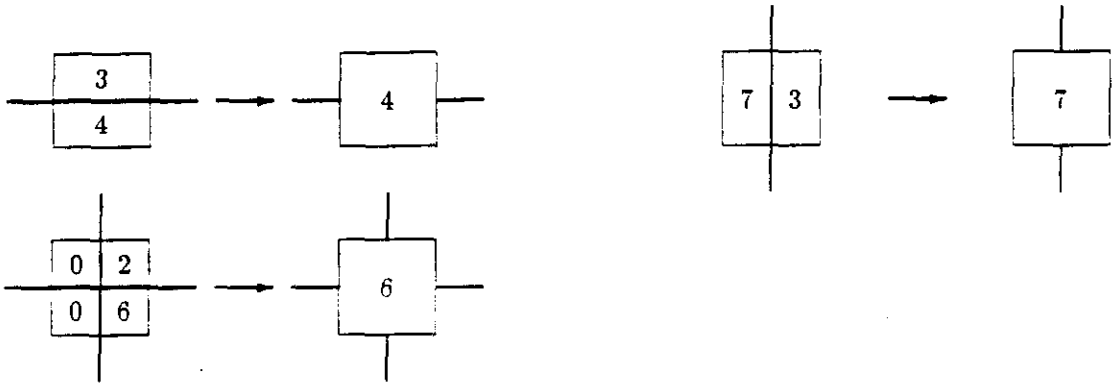

Figure 13: Examples of Partial Region Resolution
Largest subregion isolated electron code becomes the code for the composite region.

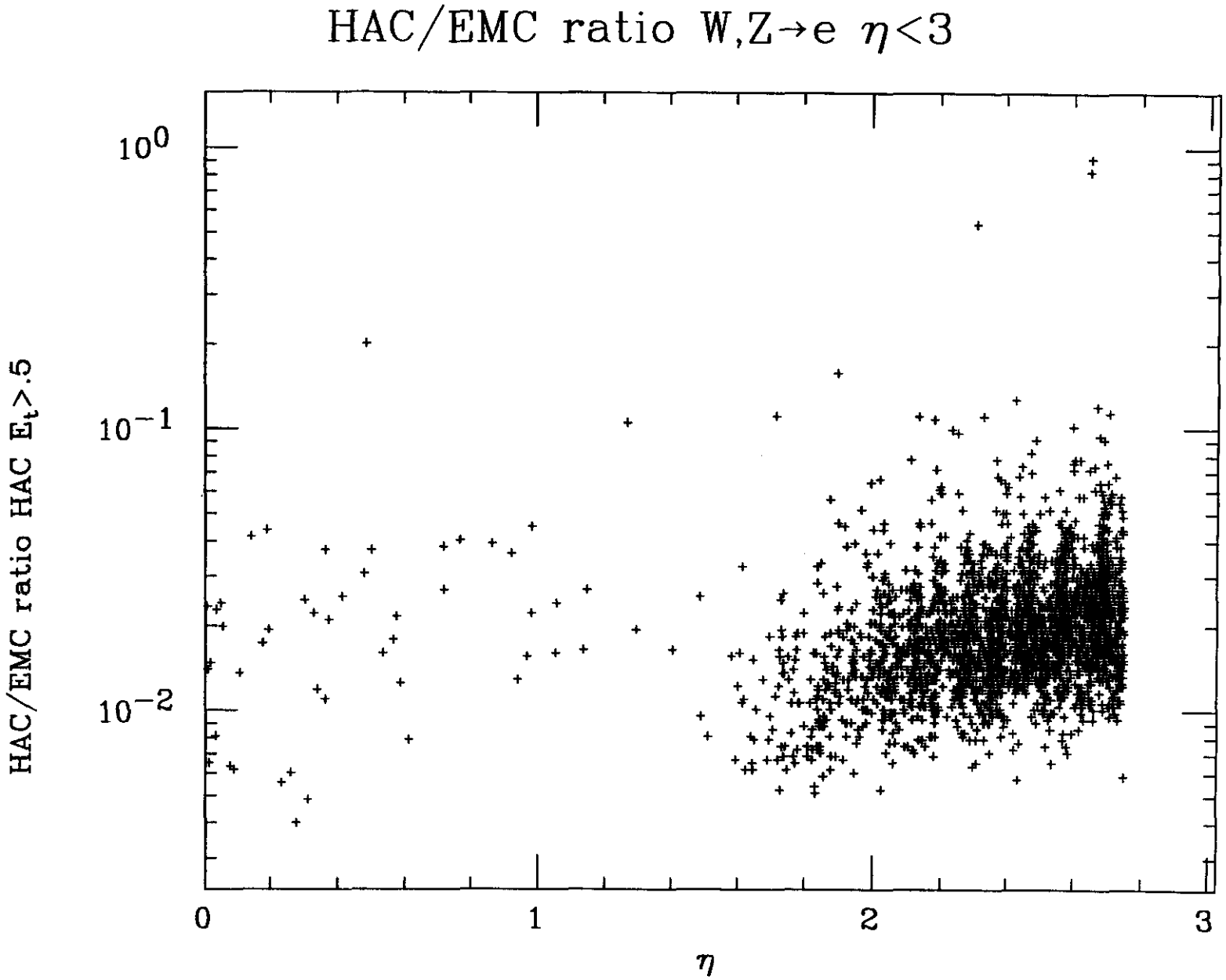

Figure 14

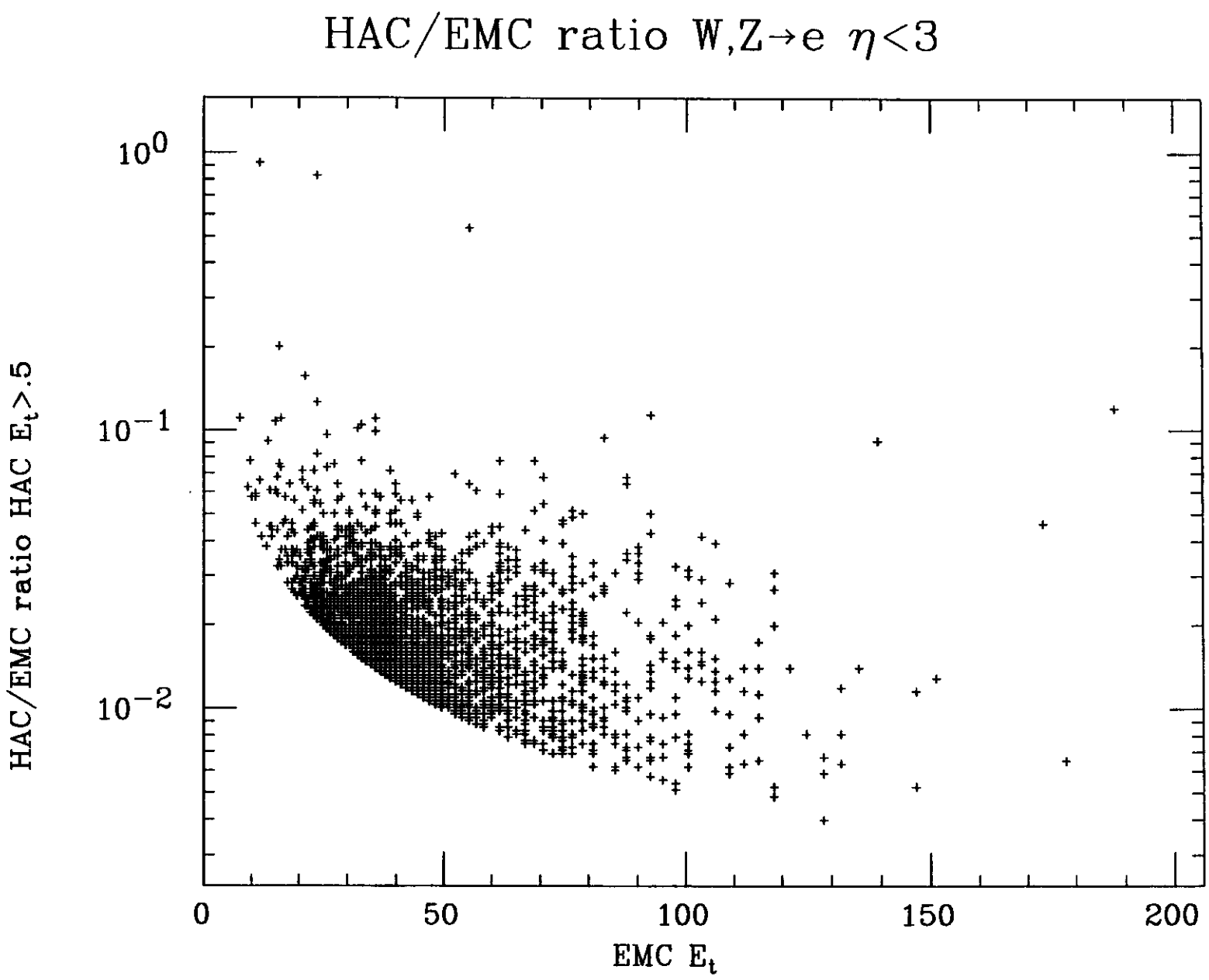
HAC/EMC ratio W,Z→e η<3
HAC/EMC ratio HAC E_t>.5
10^0
10^-1
10^-2
0
50
100
150
200
EMC E_t

Figure 15

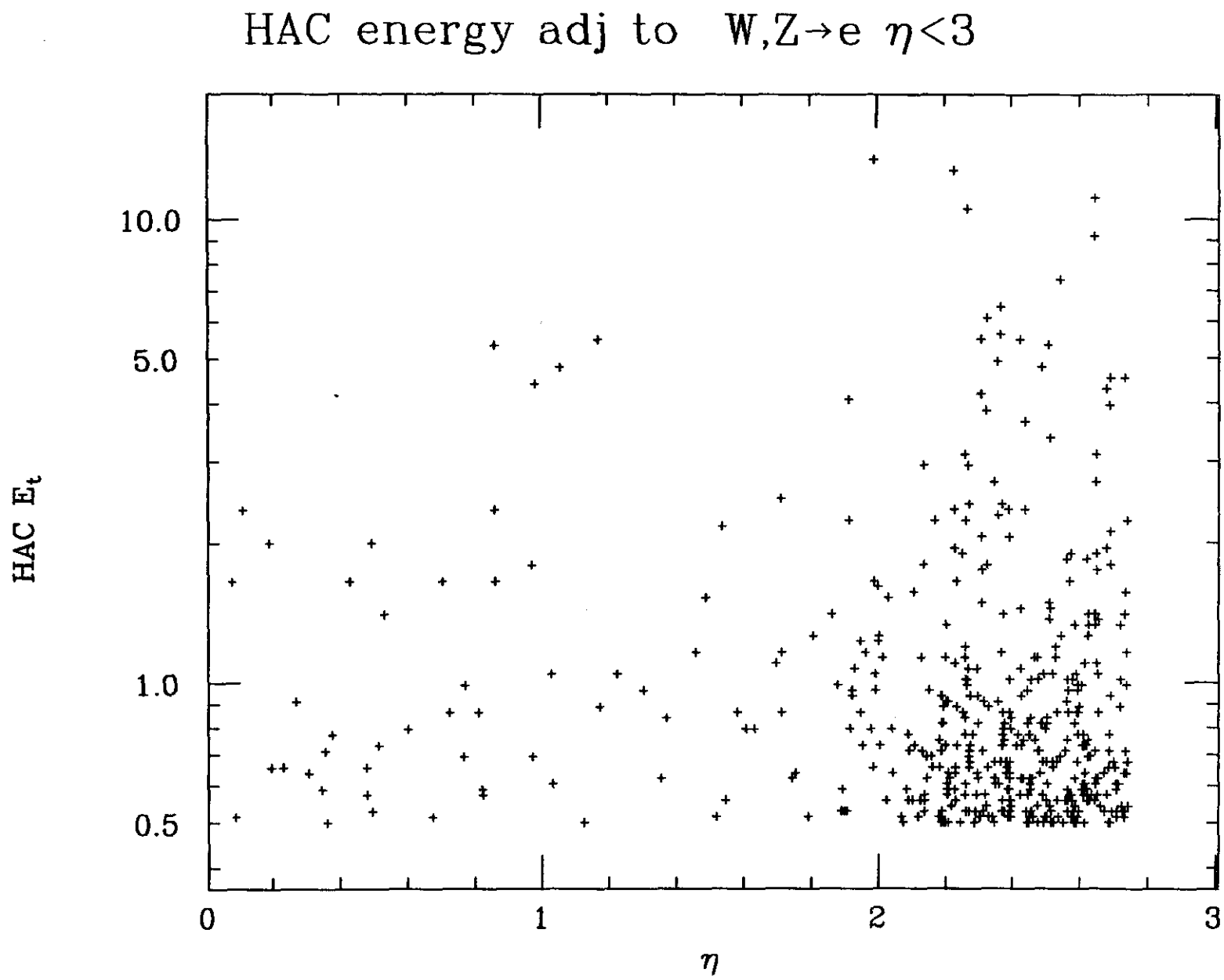

Figure 16

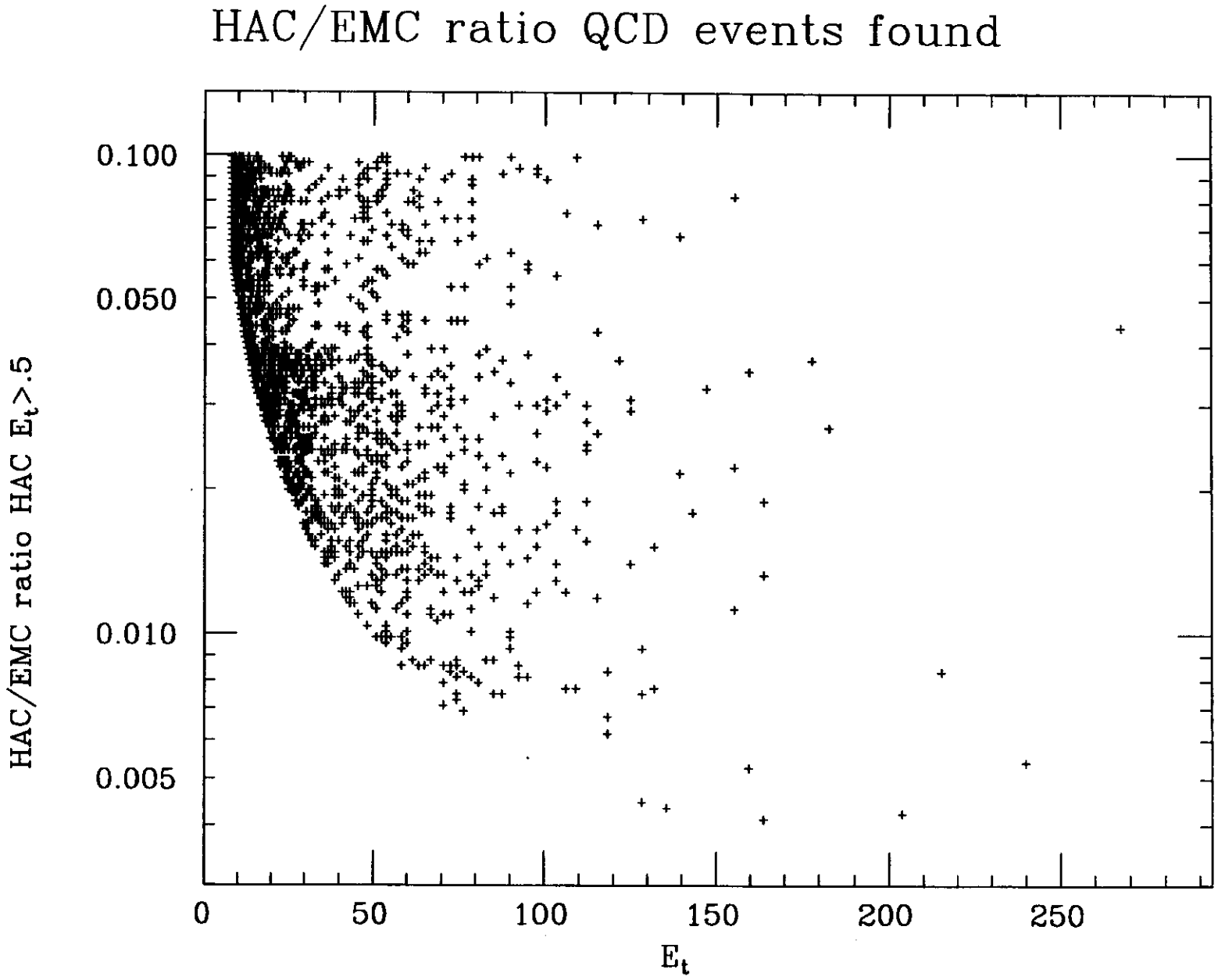
HAC/EMC ratio QCD events found
0.100
0.050
0.010
0.005
HAC/EMC ratio HAC E_t>.5
0
50
100
150
200
250
E_t

Figure 17

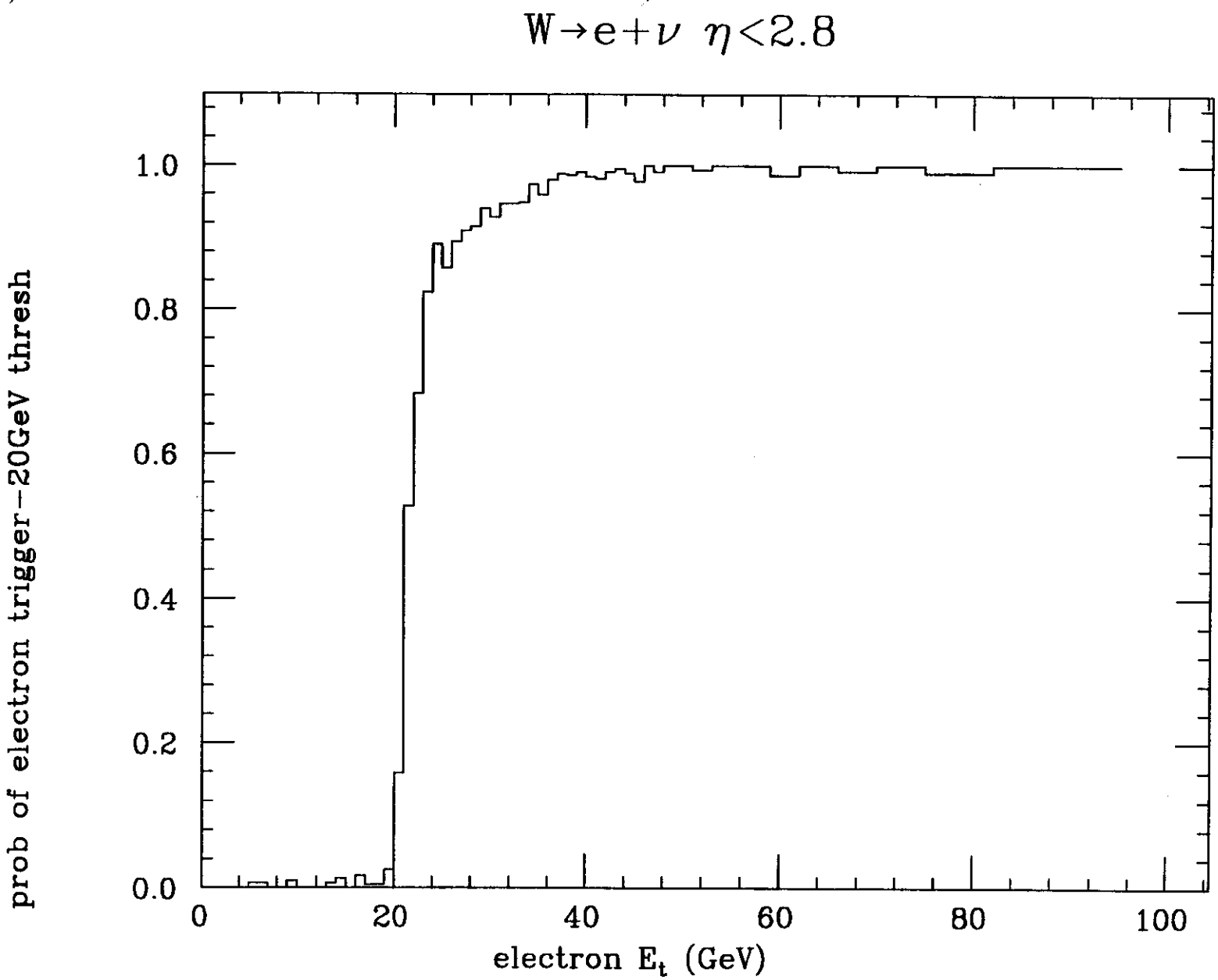
W→e+ν η<2.8
prob of electron trigger−20GeV thresh
1.0
0.8
0.6
0.4
0.2
0.0
0
20
40
60
80
100
electron E_t (GeV)

Figure 18

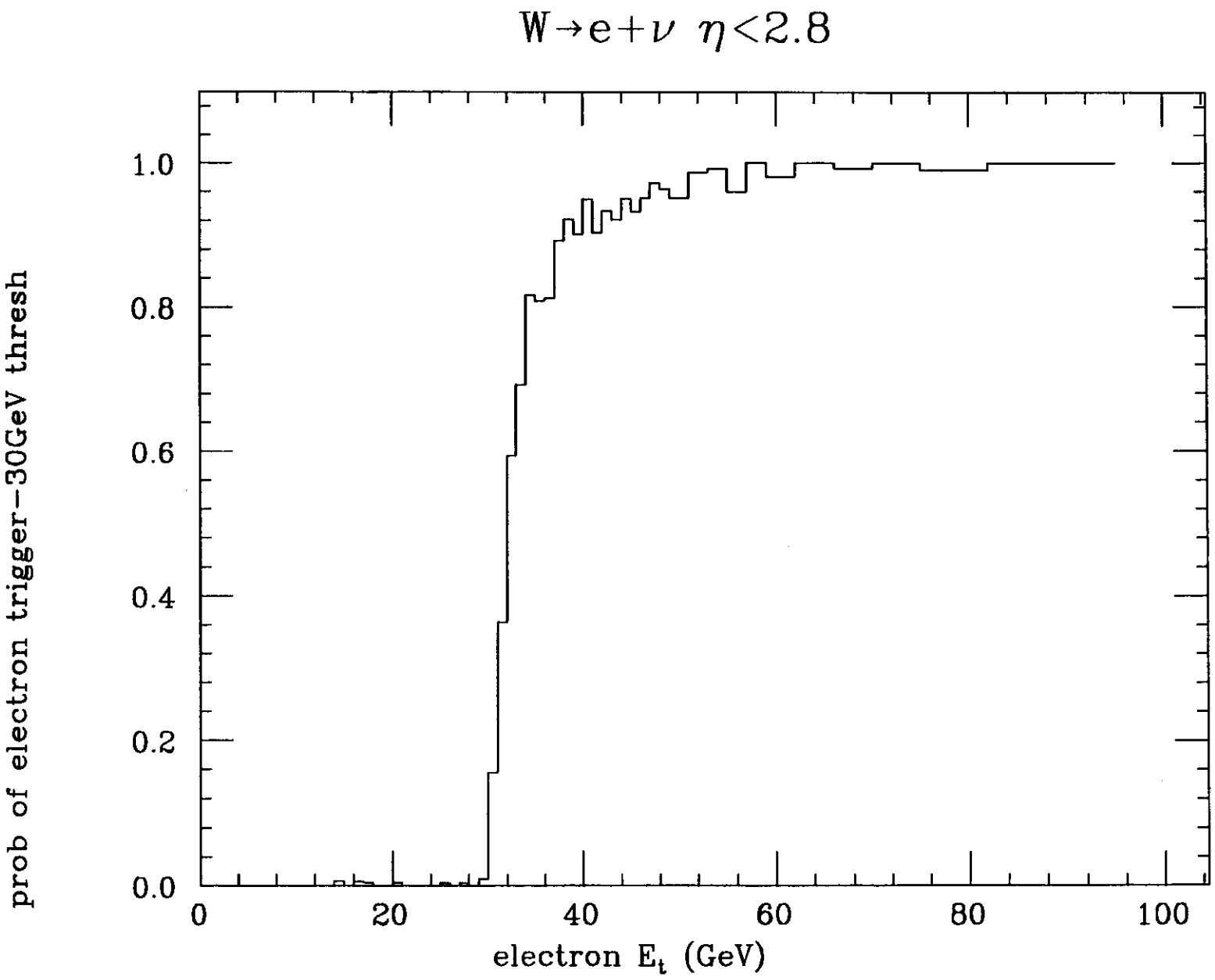
W→e+ν η<2.8
prob of electron trigger−30GeV thresh
1.0
0.8
0.6
0.4
0.2
0.0
0
20
40
60
80
100
electron E_t (GeV)

Figure 19

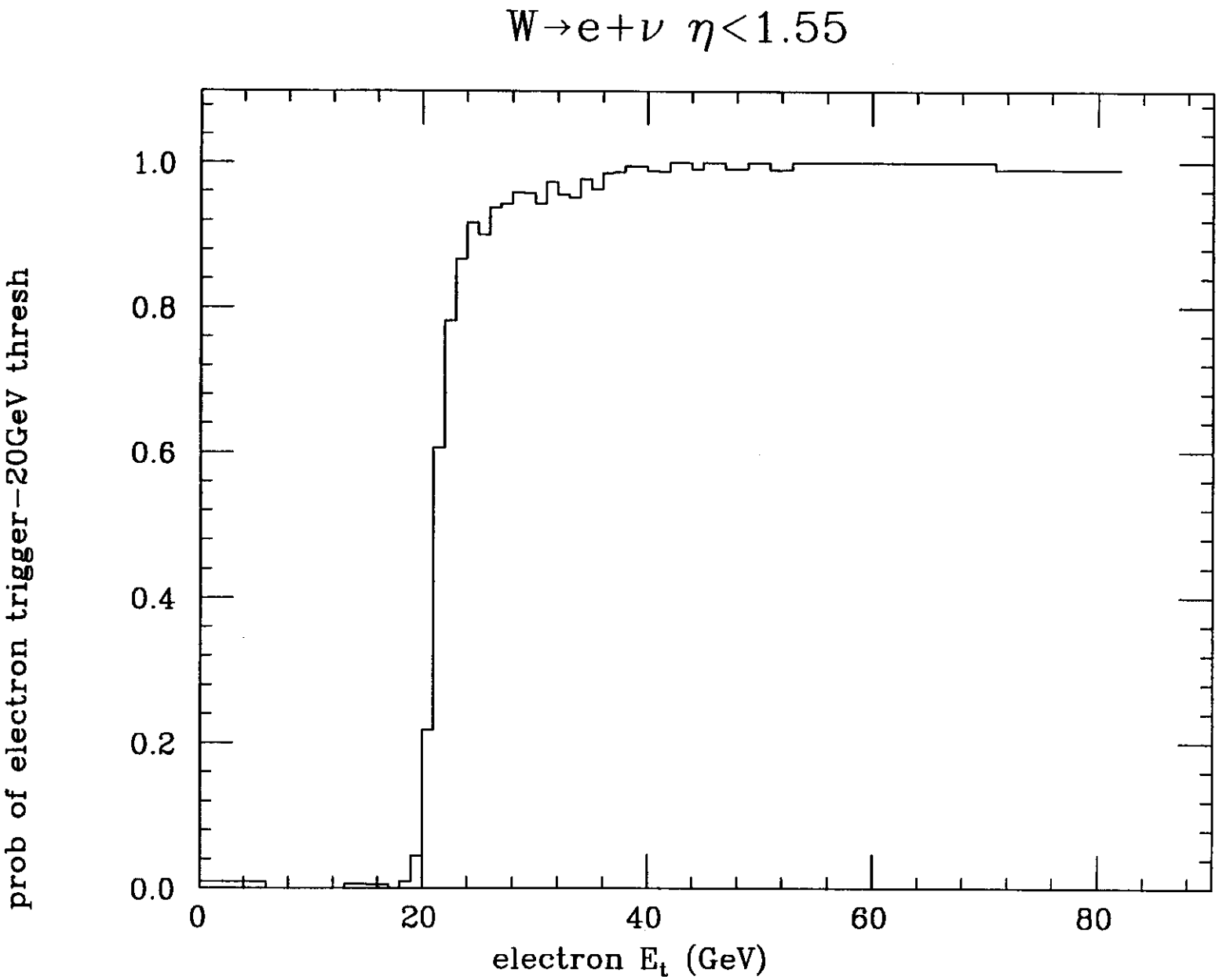
W→e+ν η<1.55
prob of electron trigger−20GeV thresh
1.0
0.8
0.6
0.4
0.2
0.0
0
20
40
60
80
electron E_t (GeV)

Figure 20

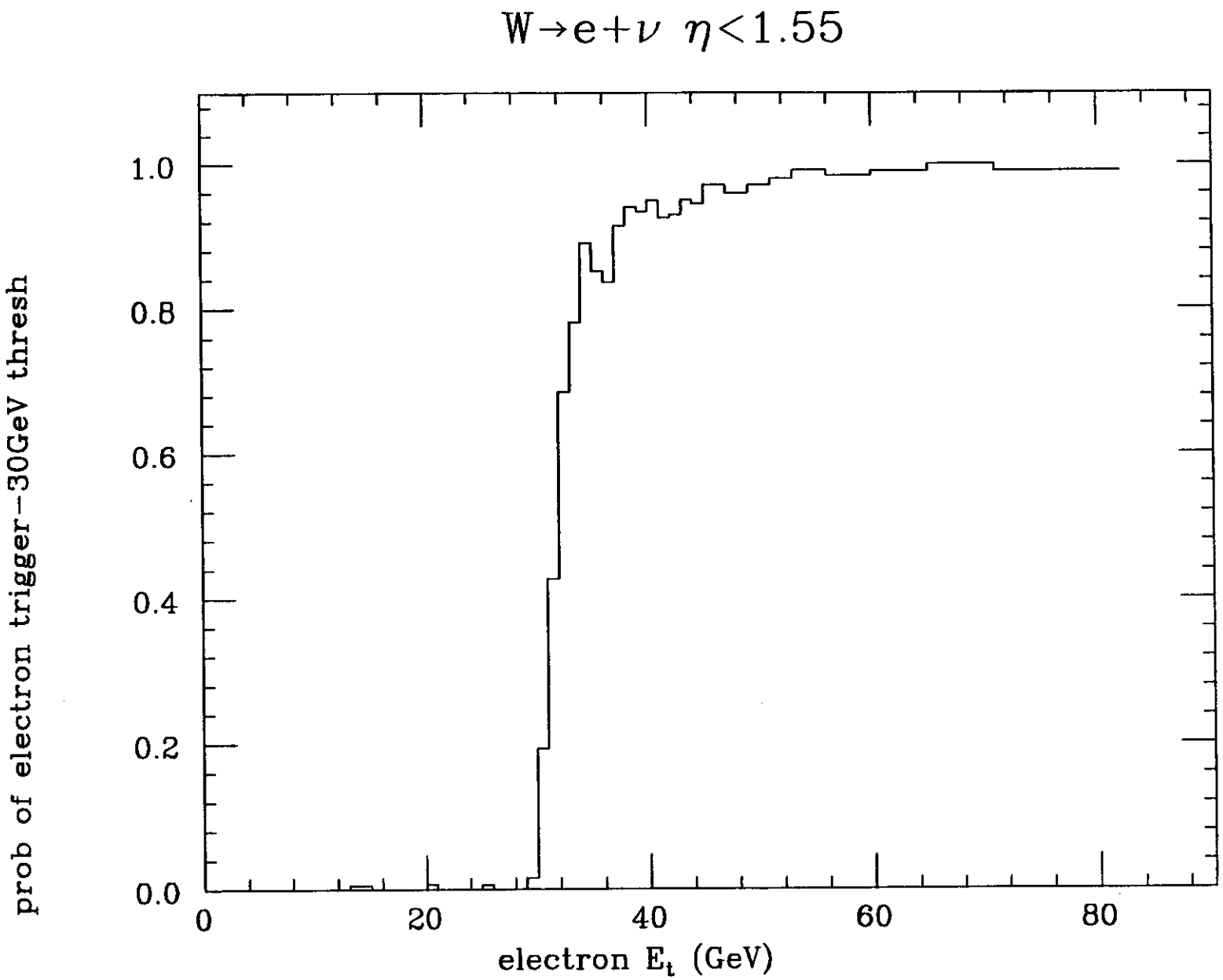
W→e+ν η<1.55
prob of electron trigger−30GeV thresh
1.0
0.8
0.6
0.4
0.2
0.0
0
20
40
60
80
electron E_t (GeV)

Figure 21

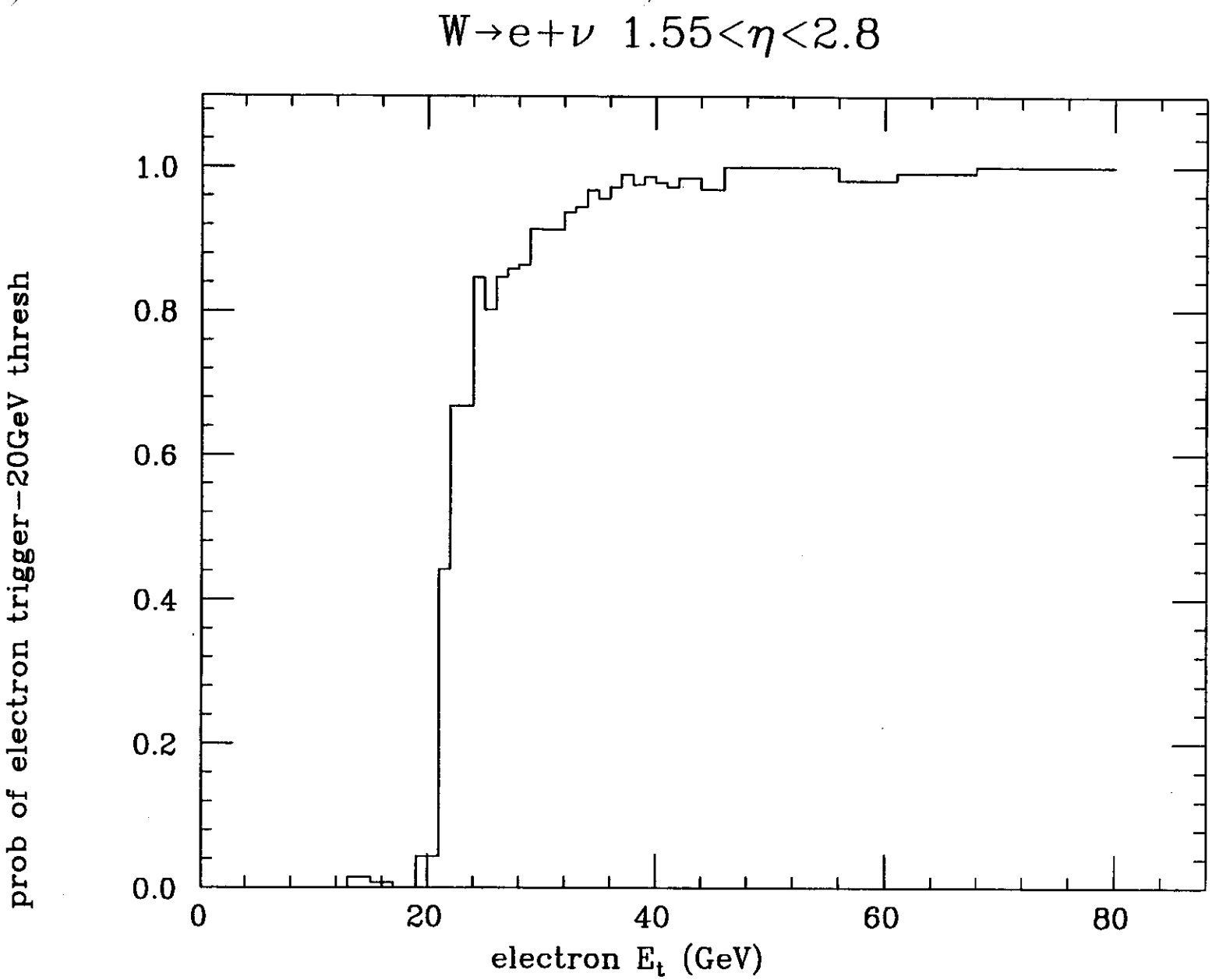
W→e+ν 1.55<η<2.8
prob of electron trigger−20GeV thresh
1.0
0.8
0.6
0.4
0.2
0.0
0
20
40
60
80
electron E_t (GeV)

Figure 22

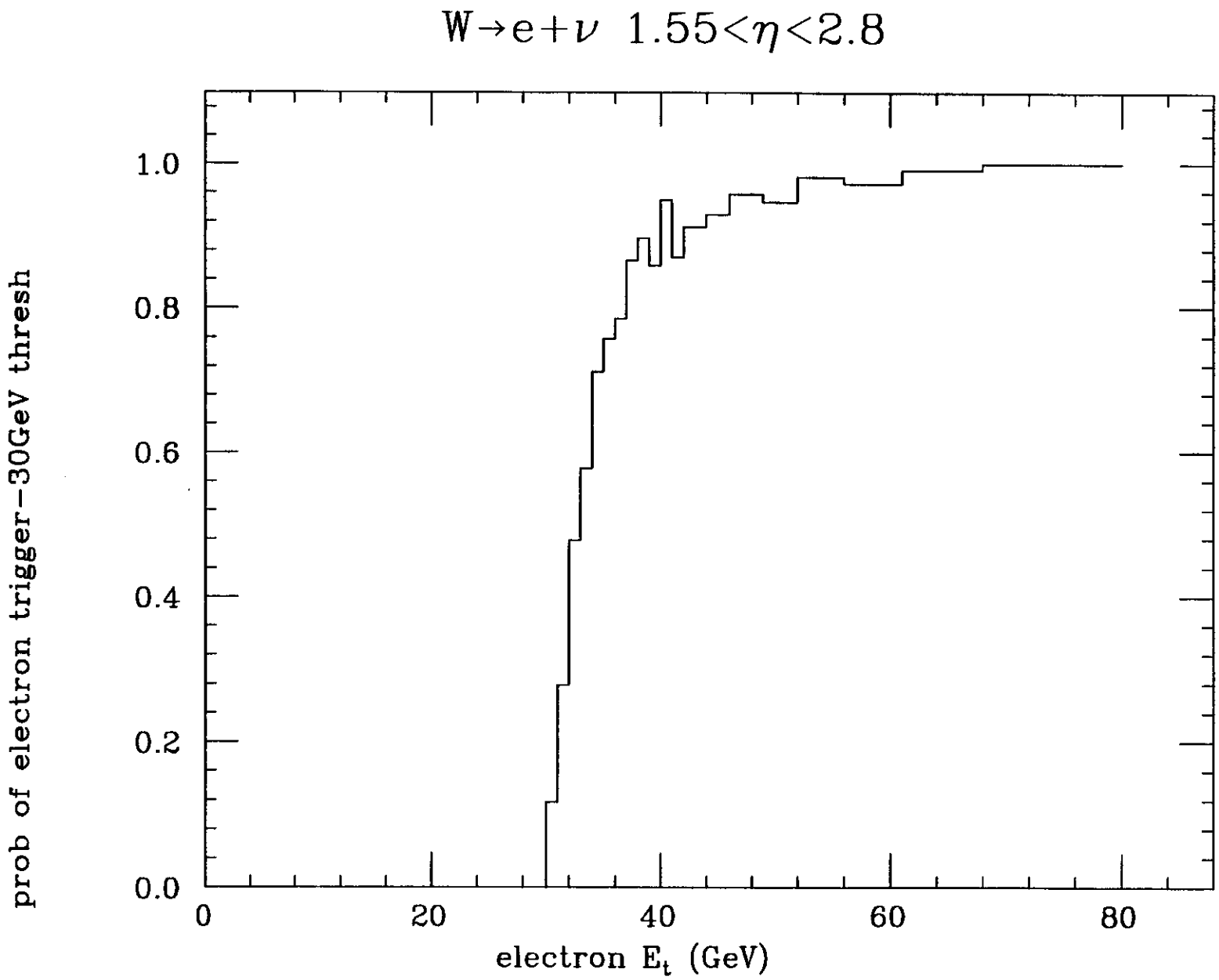
W→e+ν 1.55<η<2.8
prob of electron trigger−30GeV thresh
1.0
0.8
0.6
0.4
0.2
0.0
0
20
40
60
80
electron E_t (GeV)

Figure 23

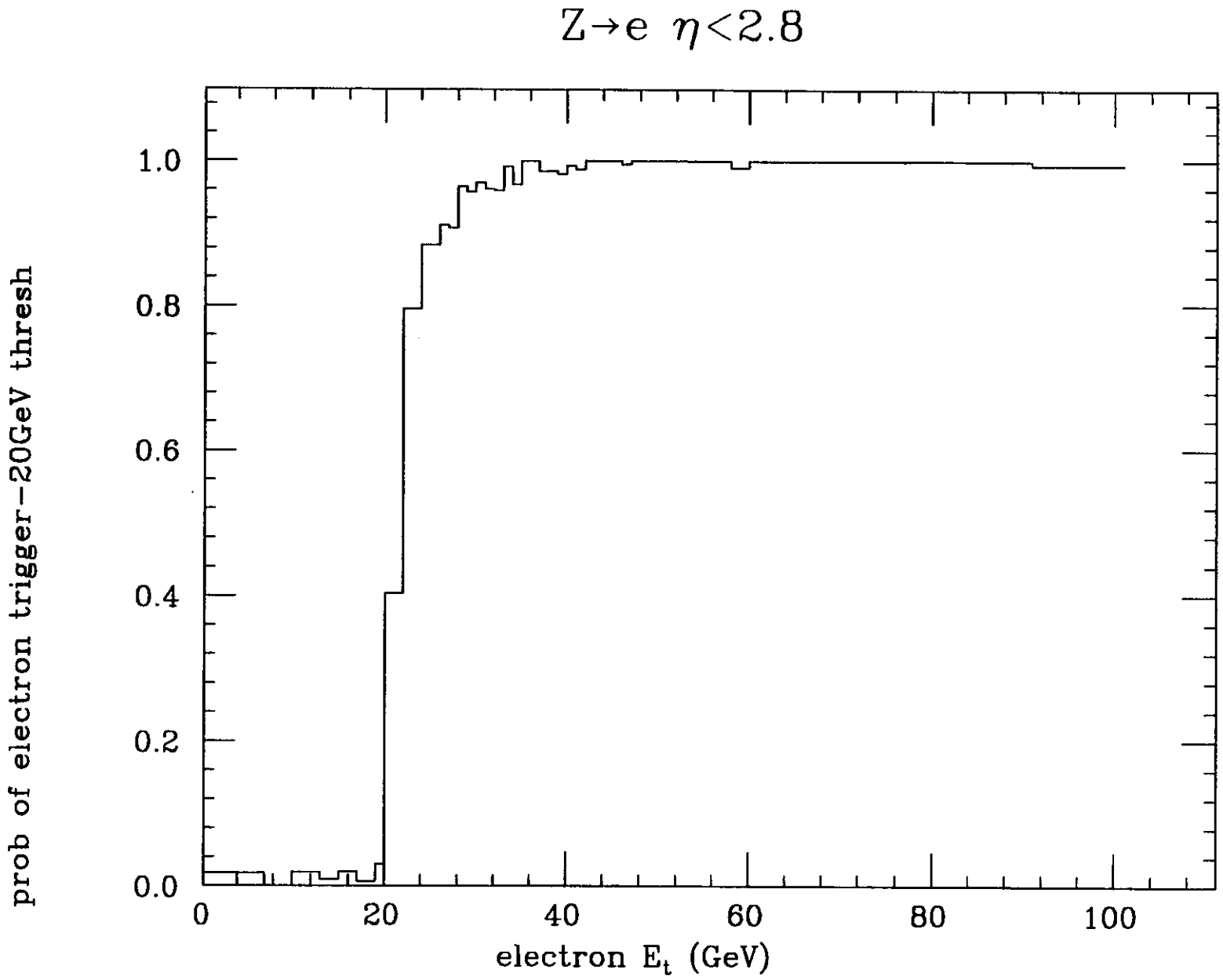
Z→e η<2.8
prob of electron trigger−20GeV thresh
1.0
0.8
0.6
0.4
0.2
0.0
0
20
40
60
80
100
electron E_t (GeV)

Figure 24

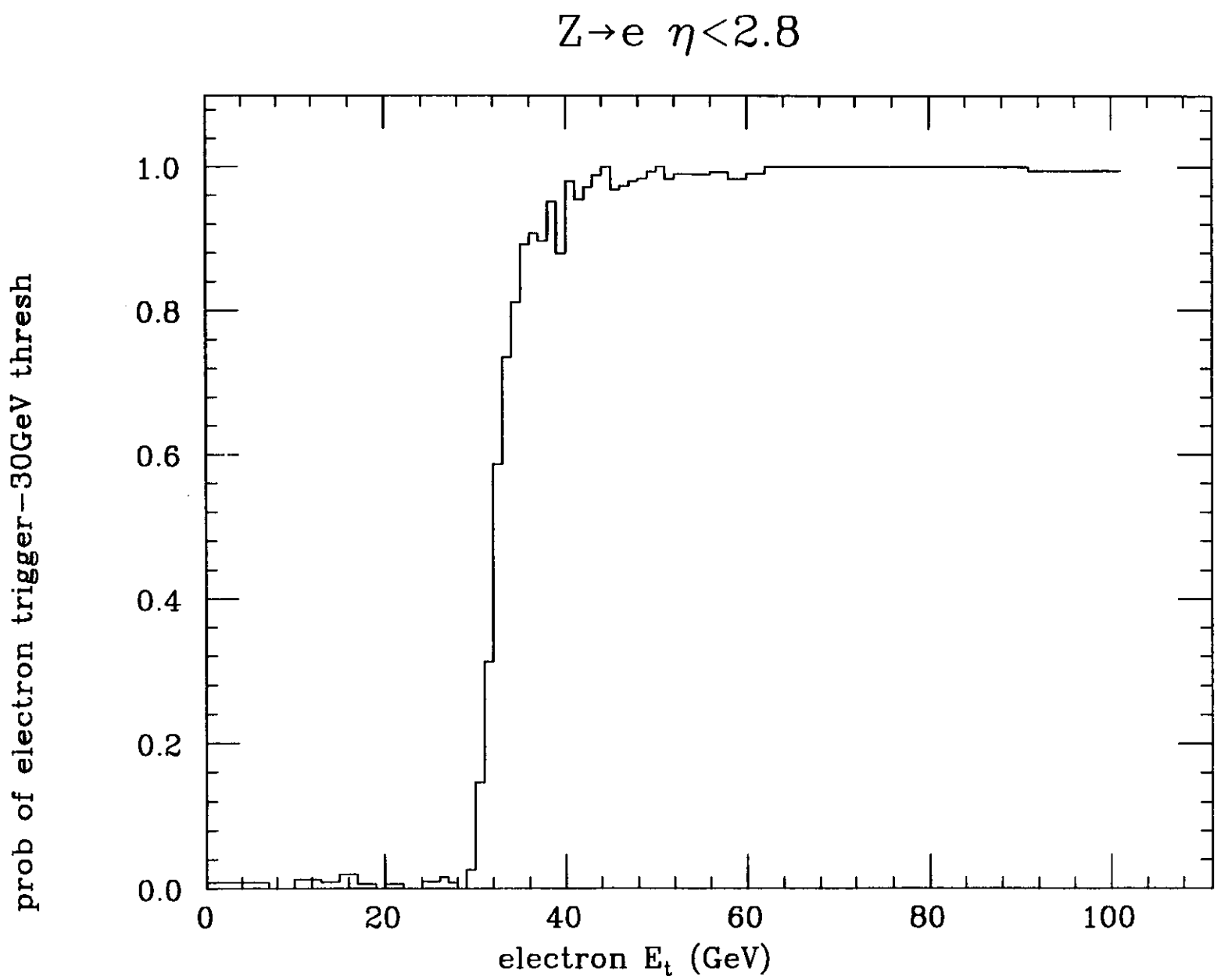
Z→e η<2.8
prob of electron trigger−30GeV thresh
1.0
0.8
0.6
0.4
0.2
0.0
0
20
40
60
80
100
electron E_t (GeV)

Figure 25

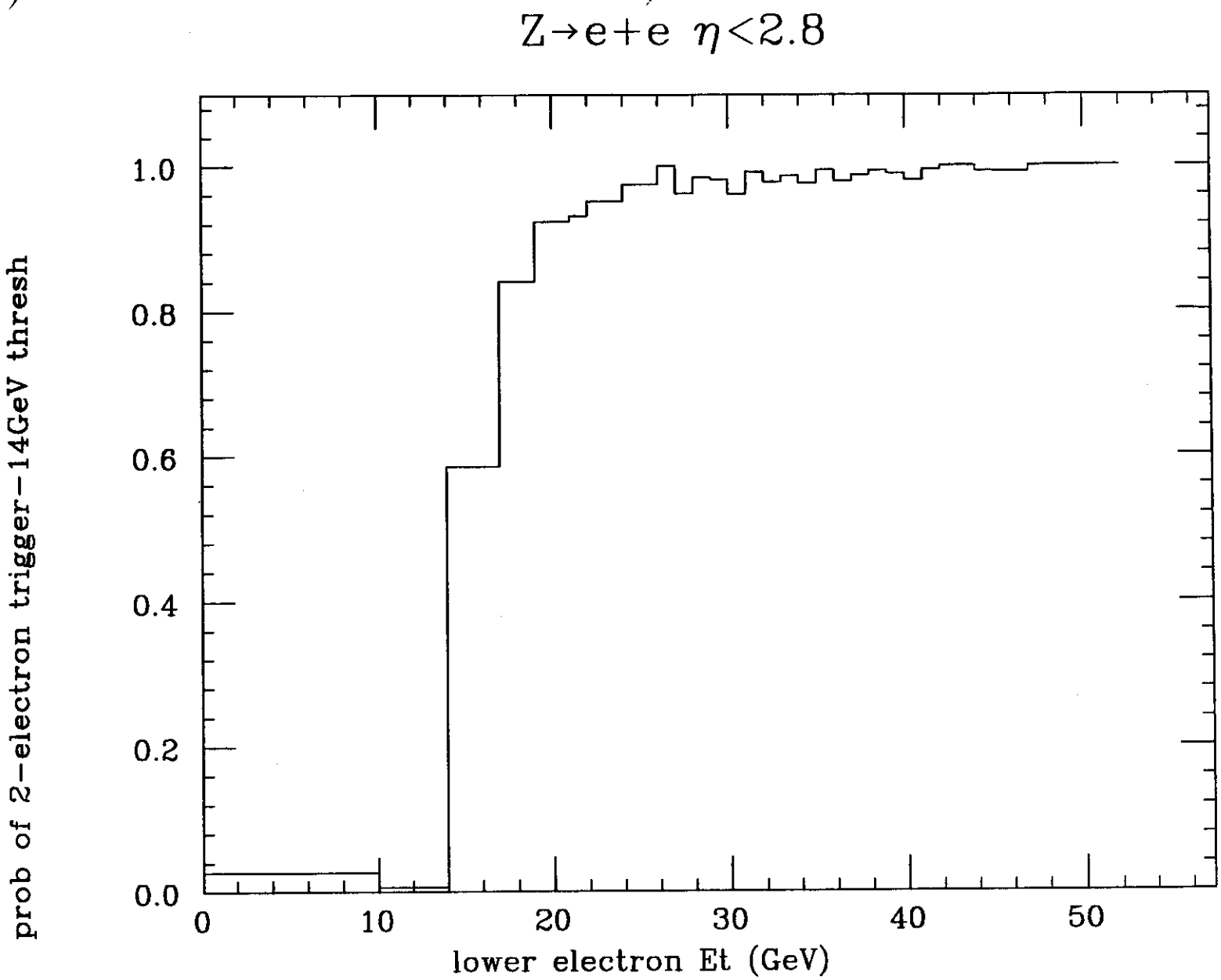
Z→e+e η<2.8
prob of 2-electron trigger-14GeV thresh
1.0
0.8
0.6
0.4
0.2
0.0
0
10
20
30
40
50
lower electron Et (GeV)

Figure 26

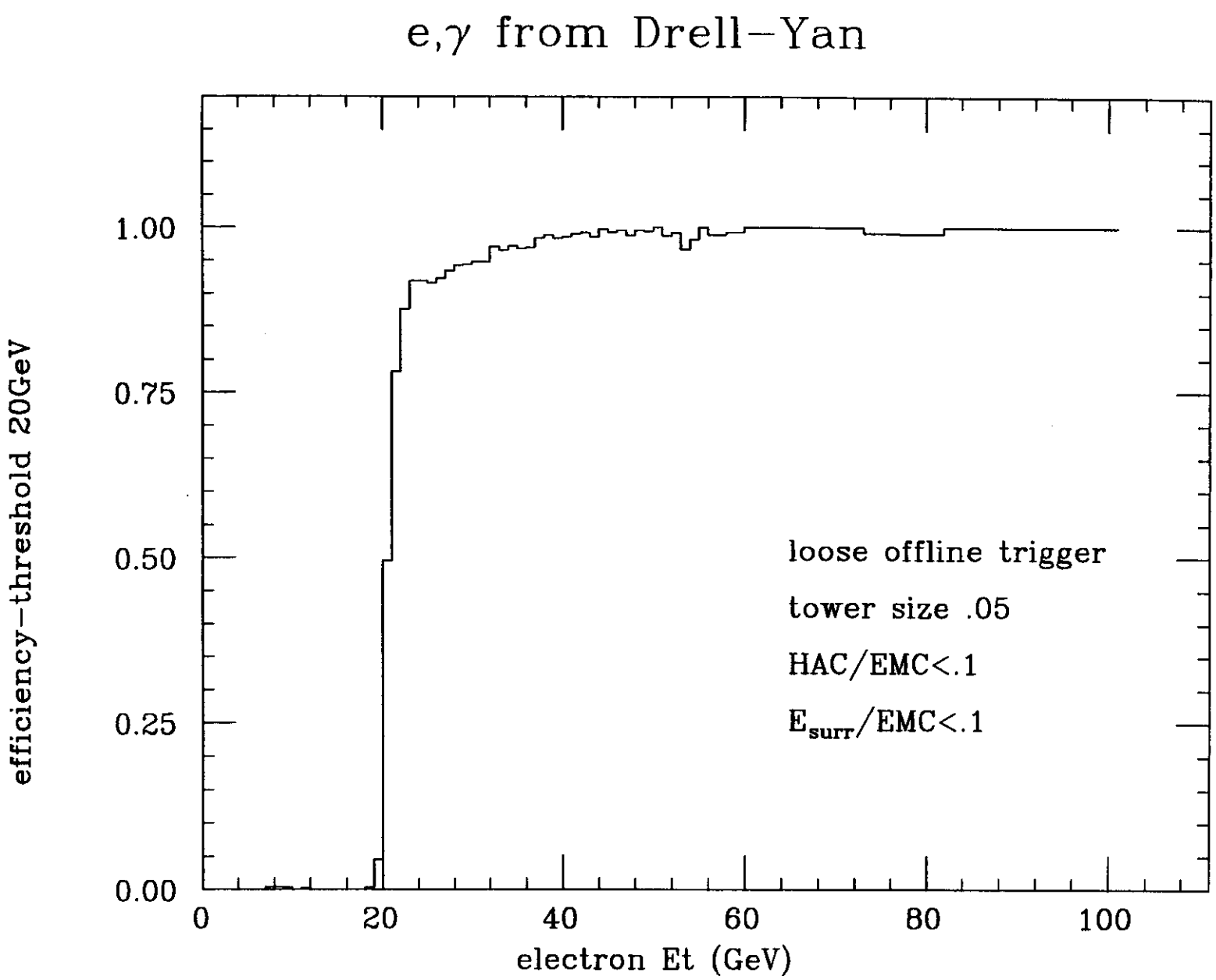
e,γ from Drell−Yan
efficiency−threshold 20GeV
1.00
0.75
0.50
0.25
0.00
0
20
40
60
80
100
electron Et (GeV)
loose offline trigger
tower size .05
HAC/EMC<.1
E_surr/EMC<.1

Figure 27

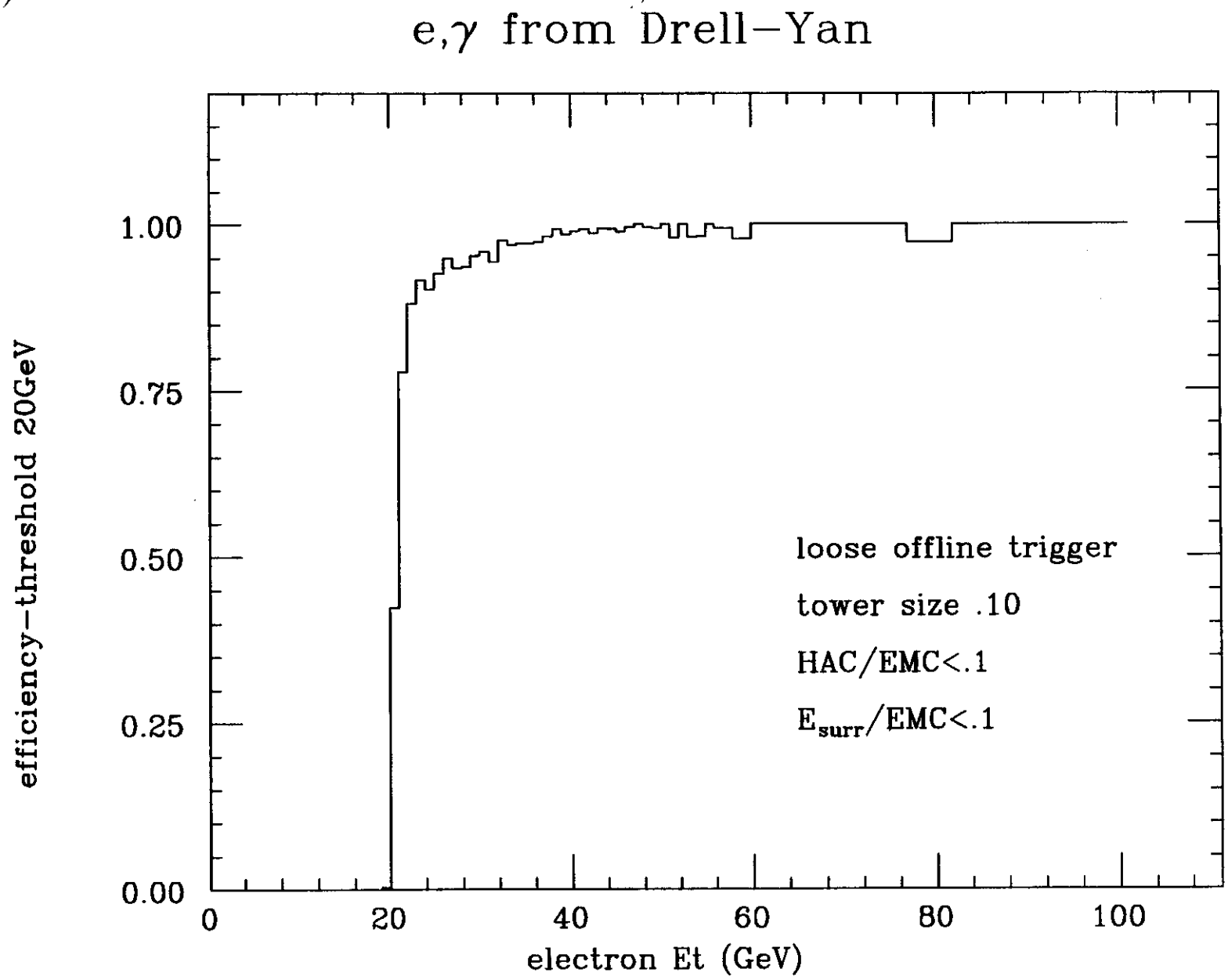
e,γ from Drell−Yan
efficiency−threshold 20GeV
1.00
0.75
0.50
0.25
0.00
0
20
40
60
80
100
electron Et (GeV)
loose offline trigger
tower size .10
HAC/EMC<.1
E_surr/EMC<.1

Figure 28

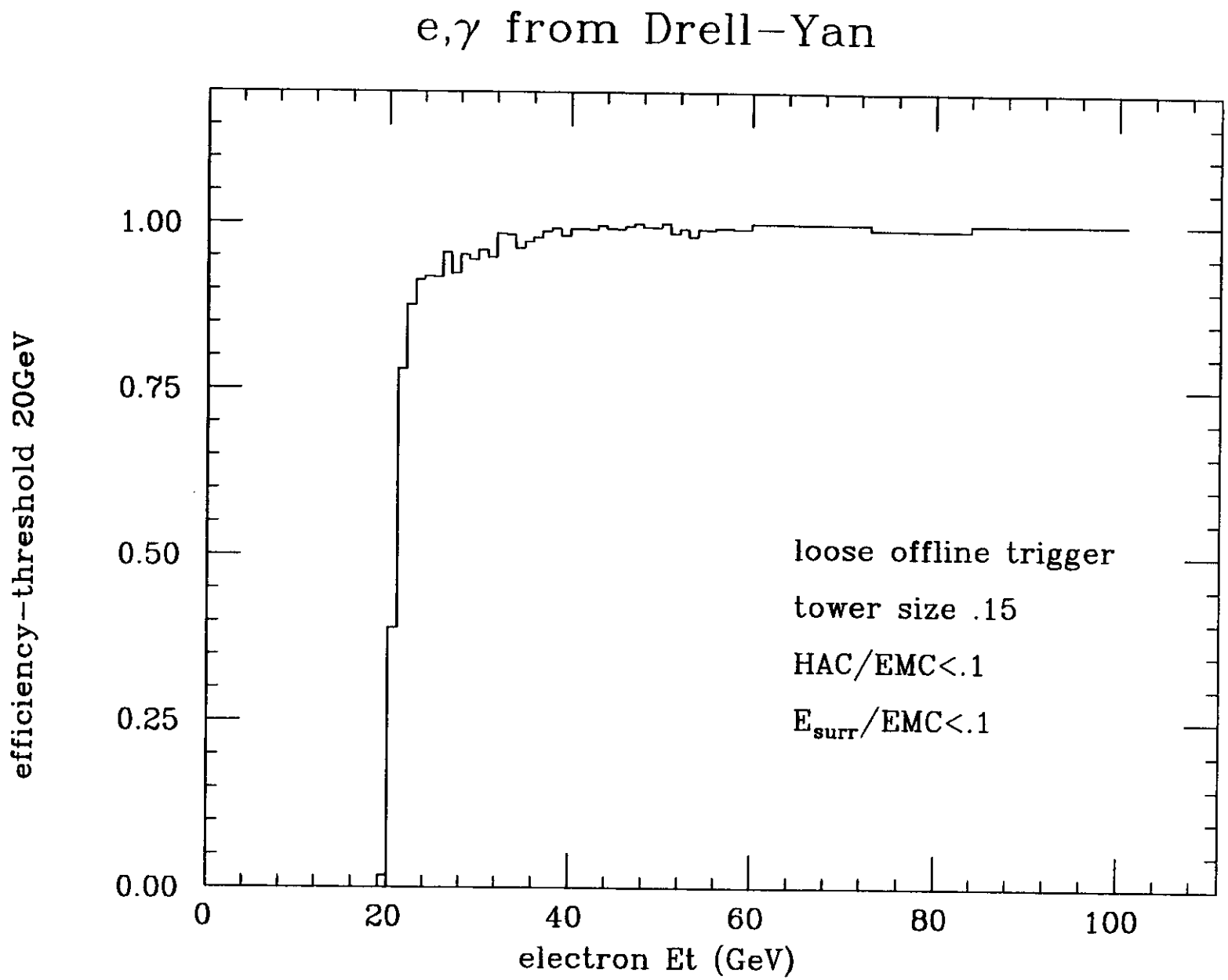
e,γ from Drell−Yan
efficiency−threshold 20GeV
1.00
0.75
0.50
0.25
0.00
0
20
40
60
80
100
electron Et (GeV)
loose offline trigger
tower size .15
HAC/EMC<.1
E_surr/EMC<.1

Figure 29

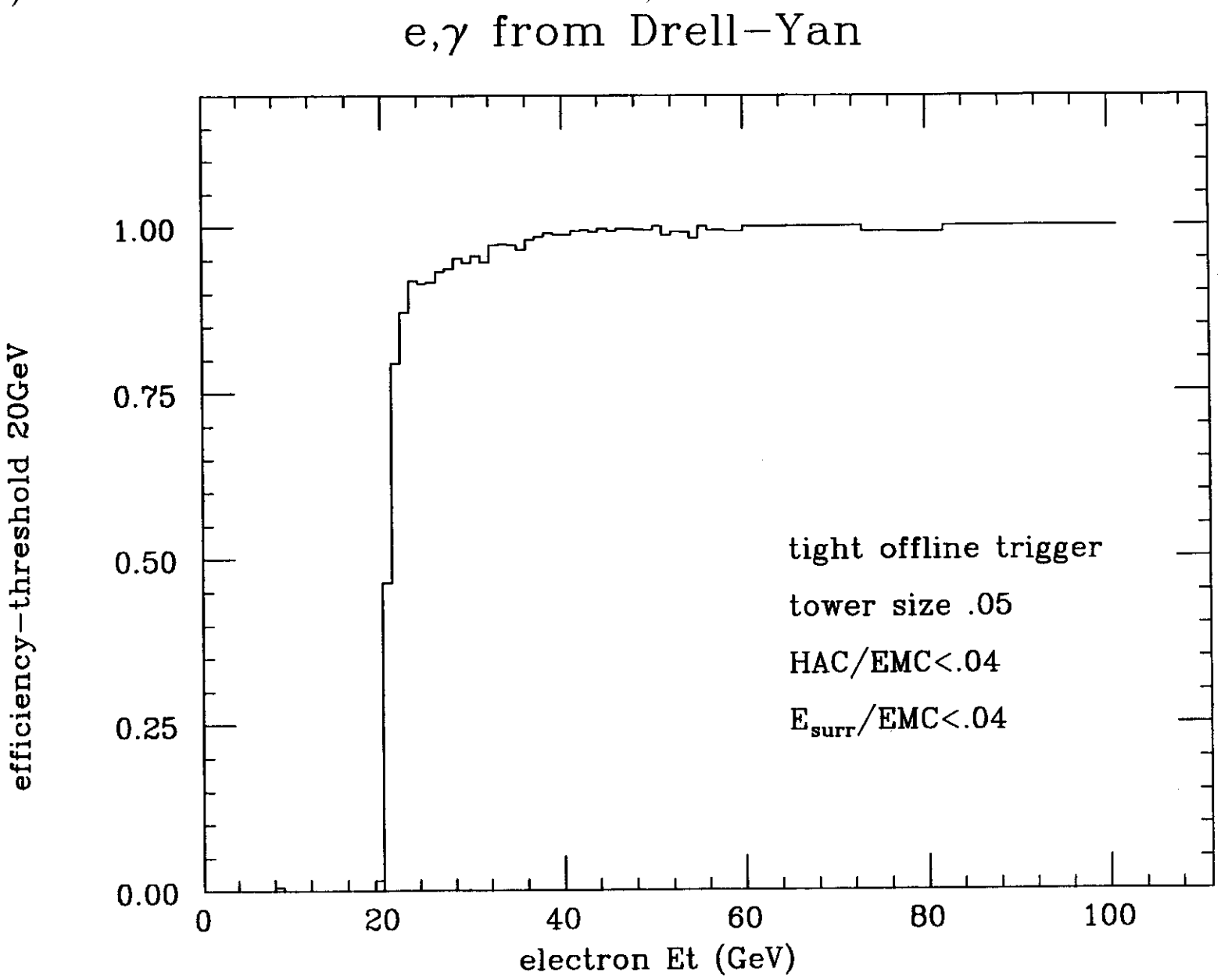
e,γ from Drell–Yan
efficiency–threshold 20GeV
1.00
0.75
0.50
0.25
0.00
0
20
40
60
80
100
electron Et (GeV)
tight offline trigger
tower size .05
HAC/EMC<.04
E_surr/EMC<.04

Figure 30

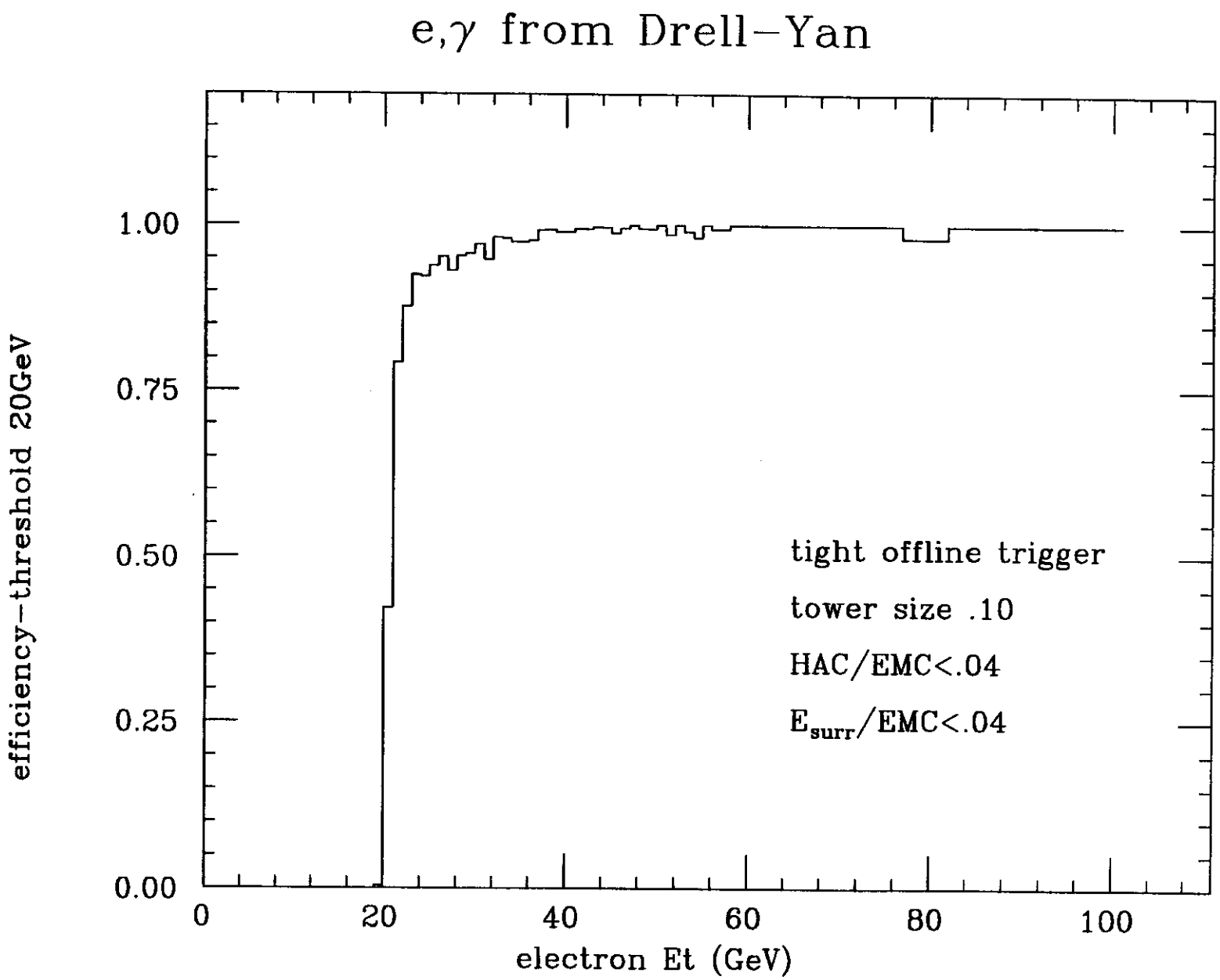
e,γ from Drell–Yan
efficiency–threshold 20GeV
1.00
0.75
0.50
0.25
0.00
0
20
40
60
80
100
electron Et (GeV)
tight offline trigger
tower size .10
HAC/EMC<.04
E_surr/EMC<.04

Figure 31

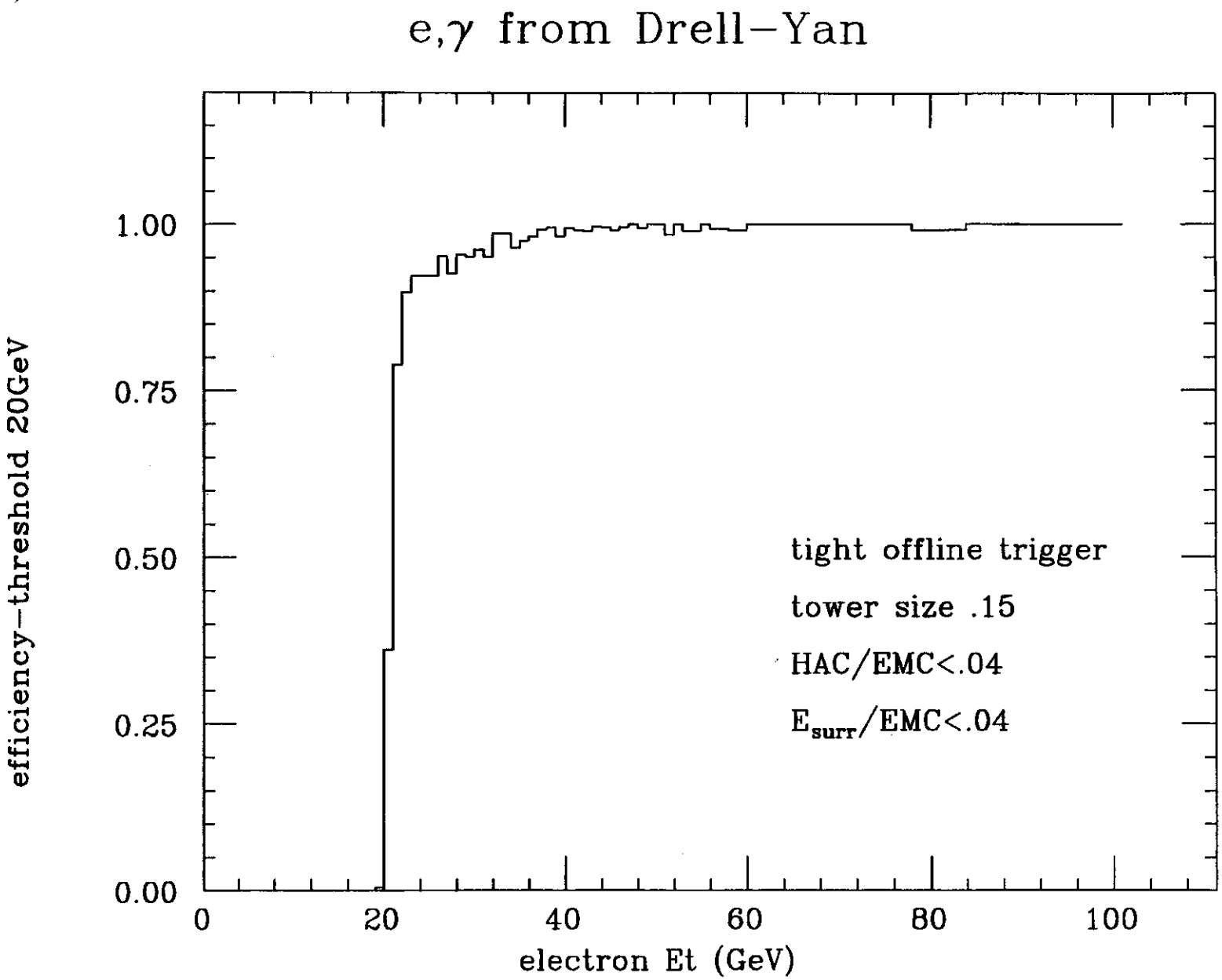
e,γ from Drell−Yan
efficiency−threshold 20GeV
1.00
0.75
0.50
0.25
0.00
0
20
40
60
80
100
electron Et (GeV)
tight offline trigger
tower size .15
HAC/EMC<.04
E_surr/EMC<.04

Figure 32

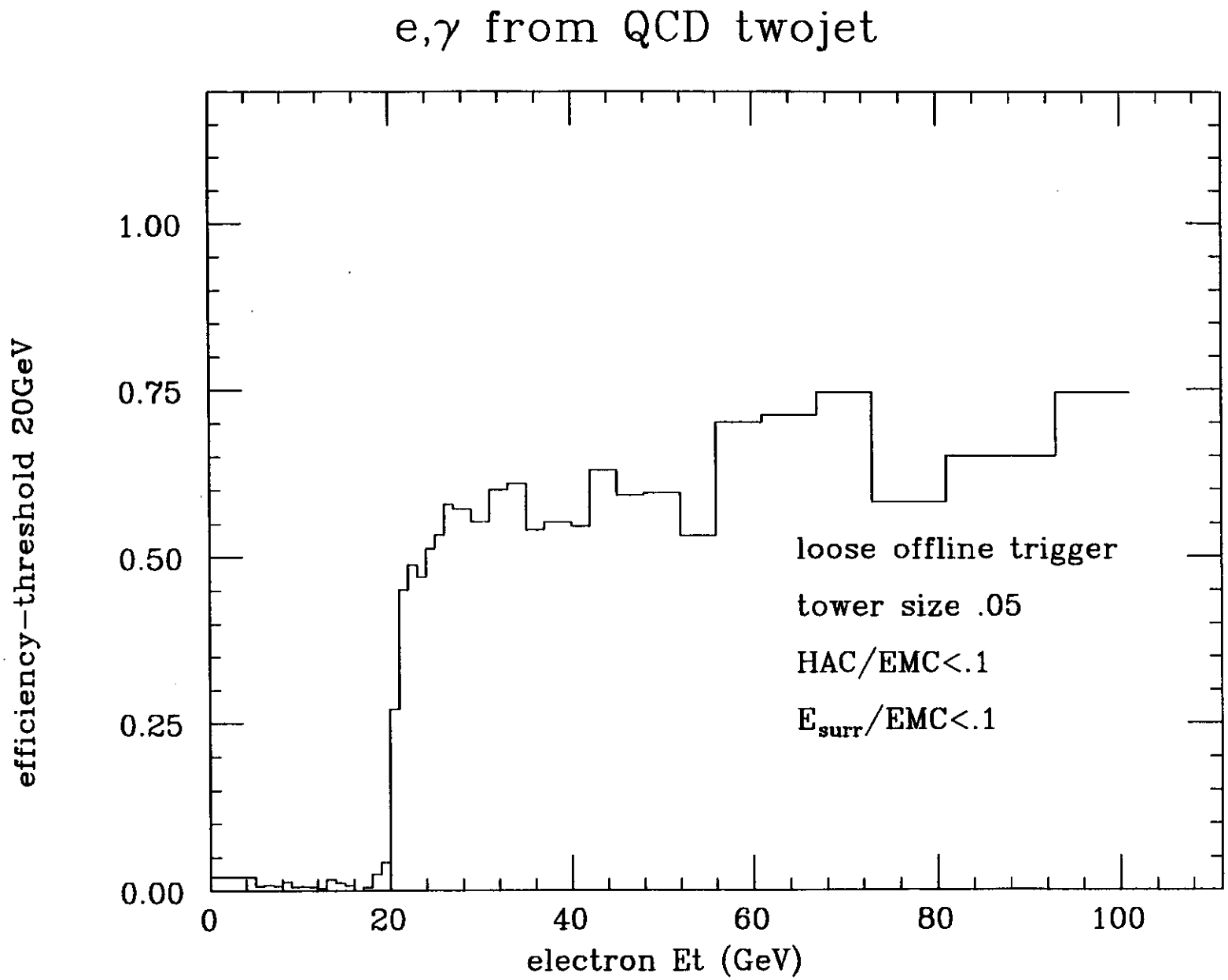
e,γ from QCD twojet
efficiency−threshold 20GeV
1.00
0.75
0.50
0.25
0.00
0
20
40
60
80
100
electron Et (GeV)
loose offline trigger
tower size .05
HAC/EMC<.1
E_surr/EMC<.1

Figure 33

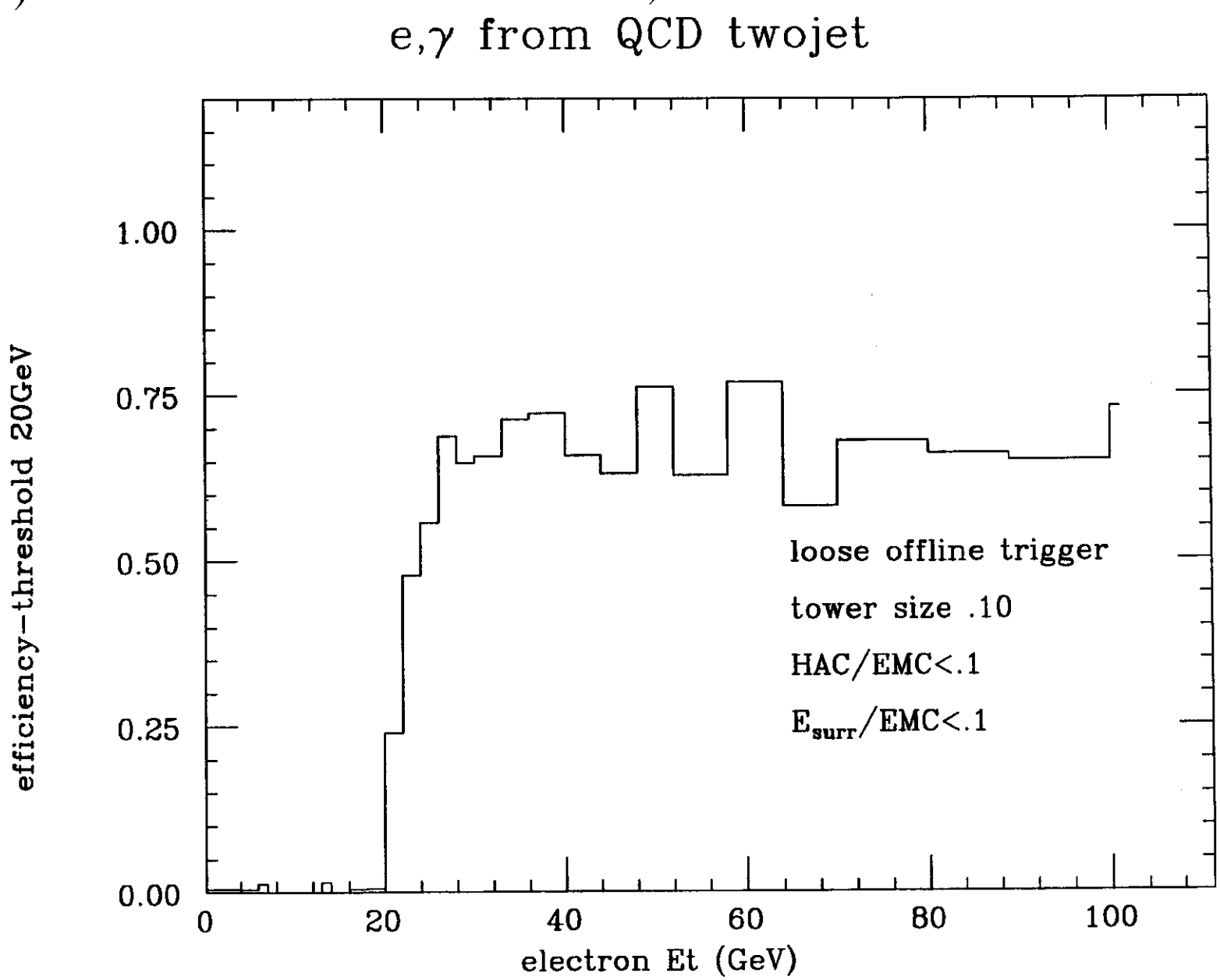
e,γ from QCD twojet
efficiency−threshold 20GeV
1.00
0.75
0.50
0.25
0.00
0
20
40
60
80
100
electron Et (GeV)
loose offline trigger
tower size .10
HAC/EMC<.1
E_surr/EMC<.1

Figure 34

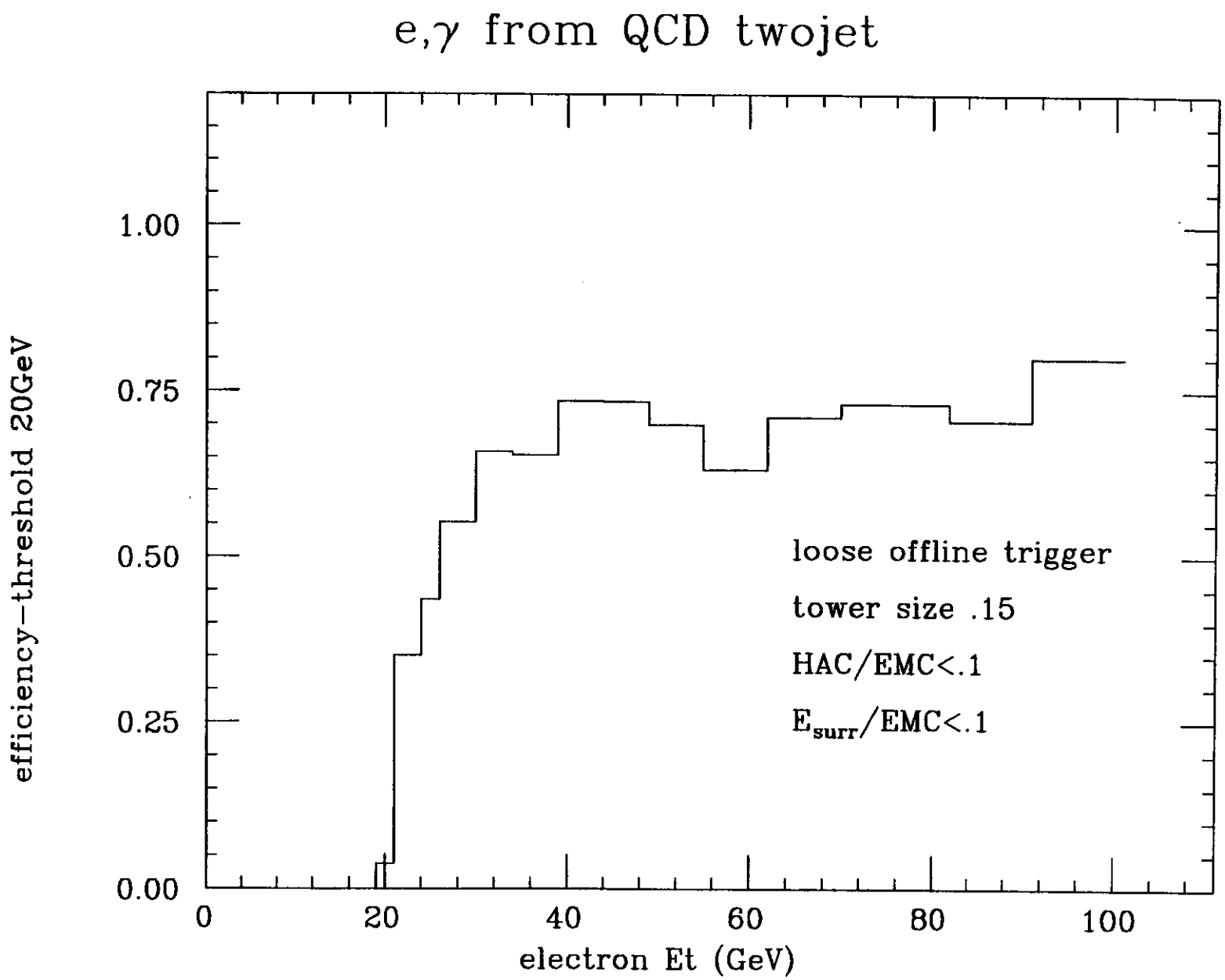
e,γ from QCD twojet
efficiency−threshold 20GeV
1.00
0.75
0.50
0.25
0.00
0
20
40
60
80
100
electron Et (GeV)
loose offline trigger
tower size .15
HAC/EMC<.1
E_surr/EMC<.1

Figure 35

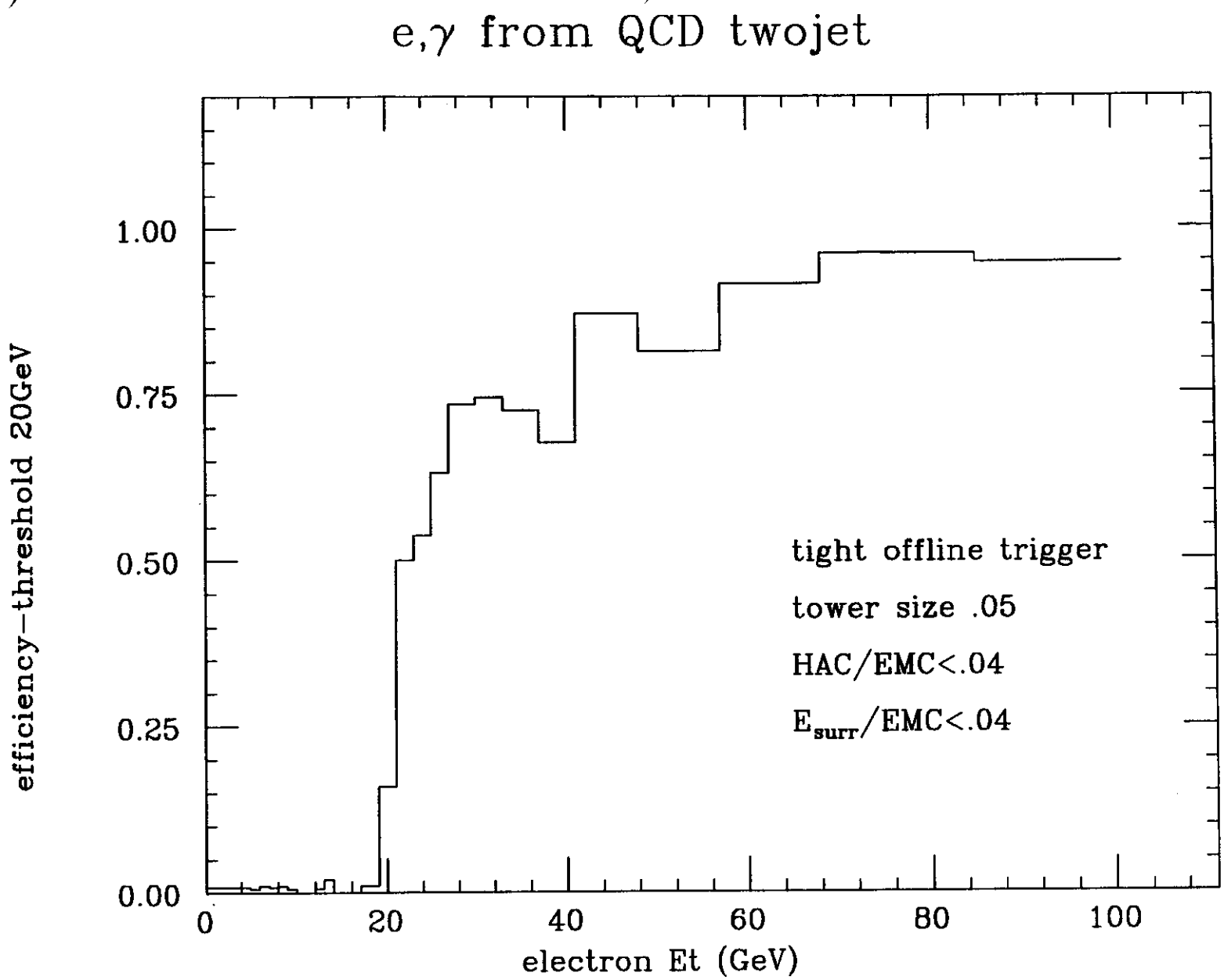
e,γ from QCD twojet
efficiency−threshold 20GeV
1.00
0.75
0.50
0.25
0.00
0
20
40
60
80
100
electron Et (GeV)
tight offline trigger
tower size .05
HAC/EMC<.04
E_surr/EMC<.04

Figure 36

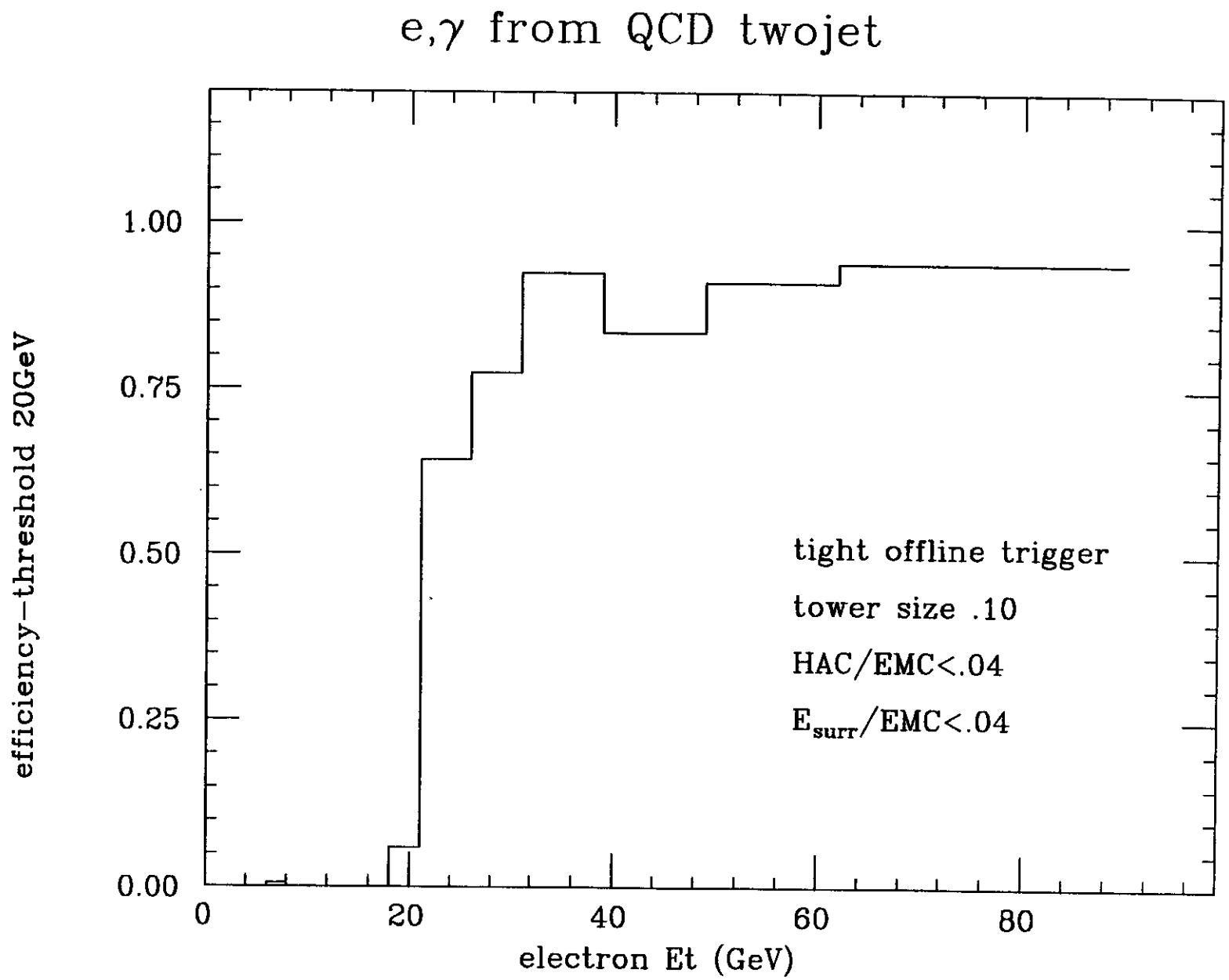
e,γ from QCD twojet
efficiency−threshold 20GeV
1.00
0.75
0.50
0.25
0.00
0
20
40
60
80
electron Et (GeV)
tight offline trigger
tower size .10
HAC/EMC<.04
E_surr/EMC<.04

Figure 37

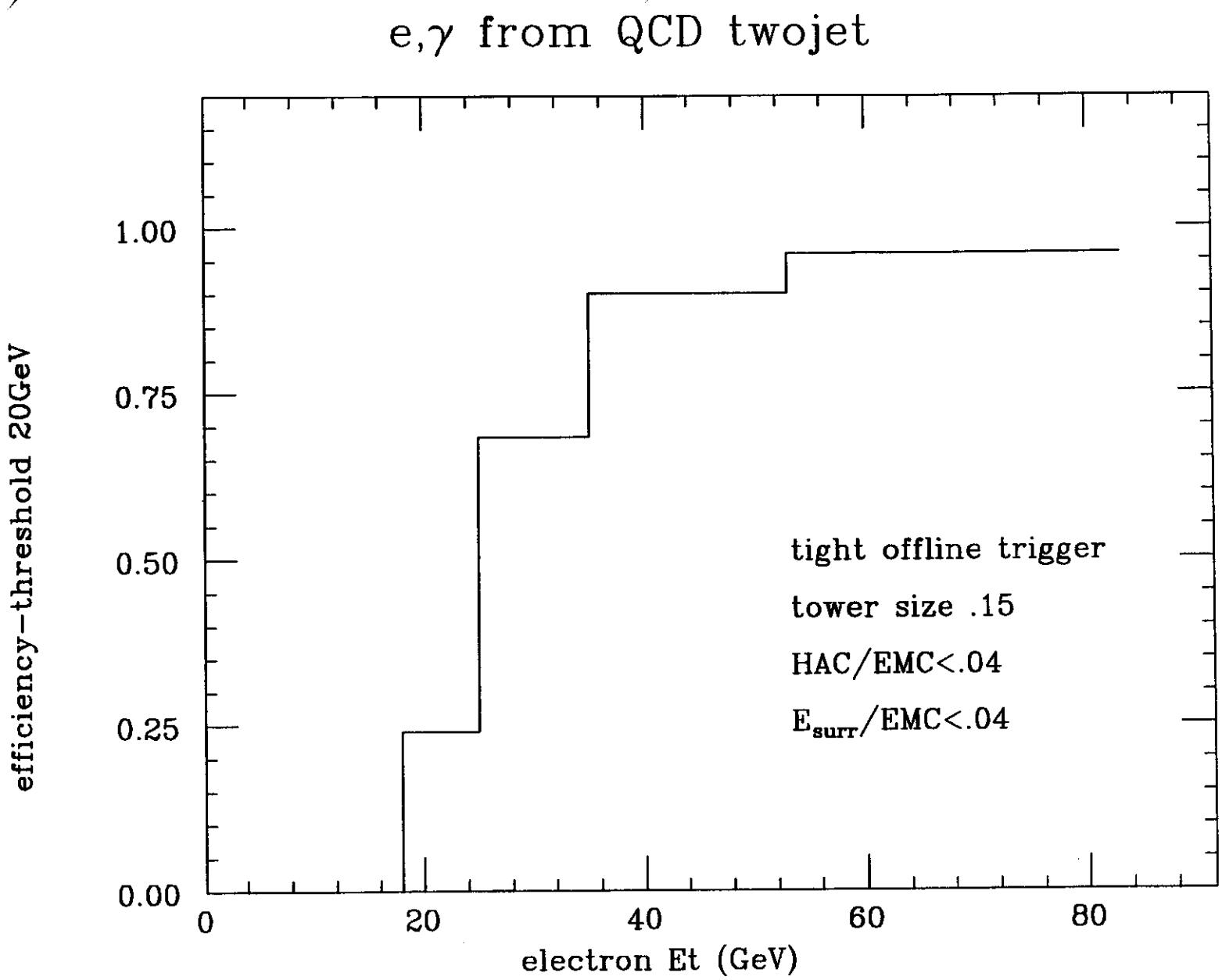
e,γ from QCD twojet
efficiency−threshold 20GeV
1.00
0.75
0.50
0.25
0.00
0
20
40
60
80
electron Et (GeV)
tight offline trigger
tower size .15
HAC/EMC<.04
E_surr/EMC<.04

Figure 38

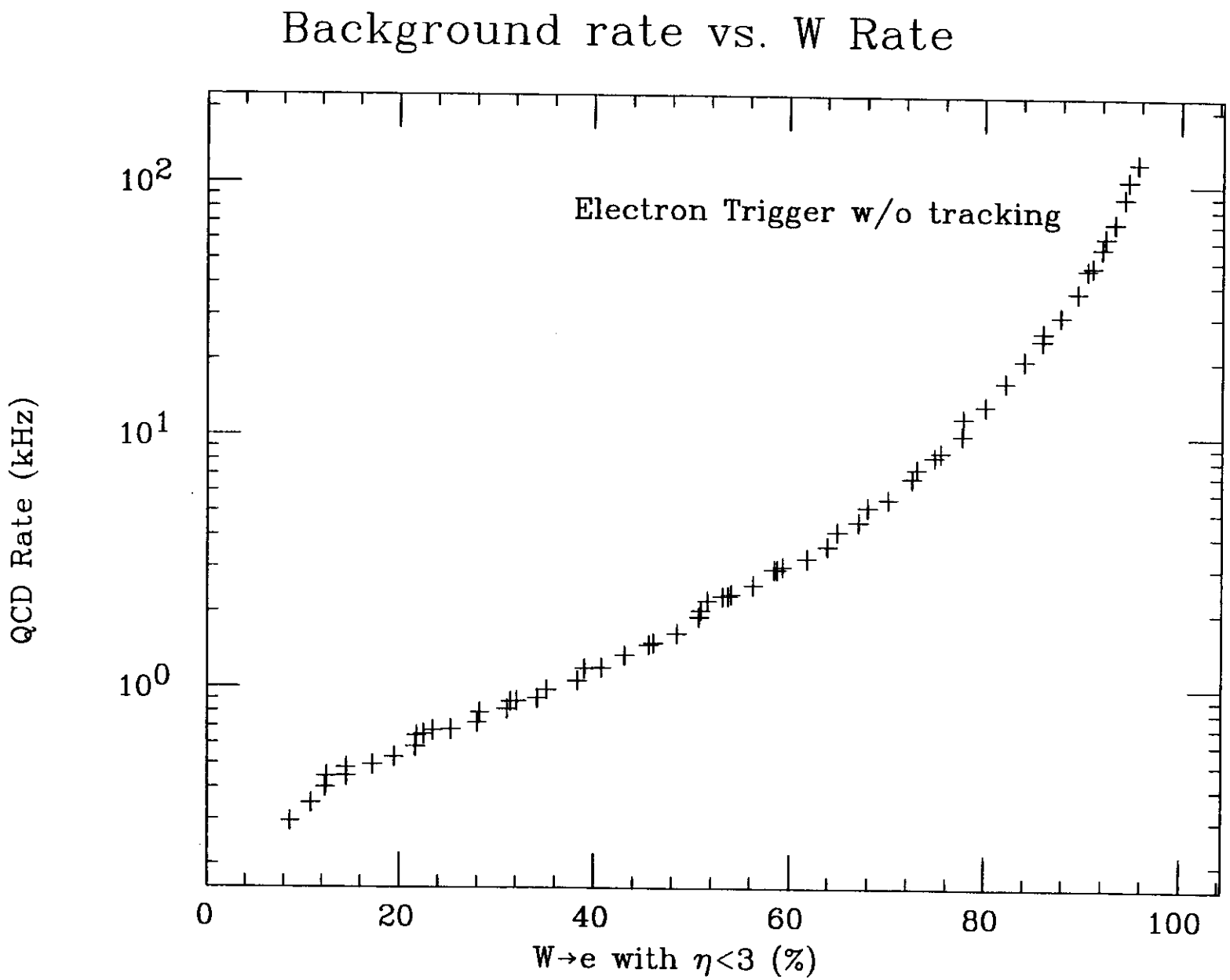
Background rate vs. W Rate
Electron Trigger w/o tracking
QCD Rate (kHz)
10^2
10^1
10^0
0
20
40
60
80
100
W→e with η<3 (%)

Figure 39

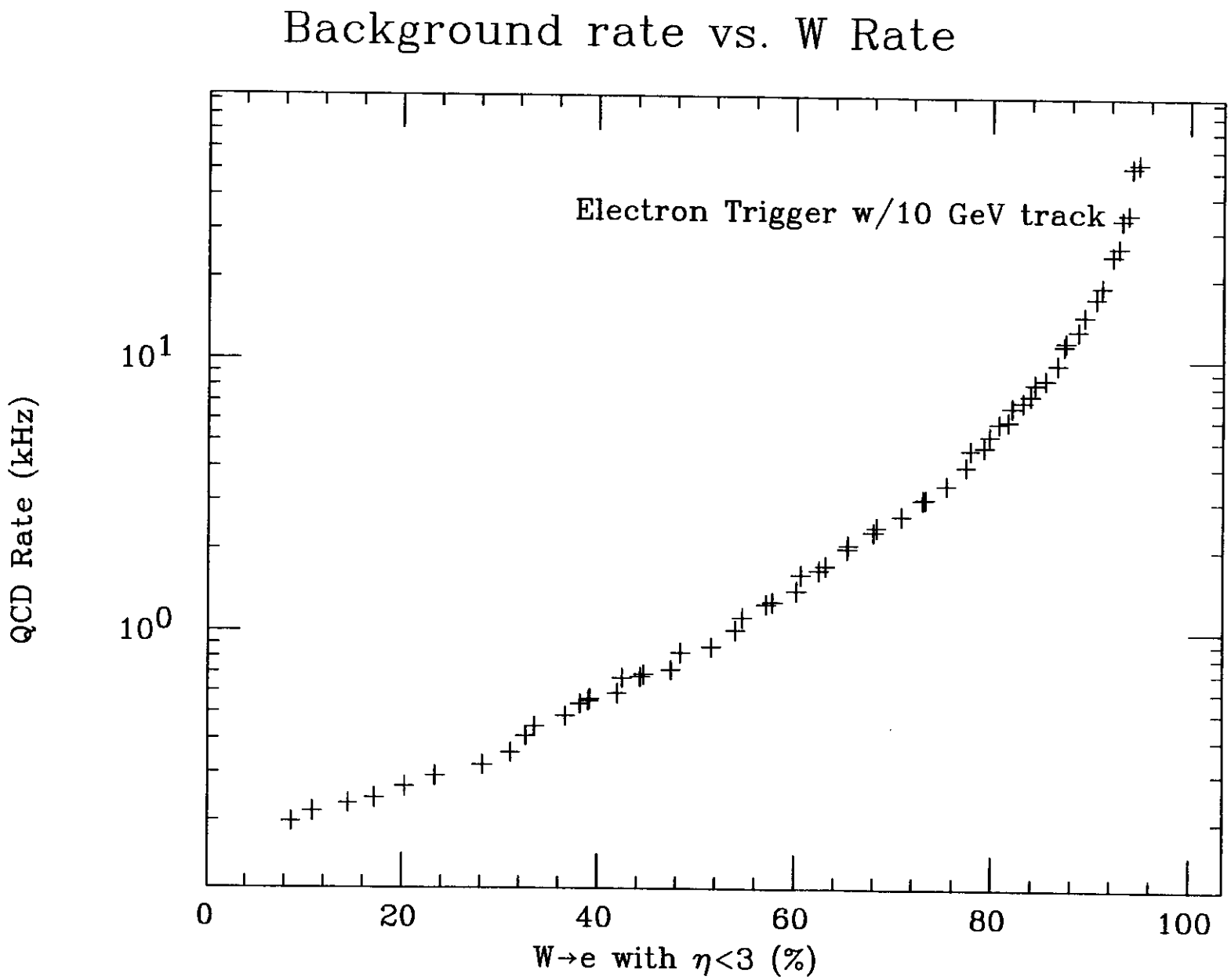
Background rate vs. W Rate
Electron Trigger w/10 GeV track
QCD Rate (kHz)
10^1
10^0
0
20
40
60
80
100
W→e with η<3 (%)

Figure 40

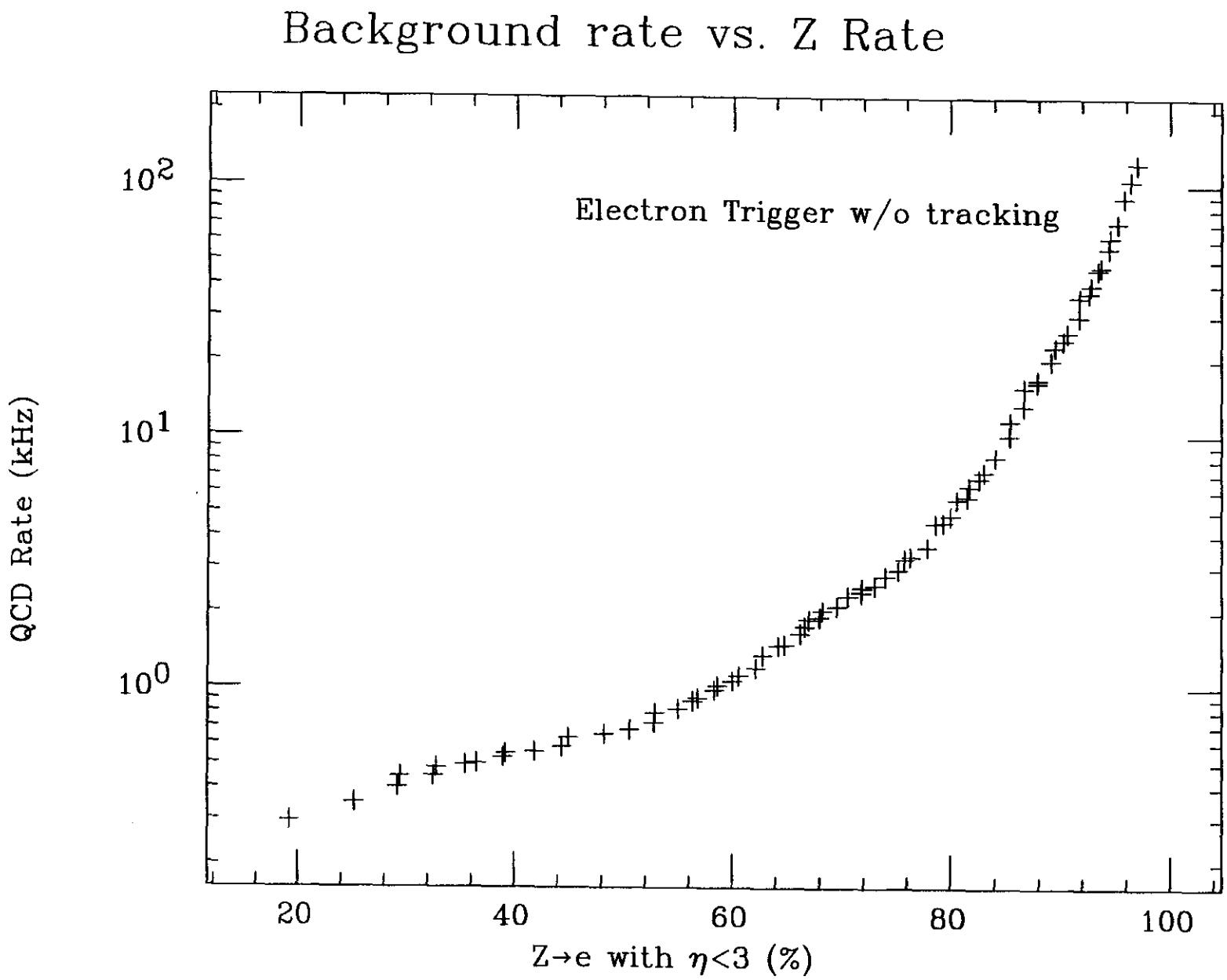
Background rate vs. Z Rate
Electron Trigger w/o tracking
QCD Rate (kHz)
10^2
10^1
10^0
20
40
60
80
100
Z→e with η<3 (%)

Figure 41

Background rate vs. Z Rate

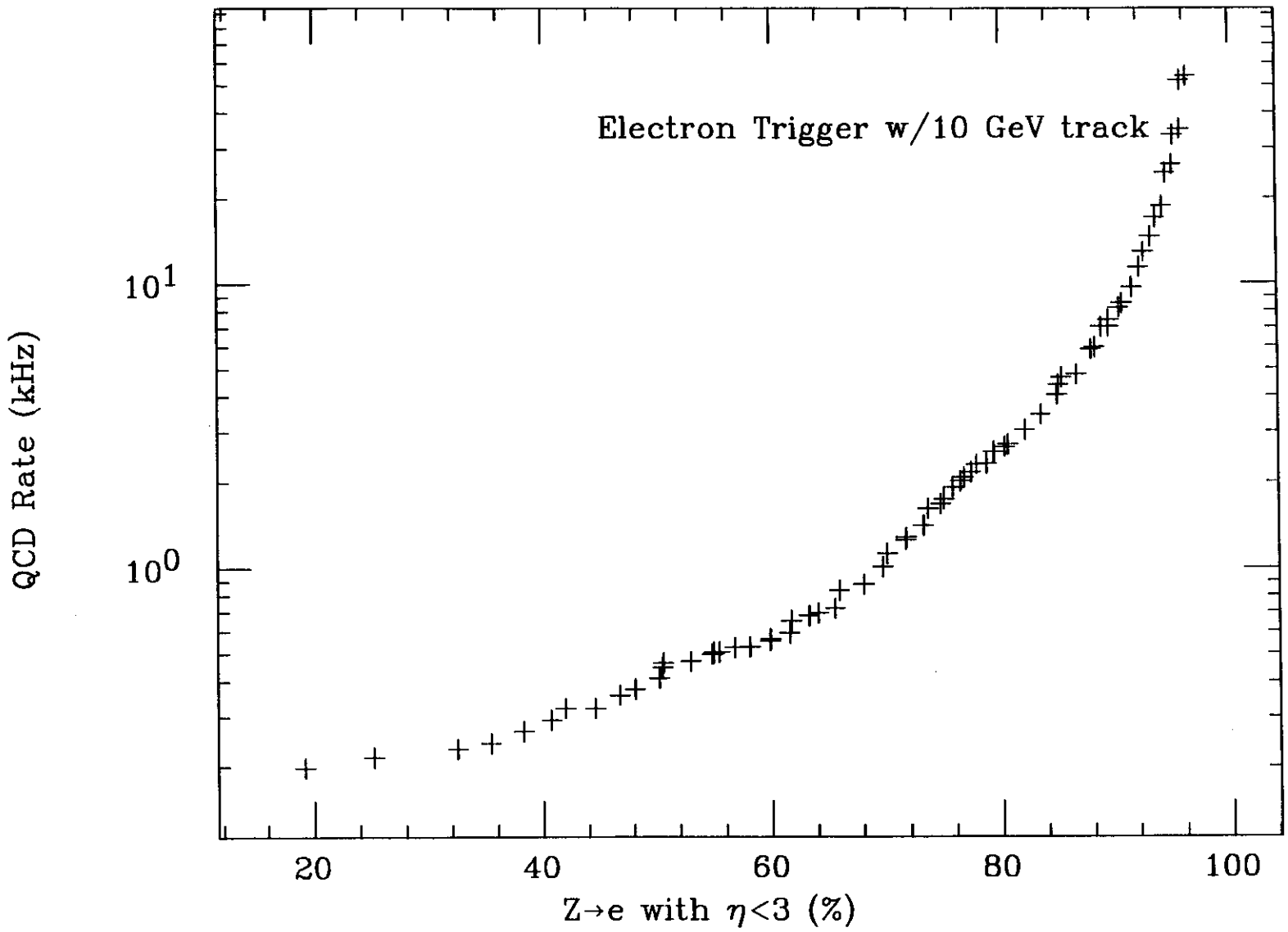

Figure 42

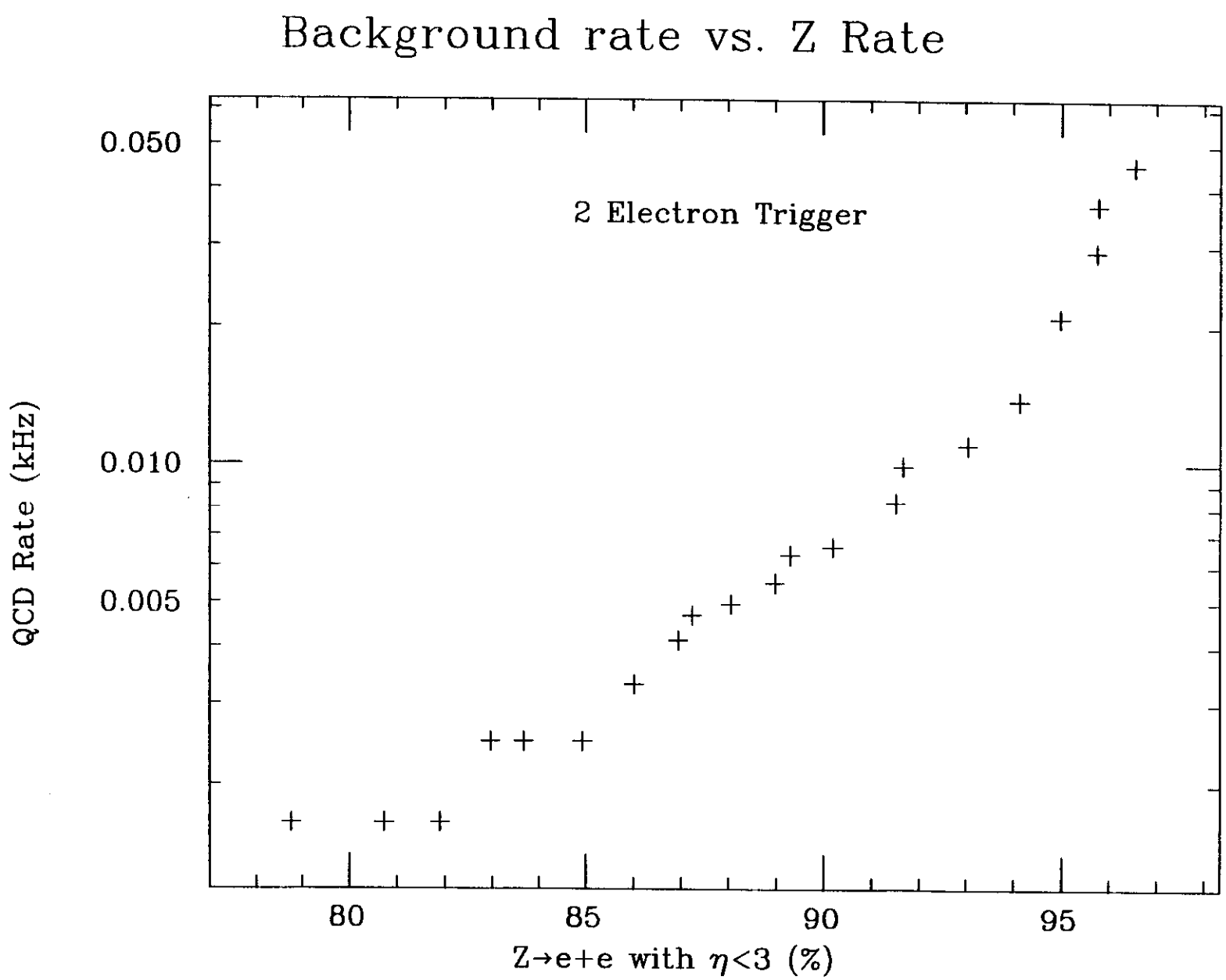
Background rate vs. Z Rate
2 Electron Trigger
QCD Rate (kHz)
0.050
0.010
0.005
80
85
90
95
Z→e+e with η<3 (%)

Figure 43

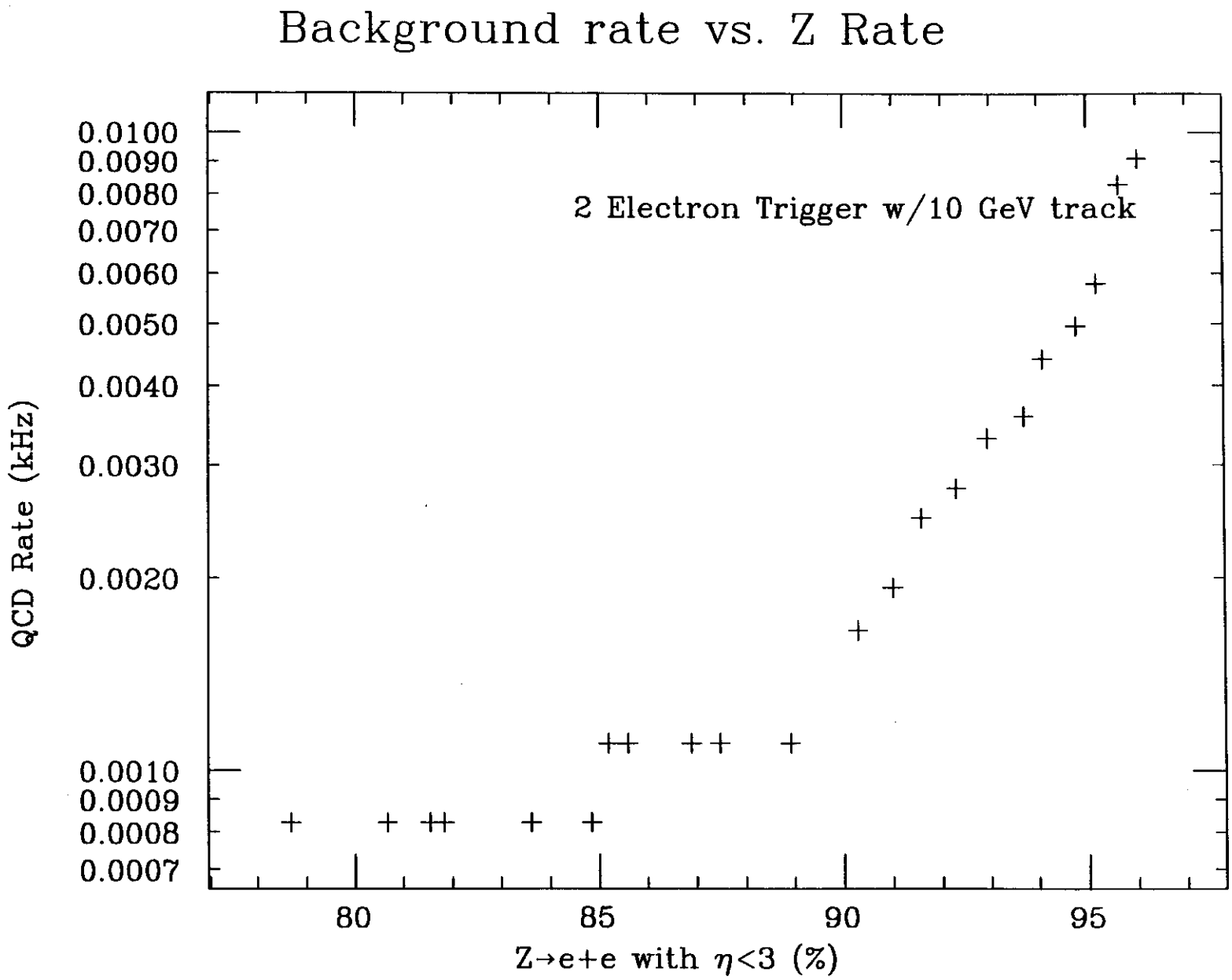
Background rate vs. Z Rate
2 Electron Trigger w/10 GeV track
QCD Rate (kHz)
0.0100
0.0090
0.0080
0.0070
0.0060
0.0050
0.0040
0.0030
0.0020
0.0010
0.0009
0.0008
0.0007
80
85
90
95
Z→e+e with η<3 (%)

Figure 44

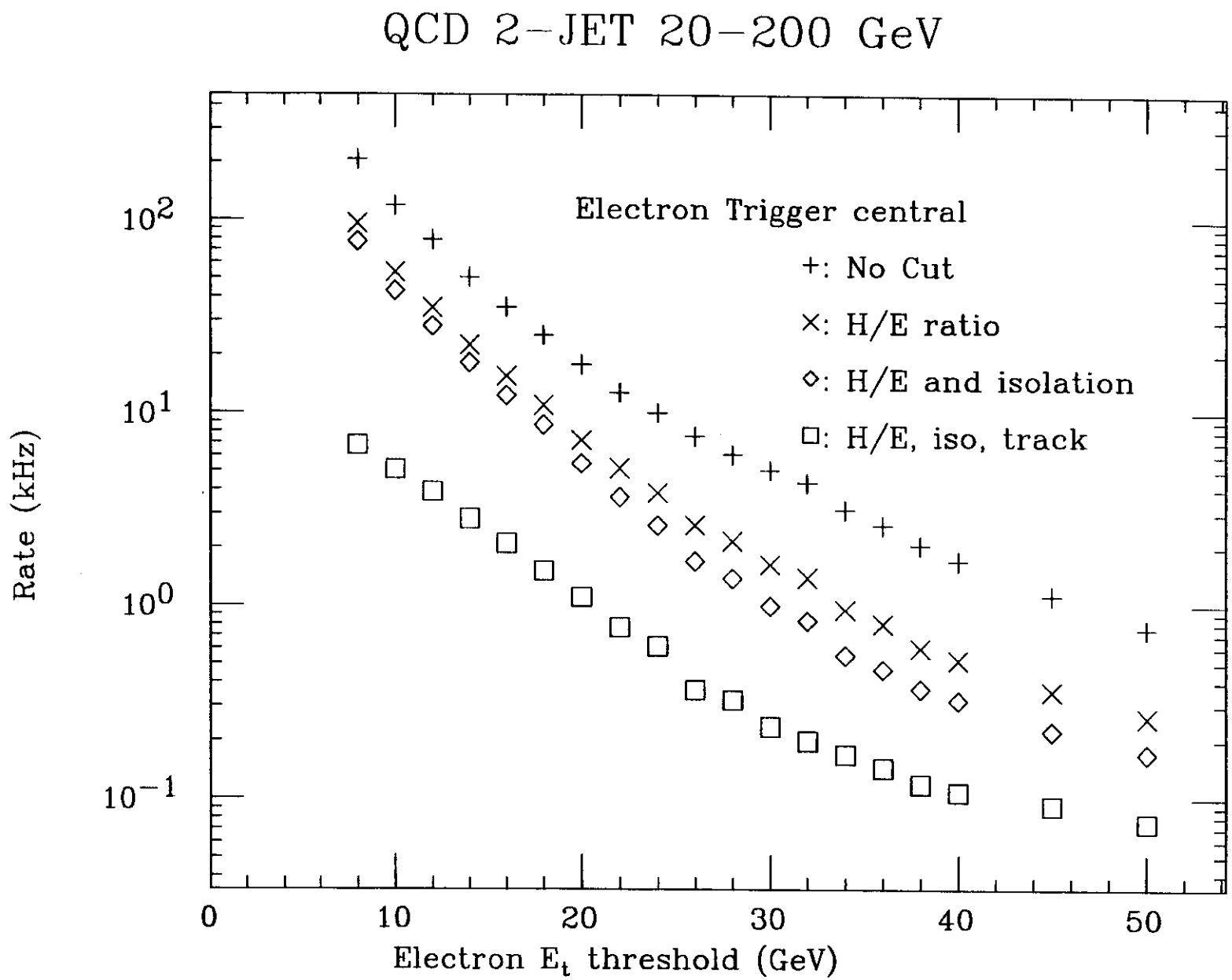
QCD 2-JET 20-200 GeV
Electron Trigger central
+: No Cut
×: H/E ratio
◇: H/E and isolation
□: H/E, iso, track
Rate (kHz)
10^2
10^1
10^0
10^{-1}
0
10
20
30
40
50
Electron E_t threshold (GeV)

Figure 45

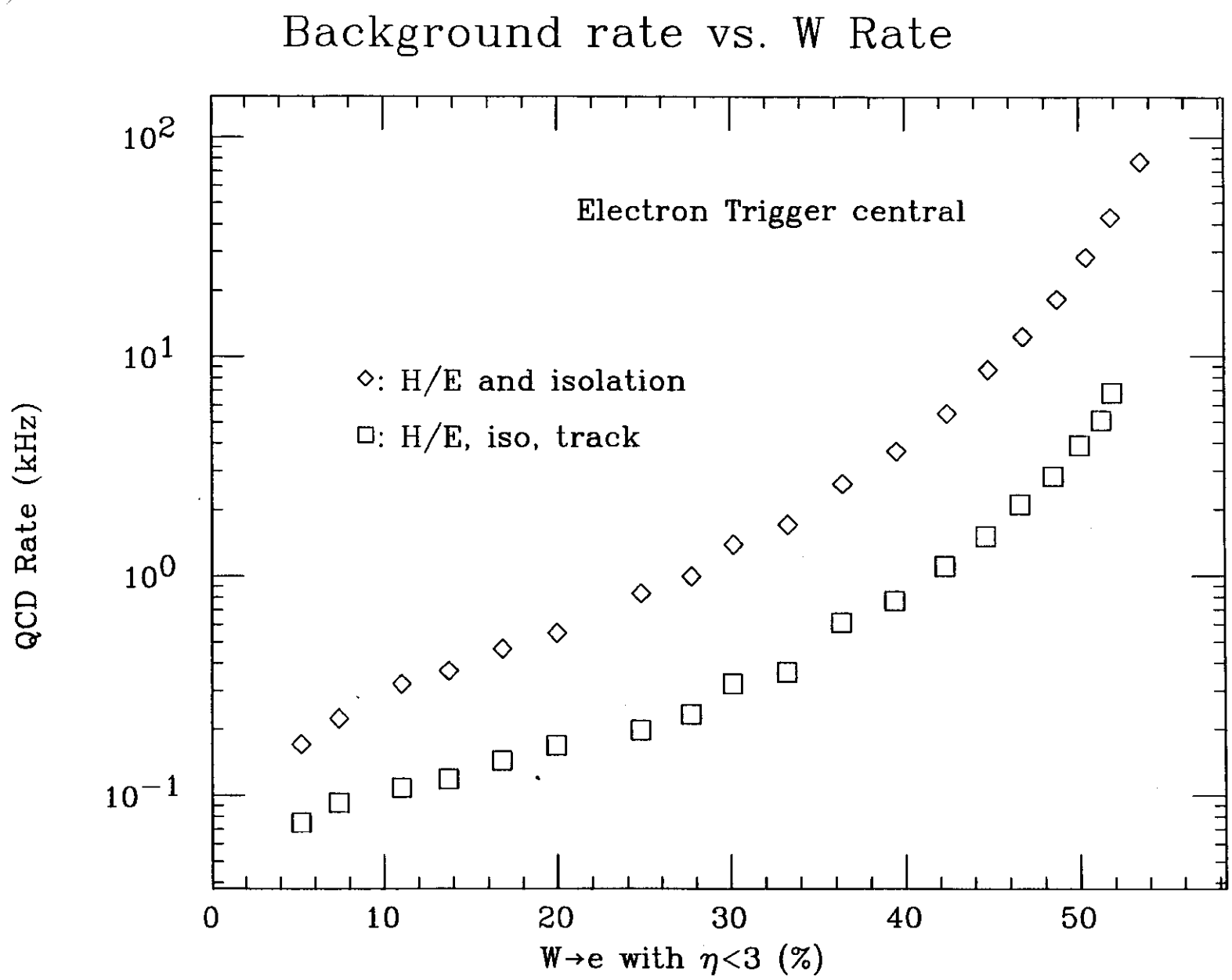
Background rate vs. W Rate
Electron Trigger central
◇: H/E and isolation
□: H/E, iso, track
QCD Rate (kHz)
10^2
10^1
10^0
10^{-1}
0
10
20
30
40
50
W→e with η<3 (%)

Figure 46

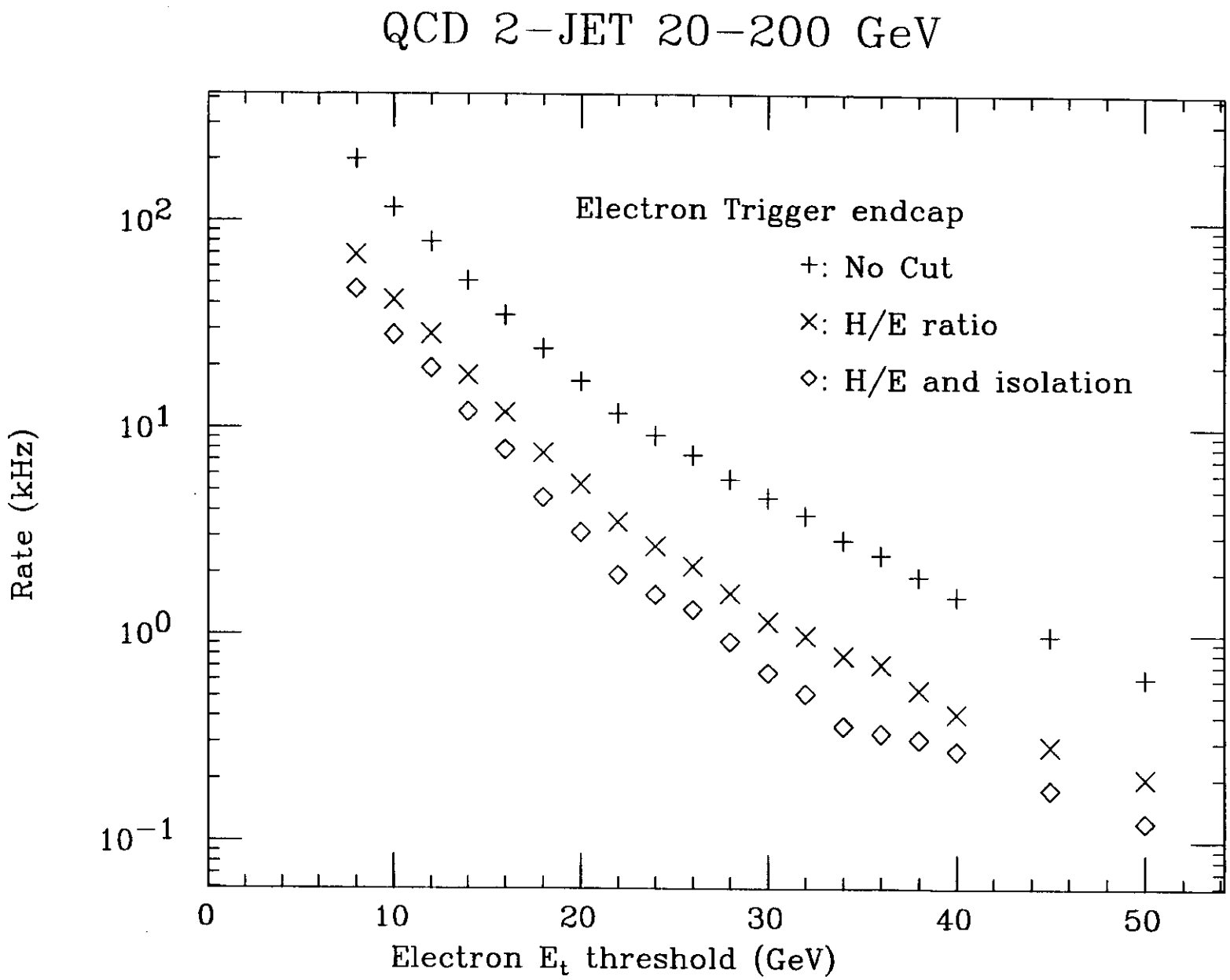
QCD 2-JET 20-200 GeV
Electron Trigger endcap
+: No Cut
×: H/E ratio
◇: H/E and isolation
Rate (kHz)
10^2
10^1
10^0
10^{-1}
0
10
20
30
40
50
Electron E_t threshold (GeV)

Figure 47

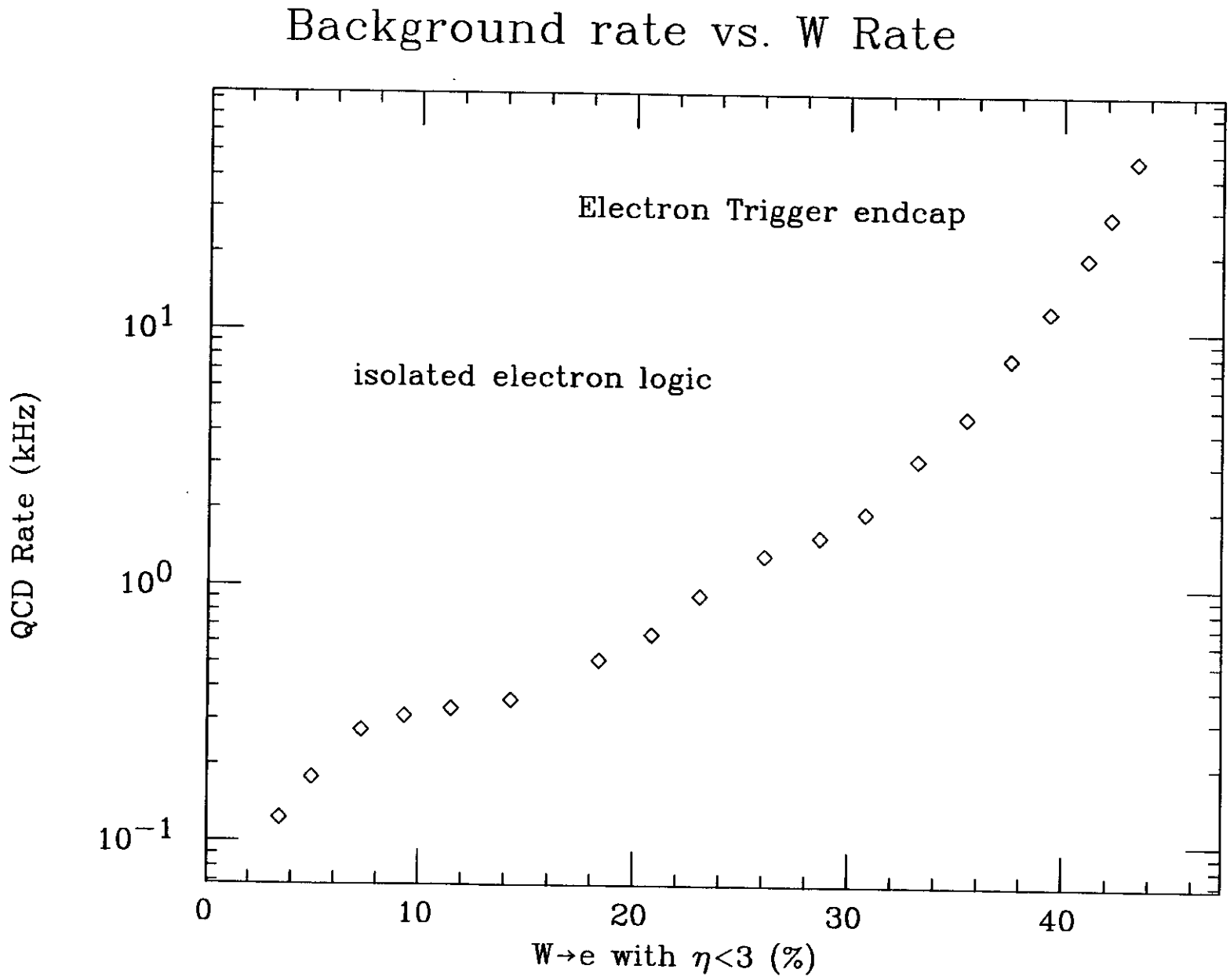
Background rate vs. W Rate
Electron Trigger endcap
isolated electron logic
QCD Rate (kHz)
10^1
10^0
10^{-1}
0
10
20
30
40
W→e with η<3 (%)

Figure 48

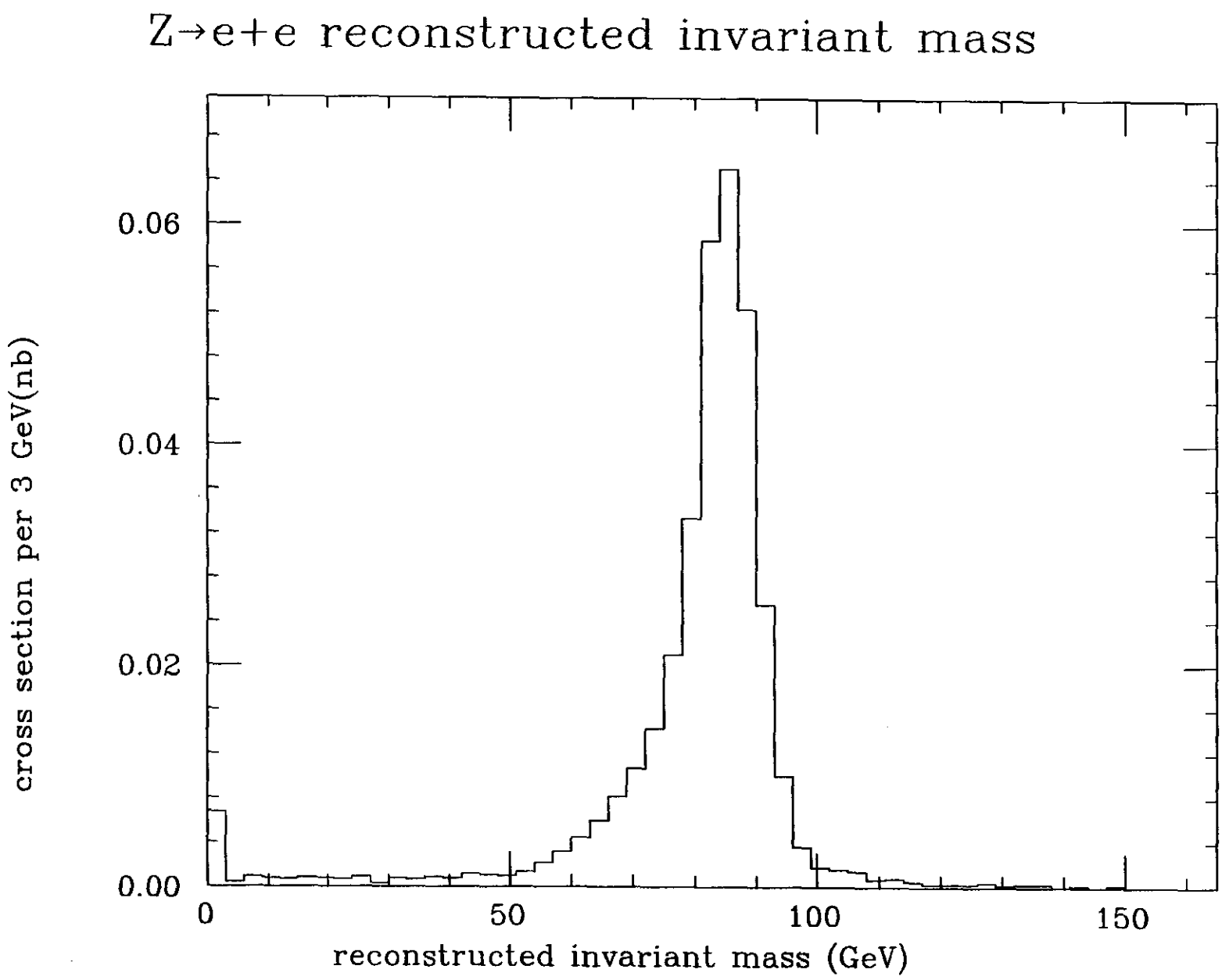
Z→e+e reconstructed invariant mass
cross section per 3 GeV(nb)
0.06
0.04
0.02
0.00
0
50
100
150
reconstructed invariant mass (GeV)

Figure 49